

**MODELLING OF THE EFFECT OF MOTION BLUR ON
PIXELATED COMMUNICATION SYSTEMS**

By
Md. Imran Khan


MASTER OF SCIENCE IN
INFORMATION AND COMMUNICATION TECHNOLOGY




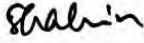
Institute of Information and Communication Technology
BANGLADESH UNIVERSITY OF ENGINEERING AND TECHNOLOGY
April, 2019


The thesis titled **“MODELLING OF THE EFFECT OF MOTION BLUR ON PIXELATED COMMUNICATION SYSTEMS”** Submitted by Md. Imran Khan, Roll No: 1014312018, Session: October 2014, has been accepted as satisfactory in partial fulfillment of the requirement for the degree of Master of Science in Information and Communication Technology on 13 April 2019.

BOARD OF EXAMINERS

1. 

Dr. Md. Rubaiyat Hossain Mondal
Associate Professor
Institute of Information and Communication Technology
BUET, Dhaka-1205
Chairman
(Supervisor)
2. 

Dr. Md. Saiful Islam
Professor and Director
Institute of Information and Communication Technology
BUET, Dhaka-1205
Member
(Ex officio)
3. 

Dr. Shahin Akhter
Assistant Professor
Institute of Information and Communication Technology
BUET, Dhaka-1205
Member
4. 

Dr. Kazi Abu Taher
Professor
Dept. of Information and Communication Technology
Bangladesh University of Professionals
Mirpur Cantonment, Dhaka-1216
Member
(External)

CANDIDATE'S DECLARATION

It is hereby declared that this thesis/project or any part of it has not been submitted elsewhere for the award of any degree or diploma.

Md. Imran Khan

DEDICATED TO MY PARENTS

Table of Contents

List of Figures	Viii
List of Abbreviations	X
List of Symbols	Xii
Acknowledgement	Xiii
Abstract	Xiv
Chapter 1 Introduction	1
1.1 Overview	1
1.2 Visible Light Communication (VLC)	2
1.3 OWC Imaging System	3
1.4 Pixelated Communication	4
1.5 Impairments in Pixelated Communication	4
1.6 Spatial OFDM for Pixelated Communication	5
1.7 Motivation of the Work	6
1.8 Objectives and Possible Outcome	6
1.9 Outline of the Thesis	7
Chapter 2 Literature Review	9
2.1 Introduction	9
2.2 Related Works	9
2.2.1 Spatial OFDM in Pixelated Communication	9
2.2.2 OFDM Based Modulation in VLC	11
2.2.3 Impairments in Pixelated Communication	13
2.2.4 Motion Blur	15

2.3	Conclusion	16
Chapter 3 Spatial OFDM Based Pixelated System		17
3.1	Overview	17
3.2	Pixelated OWC System	17
	3.2.1 A Generalized Pixelated System	19
	3.2.1.1 Transmitter	19
	3.2.1.2 Optical Channel	20
	3.2.1.3 Receiver	21
3.3	Spatial OFDM for Pixelated System	22
	3.3.1 Spatial Domain and Spatial Frequency Domain	23
	3.3.2 OFDM and Spatial OFDM	24
	3.3.3 Unipolar Optical OFDM system	27
	3.3.3.1 SDCO-OFDM system	27
	3.3.3.2 SACO-OFDM system	30
	3.3.3.2 SADO-OFDM System	30
3.4	Conclusion	32
Chapter 4 Mathematical Model		33
4.1	Introduction	33
4.2	Modelling the Effect of Motion Blur	34
4.3	Modelling the Joint Effect of Motion and Defocus Blur	38
4.4	Modelling the Effect of All Impairments	40
4.5	Conclusion	49

Chapter 5	Spatial LIM and Spatial NDC	50
5.1	Introduction	50
5.2	Spatial LED Index Modulation (Spatial LIM)	51
5.3	Spatial Non-DC Biased Modulation (Spatial NDC)	54
5.4	Simulation Results	55
5.5	Conclusion	59
Chapter 6	Practical Experiment	60
6.1	Overview	60
6.2	Experimental Set-up	60
	6.2.1 Transmitter	61
	6.2.2 Receiver	61
6.3	Angle Correction of Rotational Misaligned Image	63
6.4	BER Calculation from Perspective Distorted Images	67
6.5	BER Calculation from Motion Blurred Images	70
6.6	Conclusion	72
Chapter 7	Conclusion	74
7.1	Introduction	74
7.2	Contributions	74
7.3	Recommendations	75
	Reference	77

List of Figures

Fig. 3.1:	A point to point pixelated system	18
Fig. 3.2:	Schematic of a Pixelated OWC system	19
Fig. 3.3:	Block diagram of a pixelated OWC system.	20
Fig. 3.4:	Mapping of information to pixel values for 8×8 data set	21
Fig. 3.5:	(a) higher spatial frequency (b) lower spatial frequency	23
Fig. 3.6:	Block diagram of a Spatial OFDM system	25
Fig. 3.7:	Mapping of spatial OFDM frame to pixelated image frame	26
Fig. 3.8:	Addition of cyclic prefix (CP) and cyclic postfix (CPo)	27
Fig. 3.9:	Block diagram of an SDCO-OFDM based pixelated system	28
Fig. 4.1:	Point spread function (PSF) for motion blur	34
Fig. 4.2:	The difference between transmitted and received frames in joint presence of all spatial impairments	41
Fig. 5.1:	Block diagram of LED index modulation for pixelated communication	51
Fig. 5.2:	Block diagram of non-DC biased modulation for pixelated communication	54
Fig. 5.3:	BER vs. $E_{b(elec)}/N_0$ curve in pixelated systems for stand-alone AWGN channels	56
Fig. 5.4:	BER vs. $E_{b(opt)}/N_0$ curve for pixelated systems for stand-alone AWGN channels	57
Fig. 5.5:	BER vs. $E_{b(elec)}/N_0$ curve for pixelated systems with different impairments	58
Fig. 5.6:	BER vs. $E_{b(opt)}/N_0$ curve for pixelated systems with different impairments	58

Fig. 6.1:	Schematic diagram of practical pixelated communication system	61
Fig. 6.2:	Transmitter block diagram of pixelated system	61
Fig. 6.3:	Receiver block diagram of pixelated system	62
Fig. 6.4:	(a) Transmitted image (b) Received image (c) Segmented ROI (d) Decoded image	63
Fig. 6.5:	Coordinate changing for image rotation	64
Fig. 6.6:	(a) Rotational misaligned image, (b) Rotational alignment corrected image, (c) Reference Image, (d) Segmented ROI	66
Fig. 6.7:	Geometric transformation for perspective distortion	67
Fig. 6.8:	(a) Reference image, (b) Received distorted image, (c) Image after projective transformation	69
Fig. 6.9:	BER curve (distorted images)	70
Fig. 6.10:	BER curve (projective transformed images)	70
Fig. 6.11:	Image with higher frequency	71
Fig. 6.12:	Image without higher frequency	71
Fig. 6.13:	Transmitted image	71
Fig. 6.14:	Received motion blurred image	71
Fig. 6.15:	Segmented ROI	72
Fig. 6.16:	Recovered image	72
Fig. 6.17:	BER using higher frequency	72
Fig. 6.18:	BER without using higher frequency	72

List of Abbreviations

PSF	Point Spread Function
RF	Radio Frequency
OWC	Optical Wireless Communication
IR	Infrared
UV	Ultraviolet
LED	Light Emitting Diode
ITS	Intelligent Transport System
VLC	Visible Light Communication
SNR	Signal to Noise Ratio
MIMO	Multiple Input Multiple Output
FOV	Field of View
LCD	Liquid Crystal Display
OFDM	Orthogonal Frequency Division Multiplexing
SACO-OFDM	Spatial Asymmetrically Clipped Optical OFDM
SDCO-OFDM	Spatial DC bias Optical OFDM
SADO-OFDM	Spatial Asymmetrically DC biased Optical OFDM
CCD	Charged Coupled Device
OOK	On-Off Keying
PPM	Pulse Position Modulation
ICI	Inter Carrier Interference

QAM	Quadrature Amplitude Modulation
CP	Cyclic Prefix
CPo	Cyclic Postfix
SF-ICI	Spatial Frequency Inter Channel Interference
BER	Bit Error Rate
SLIM	Spatial LED Index Modulation
SNDC	Spatial Non DC Bias
D2C	Display to Camera
PAM	Pulse Amplitude Modulation
DPSK	Differential Phase Shift Keying
QPSK	Quadrature Phase Shift Keying
SURF	Speeded Up Robust Feature
ISI	Inter Symbol Interference
LFM	Linear Fractional Misalignment
IFFT	Inverse Fast Fourier Transform
FFT	Fast Fourier Transform
SDM	Spatial Domain Modulation
NCS-OFDM	Noise- Cancelled Spatial OFDM

List of Symbols

$\{\blacksquare\}$	Expectation Operator
μ	Proportionality constant
Σ	Summation
σ	Standard deviation
*	Complex conjugate operator

Acknowledgement

First of all, I would like to thank Allah for giving me the ability to complete this thesis work. I would like to express my sincere gratitude to my supervisor, Dr. Md. Rubaiyat Hossain Mondal, Associate Professor of IICT, BUET. This thesis would not have been completed without his support and guidance. I would like to express my great thanks and gratefulness for instructions, continuous encouragement, valuable discussions and careful review during the period of this research. I have learned many valuable lessons and concepts of optical wireless communication from him through my study, which I have utilized to develop my abilities to work innovatively. His constant encouragement gave me the confidence to carry out my work.

I would like to thank Professor Dr. Md. Saiful Islam, Director of IICT, BUET for his support and inspiration during my candidature. I would also like to thank all the teachers and staffs of IICT, BUET for their cordial help and assistance during my study period.

Finally, I would like to thank my parents. Their unconditional support made it possible for me to finish this thesis.

Abstract

Optical wireless communication (OWC) is becoming popular nowadays due to high data rate and more security features than the radio frequency (RF) communication. One of the major branches of OWC is optical camera communication (OCC) which can be categorized into visible light communication (VLC) and pixelated communication. The screen of a digital gadget like smartphones/tablets/laptops is used as transmitter and camera of any of those digital gadgets is used as receiver to transfer images in pixelated OWC. A pixelated system is susceptible to different spatial impairments such as motion blur, defocus blur, rotational misalignment and perspective distortion. This thesis analyses the impact of motion blur in the context of pixelated systems for the first time and also finds the combined impact of all spatial impairments mathematically. At first the effect of stand-alone motion blur is derived and it is found that the impact of motion blur depends on motion length and subcarrier index. Next, the joint impacts of defocus and motion blur are modeled which show that the impact of both blurs are independent to each other and the attenuation due to defocus blur depends on point spread function (PSF) of defocus blur and subcarrier index. Finally the combined effect of all the impairments are modeled which indicate that the impact of each impairment does not depend on others and the combined effect is the joint attenuation due to motion blur, defocus blur, linear fractional misalignment (LFM), and vignetting. On the other hand, the performance of non-DC biased optical OFDM (NDC-OFDM) and LED index modulation optical OFDM (LIM-OFDM) are evaluated and compared with different forms of spatial orthogonal frequency division multiplexing (spatial OFDM) including spatial DC biased optical OFDM (SDCO-OFDM), spatial asymmetrically clipped optical OFDM (SACO-OFDM) and spatial asymmetrically clipped DC biased optical OFDM (SADO-OFDM) for both VLC and pixelated OWC systems to find out the best candidate in terms of electrical and optical power efficiency. Simulation results show that without the presence of impairments, SLIM shows better optical power efficiency than SNDC when only AWGN is present. On the other hand, SNDC performs better than SLIM, SACO and SDCO when channel is modeled with different spatial impairments like motion blur, linear fractional misalignment, vignetting along with channel noise. Practical experiments are also conducted for SDCO-OFDM modulation to realize the practical impact of these impairments and some techniques are followed to reduce the impact from practically impaired received images.

CHAPTER ONE

INTRODUCTION

1.1 Overview

The demand for wireless multimedia data is increasing quickly every year. *Optical wireless communication* (OWC) [1-3] means wireless transmission in the optical spectrum used as alternative of *radio frequency* (RF) transmission as data rate of RF transmission is only several hundred Mbits/s[4-6]. Local and international authorities strictly regulate the use of this RF band. Ordinarily, certain operators like television broadcasters, point-to-point microwave links and cellular phone operators have the license of entire RF sub-bands [7]. To cope up with high-density and high-capacity networks, the optical spectrum is considered as a promising solution. OWC-based network technologies offer unique advantages in comparison with RF-based networks. For communication distances ranging from a few nanometers to more than 10,000 km, OWC systems can provide high-data-rate services. For both indoor and outdoor services it can perform well.

Information is converted to optical signal from electrical signal and free space is used as channel in OWC. The optical spectrum consists with infrared (IR), ultraviolet (UV), and the visible light wavelengths. Before transforming data into an optical signal through an optical modulator such as *light emitting diode* (LED), *LASER diodes* (LDs), firstly data is modulated in the electrical domain. In receiver, photo-detector such as photodiode is used to generate equivalent electrical signal from received optical power and then demodulation is performed for data recovery [8-10].

In OWC system, at first, the data is modulated by an electrical modulator in electrical domain to produce a signal x_t . Then this electrical signal x_t is converted to optical signal p_t by optical modulator. The optical signal p_t is then transmitted through optical wireless channel. At receiver the received optical signal q_t is transferred into equivalent electrical signal using optical demodulator. Finally original data are recovered after electrical demodulation. Due to optical

noise an equivalent electrical noise z_t is considered here.

The prime advantage of OWC is that the optical spectrum does not need any licensing. This specific feature makes OWC eminent over the congested RF spectrum. Furthermore, OWC provides higher directivity, privacy against eavesdropping, higher degree of communication security and higher data rate as optical signal can be restricted in compact boundaries. Besides, coexistence with existing RF system is possible without any electromagnetic interference as optical signal of OWC system does not interfere with RF signal [8-12].

OWC is more suitable for secure communications for these features. OWC systems also have applications like chip-to-chip communication [13-16], inter-building connections [17], *wireless body area network* (WBAN), *wireless personal area network* (WPAN), Underwater communications [18-20], inter-satellite, satellite-earth, satellite-to-airplane, airplane-to-satellite, airplane-to-airplane, and airplane-to-ground links [21-22], VLC-based WLANs and vehicular communication [23-25]. However, optical noise causes by ambient light, path loss in free space and limited capability of switching of optical modulator and demodulator limits the data rate of OWC [9, 26, 27].

1.2 Visible Light Communication (VLC)

In the past decade, *visible light communication* (VLC) which is a subcategory of OWC, has emerged as a promising technology. The VLC technology is nothing but communication through visible light using the intensity modulation of LDs or LEDs. LEDs or LDs can be switched on and off at a very high rate according to the electrical information [28] which enables communications through visible light. For upcoming high-density and high capacity 5G wireless networks LEDs or LDs based VLC can be a promising solution. VLC could play an important role in Internet of things (IoT) [29] because it needs to allow a connection among large number of devices for resource sharing, sensing and monitoring purposes. As RF-based technologies suffer for 10,000 times less bandwidth capacity than VLC technology, VLC become popular [30]. Moreover, VLC is preferable as it uses visible light

spectrum which is related to eye safety. VLC has vast application including roadside, cars, homes, airplanes, trains, and offices [31].

On the other hand, some constraints of this technology are: (i) for outdoor applications it is not effective; and (ii) long distance communication is not possible using this technology. The data rate of VLC largely depends on the switching rate of LEDs. LEDs have a unique feature which is not available in other devices as it can change its intensity levels very fast and this change cannot be detected by the human eye [32-34]. Hence, for illumination, communication, and localization these energy-efficient LED devices can be used [35]. LEDs based VLC can provide more than 10 Gbps data rates [36] where a single color LED can provide a data rate of 3 Gbps [37]. Sometimes LDs are used as alternatives in VLC as LEDs can't provide higher bandwidth and higher optical efficiency at the same time. LDs based VLC provides 100 Gbps data rate in case of indoor communication [36].

1.3 OWC Imaging System

To obtain spatial diversity imaging lens at the receiver are used as optical concentrators in OWC imaging system. The information is converted to the optical signal which is transmitted from the transmitter array and then refracted by the imaging lens. Finally the optical signal is collected by photo detector array at the receiver side of OWC imaging system [1, 11, 38, 39].

The array of pixels are used in transmitter as transmitting units just to enlarge the *field of view*(FOV) because a single pixel could only accumulate data from its surroundings resulting narrow FOV, whereas an array of pixels will collect data according to their individual range and after accumulating will provide a much larger FOV [40,41]. Equivalent electrical current proportional to the collected optical power is then generated in the receiver. Conversely, the limiting factor of this type of receiver is that it is not fitted to a system which needs higher mobility. Because of movement of the receiver, focal point changes with different incident angle of light. From the uncorrelated channel matrix the receiver pixels can easily distinguish the optical signal coming from different directions. In case of large number of transmitting pixels and receiving pixels higher order of channel matrix can be implemented [42].

1.4 Pixelated Communication

Another form of imaging system is pixelated scheme. In pixelated imaging system, the data are encoded in two dimensional (2D) image space known as the 2D spatial domain [43 -58]. To achieve high data rates in pixelated imaging system, a series of time varying images are produced and transmitted which are nothing but the representation of encoded data. Fig. 1-3 illustrates one such image frame. Here the value of data determines the intensity of the pixels of the image frame. Generally *intensity modulation and direct detection* (IM/DD) is applied for the pixelated system. A *liquid crystal display* (LCD) or a LED screen of a computer is used as transmitter; and a camera is used as receiver. Moreover, a receiver [43] can also consist of an imaging lens with an array of photodiode. Despite the fact of offering limited mobility of pixelated systems, it has the potential for a number of indoor and outdoor applications. Pixelated systems are widely used in near field communication for example secure communication, data exchange in high concentration scenario and mobile advertisement. The next chapters will elaborate this system in details.

1.5 Impairments in Pixelated Communication

The performance of pixelated communication is affected by various types of spatial channel impairments which are introduced below:

Motion: Motion blur is one of the most prominent spatial impairments for pixelated communication. This blur is created due to motion of either transmitting device or receiving device or both at the same time which affect the communication performance. In case of motion blur, data cannot be estimated correctly in receiver section as original information is distorted due to blur. To remove the noise created for motion blur, it is important to know the effect of motion blur first. The effect of motion blur in spatial frequency domain is not studied yet.

Defocus: Due to imperfect focusing of the imaging lens another blur is generated called defocus blur which is another important impairment of pixelated communication system. As the distance between the transmitter and the receiver usually does not remain fixed, defocus is likely to occur in a pixelated system. As a result the data recovery process produce incorrect data as lens of

receiver is out-of-focus. Literature review [43, 45] shows that defocus blur act as low pass filter which allows the low frequency term unchanged in image frame.

Linear misalignment: Linear misalignment occurs if the borders of the data-carrying received images are misaligned with respect to those of the transmitted images along straight lines. If the length of the misalignment is equal to the integer number of pixels then it is called as linear integral misalignment has been reported in previous research paper [43, 58, 59]. In practical scenario, the amount of misalignment is often equal to the variable factor of fraction number of pixels which is known as linear fractional misalignment (LFM).

Vignetting: A pixelated system may also be impaired by *vignetting*, which is the gradual illumination fall-off from the center to the corners of the received images [60-63].

1.6 Spatial OFDM for Pixelated Communication

The encoded data are organized in 2D image space which is known as spatial domain. Before transmission data are encoded in spatial domain which is equivalent to its spatial frequency domain and then it is transmitted through optical channel as image frame. *Spatial orthogonal frequency division multiplexing* (spatial OFDM) is one of the forms of spatial frequency domain encoding. With comparing to spatial domain, in spatial frequency domain the main advantage is easier and simpler equalization process which makes spatial OFDM popular. Consequently, in pixelated systems, one form of spatial frequency domain encoding- Spatial-OFDM is usually used. As spatial OFDM can produce complex and negative values, data is then processed such a way so that it can be converted to pixel intensity and transmitted in optical channel.

For two dimensional VLC and pixelated systems, two spatial OFDM modulation named *Non-DC biased OFDM* (NDC-OFDM) [64], *LED index modulation OFDM* (LIM-OFDM)[65]; and three unipolar spatial OFDM such as *spatial asymmetrically clipped optical OFDM* (SACO-OFDM)[47], *spatial DC biased optical OFDM* (SDCO-OFDM) [66] and *spatial asymmetrically clipped DC Biased optical OFDM* (SADO-OFDM)[67] have been discussed in the literature respectively.

1.7 Motivation of the Work

OWC can be categorized into different classes including VLC and pixelated communication. A pixelated OWC is an image transfer based data communication scheme where the screens of smartphones/tablets/laptops are used as transmitters and cameras of smartphones or webcams as receivers [50,51,58,59]. A pixelated system is susceptible to different spatial impairments such as motion blur, defocus blur, rotational misalignment and perspective distortion [51]. However, the impact of motion blur has only been simulated but not mathematically analyzed for pixelated systems. On the other hand, different forms of spatial OFDM have been proposed as modulation schemes for pixelated OWC. SADO-OFDM [67] has recently been shown to be more power efficient than other spatial OFDM formats. NDC-OFDM and LIM-OFDM [64,65] are recently shown to be effective for VLC. The spatial forms of NDC-OFDM and LIM-OFDM are yet to be developed for pixelated OWC. This research focuses on the adaptation of these two spatial OFDM formats, as well as the modelling and analysis of motion blur.

1.8 Objectives and Possible Outcome

The objectives of this work are to analyze the performance of spatial OFDM based pixelated systems in the presence of motion blur. These objectives are:

1. To analyze the impact of motion blur on pixelated communication systems.
2. To develop SLIM-OFDM and SNDC-OFDM modulation forms and comparing their power efficiency with existing SADO-OFDM based pixelated systems.
3. To evaluate the performance of spatial OFDM based system in the presence of motion blur.

The possible outcome of this research is the development of an appropriate spatial OFDM form suitable for pixelated systems affected by motion blur.

1.9 Outline of the Thesis

This thesis consists of major five sections by which the effect of motion blur in pixelated systems is explored. The first part starts with the basic concepts of pixelated systems and spatial optical OFDM. The second part of the thesis will show the previous research works related to VLC, pixelated systems and impairments of pixelated systems. The third part is responsible for exploring the theoretical model of the effect of motion blur along with other impairments in case of pixelated communication system. The fourth part will develop the SLIM-OFDM and SNDC-OFDM for pixelated communication system and comparing the performance of these optical spatial OFDM methods with other uniform optical spatial OFDM methods. The final part will deal with the practical demonstration of capturing impaired pixelated image frames and some techniques to remove the impairments. The descriptions of the chapters are the followings which are given below.

Chapter 2 will show the review of previous research work related with VLC, pixelated communication, impairments of pixelated communication system and motion blur. The achievable data rates and different impairments that affect the system discussed in previous papers will also be presented here.

In **Chapter 3**, pixelated system will be explained in detailed with the help of necessary block diagrams of transmitter and receiver. Spatial optical OFDM modulation will explained also as it is necessary in pixelated system. The basic concepts of spatial domain and spatial frequency domain will be discussed in order to understand spatial OFDM. Specifically, SDCO-OFDM, SACO-OFDM and SADO-OFDM will be explained with proper diagrams in this chapter.

In **Chapter 4**, the effect of linear and angular motion blur will be determined first. Then the joint effect of defocus and motion blur will be derived mathematically. After that, the effect of all spatial impairments like motion blur, defocus blur, LFM, vignetting and channel noise will be modeled to understand the practical worst scenario when all impairments are present.

In **Chapter 5**, LIM-OFDM and NDC-OFDM are extended to spatial domain to form spatial LIM-OFDM (SLIM-OFDM) and spatial NDC-OFDM (SNDC-OFDM) for pixelated communication systems. The electrical and optical power efficiency of SLIM-OFDM, SNDC-

OFDM along with other optical spatial OFDM methods will be compared considering both *Additive White Gaussian Noise (AWGN)* channel noise and channel with joint presence of all impairments.

Chapter 6 is for practical demonstration of a pixelated system which will describe the process of practical experiment including set up of practical a pixelated system, block diagram of transmitter and receiver. It will explain the procedure of capturing motion blur impaired images from practical experiment and data recovery along with *bit error rate (BER)* calculation. This chapter will also deal with angle correction of rotational misaligned image and BER calculation from captured images with perspective distortion impairment.

Finally **Chapter 7** will present the concluding remarks and future research direction of the thesis.

CHAPTER TWO

LITERATURE REVIEW

2.1 Introduction

A vast research works has been done about pixelated systems since 2004. Different research papers claim different data rates after conducting various experiments of pixelated systems. Similarly, various researches are done to highlight the impairments of the pixelated system and many techniques are proposed to overcome these effects of impairments in receiver side.

2.2 Related Work

The previous works related to spatial OFDM and pixelated systems are mainly categorized into four subsections. The summary of research works related to spatial OFDM based modulation in pixelated communication is presented in Section 2.2.1. Section 2.2.2 presents the research works related to OFDM based modulation in VLC. Section 2.2.3 presents the impairments in a pixelated system mentioned in different research papers. Lastly the summary of various papers based on motion blur is presented in subsection 2.2.4.

2.2.1 Spatial OFDM in Pixelated Communication

Pixelated system is a promising technique introduced in [43], defined as short range wireless communication using line of sight with high data rate by transmitting and receiving of time varying images composed of a number of pixels. Recently IEEE 802.15.7m standard is declared by OWC task group where pixelated communication is explained as screen modulation based optical camera communication (OCC) which is used generally to communicate within several meters with a data rate up to several Mbps suited for short range communication with a typical camera receiver [94]. Pixelated communication is termed as flicker modulation based communication using Nyquist sampling in [95] where a survey is done on various works based on pixelated communication along with other branches on OWC. It is reported that 2D color code based pixelated system provides high throughput with low resolution based transmitted images

than other schemes. Authors in [96] propose interframe encoding method where actual information is derived from every two consecutive image frames in the receiver section which made the pixelated system flickerless and enhances the BER performance even the distance between transmitting screen and receiving camera is increased.

Spatial DC-biased optical OFDM (SDCO-OFDM) [43, 45, 58, 66] and spatial asymmetrically clipped optical OFDM (SACO-OFDM) [47] are developed for pixelated systems. Both methods are unipolar spatial optical OFDM methods which convert complex bipolar OFDM signal into real and nonnegative so that data can be suited for transmission in IM/DD system. In SDCO-OFDM, spatial frequency domain data is modulated and converted into spatial domain data using 2D IFFT. These spatial domain data are complex and bipolar. Hermitian symmetry is applied on spatial domain data and finally a DC bias is added to make spatial domain data real and unipolar. The method of making bipolar OFDM symbol to unipolar is different in SACO-OFDM. In SACO-OFDM, only odd subcarriers carry data and even subcarriers become null. After applying Hermitian symmetry, the negative portion of bipolar OFDM symbol is asymmetrically clipped to zero level. For a given overall data rate, it is shown in [47, 50] that, SACO-OFDM requires less optical power than SDCO-OFDM. Due to the use of a large DC bias [50] to form non-negative electrical signals required to modulate pixelated images the efficiency in SDCO-OFDM is not as high as SACO-OFDM. By choosing the optimum DC bias the power efficiency of SDCO-OFDM can be improved.

A prototype is experimented in [49] where transmitter and receiver array are a 512×512 pixel LCD panel and a 154×154 pixel CCD camera, respectively. In a distance of 2 m, the achieved data rate is up to 1.7kb/Hz and the resulting frame rate is 22.4frames/second. High speed can be achieved from this type of experiment if strict alignment of transmitter and receiver is maintained. LCD or LED panel to smartphone communication through camera is proposed in [89]. To help blind people or people with low vision by sensing LED panel or 7 segment LCD panel, an image processing algorithm is implemented at Symbian smartphone. By pushing a button within 2 seconds, the software can read the display.

Display to camera (D2C) link is presented in [90] where the fundamental design is implemented and performance analysis is presented. An electronic screen is used as a transmitter and a digital

camera which is in line of sight of transmitter is used as the receiver in this system. The transmitted images consist of embedded data oriented in spectral domain. In between two data embedded image frames, a reference image is inserted for differentiating the original data from the embedded image. Based on different frequency sub-bands of the image frame, the original data are embedded. During performance evaluation, various distortions are taken into account. For image size of 256×256 pixels and constellation size of 16, this system can provide data rates up to 9.5 kbps using QAM modulation. New data modulation is proposed in [91] where differential phase shift keying (DPSK) and OFDM are combined and implemented. In this method, the problem of phase distortion due to movement of the handheld devices is mitigated by using DPSK instead of *quaternary phase shift keying* (QPSK) before OFDM. Less than 8% error rate is observed for this system instead of 30% provided by *pulse amplitude modulation* (PAM) and QPSK. In another research [97], comparison is accomplished among three smartphones of different companies and models where various shades of grey color is used to transmit images through LCD screen where smartphone is used as receiver. It is shown that the sensitivity of these three smartphones for the same illumination of LCD screen are not the same. Interestingly, high sensitivity to brightness of transmitted screen does not provides guarantee of low BER shown in [97]. TEtra-TRansmISsion (TETRIS) is proposed in [98], where smartphone to smartphone based pixelated system is developed with RGB plane used to represent data block in transmitted image frame and achieved throughput of 311.22 Kbps with 90% accuracy. This research suggests using of feedback channel between transmitter and receiver, using at least 8 different colors and improving the condition of ambient light for high throughput in future.

2.2.2 OFDM Based Modulation in VLC

For indoor mobile communications scenarios visible light communications (VLC) systems could be the optimal solution due to the existing infrastructure, which can be reused and lighting and communication systems can be combined. VLC operates between the 400-800 nm range. Due to moderate and high data rates and frequency-selective behavior of the VLC channels, orthogonal frequency division multiplexing (OFDM) and its modified versions for intensity modulation/direct detection (IM/DD) systems in VLC have attracted significant attention [1]. Several OFDM based modulation in case of VLC are presented in various papers. Like pixelated systems, DCO-OFDM and ACO-OFDM are also investigated in case of VLC [2-3]. ADO-OFDM

[67,77] is another modulation technique that performs better than ACO-OFDM and DCO-OFDM under some conditions. In ADO-OFDM the odd subcarriers are clipped at zero level and a DC bias is added with the even subcarriers after Hermitian symmetry. In the receiver side, estimator is used to estimate the even subcarriers and finally using FFT and demodulation data can be recovered. ADO-OFDM [77] is more optical power efficient than ACO-OFDM and DCO-OFDM for a bit rate/normalized bandwidth of 4, 5 and 6. ADO-OFDM needs 3.68 dB lower optical power to achieve same SNR of 1024-QAM ACO-OFDM. Similarly, for a constellation size 64, DCO-OFDM needs 1.9 dB more optical power than ADO-OFDM with a 8.99 dB DC bias level.

The power efficient and high performance providing scheme is NDC-OFDM presented in literature [64]. Research shows that NDC-OFDM is better than unipolar OFDM method while comparing different constellations. It needs 5dB less power than DCO-OFDM to achieve same spectral efficiency for constellation size 8, 32 and 128. This scheme does not require the addition of DC bias to make non negative value to positive. According to this scheme, the input bit stream is transformed into complex symbols by an M-QAM modulator. Hermitian symmetry is imposed to convert complex symbol into real without changing the original information. But still the OFDM symbols are bipolar which are not fit for IM/DD system. The trick of NDC-OFDM is it allows LEDs only to send the absolute value of symbol and the polarity of the symbol are encoded by the index of the corresponding LED like LIM-OFDM. As a result, only one LED is activated during one symbol time. The first LED will be activated to send the symbol if the transmitted symbol is positive. Otherwise, second LED will send information. NDC-OFDM is free from any DC voltage addition in OFDM symbols due to this principle.

Generalized LIM-OFDM which is a novel 4×4 *multiple input multiple output* (MIMO) transmission-based technique is also drawing attention as this scheme requires no Hermitian symmetry and DC bias to operate over frequency flat VLC channels [65]. According to this scheme, after modulation the real and imaginary parts of the complex time-domain OFDM signals are separated into their real and imaginary parts. Then based on active LED indices index modulation is performed and these signals are transmitted over the MIMO-VLC channel. The polarity information of the complex signals is encoded to the location of transmitting LEDs and these way higher spectral and power efficiencies are achieved. To estimate those real and imaginary parts of the OFDM signals a novel conditional maximum a probability estimator is

employed at the receiver. Modifying the generalized LIM-OFDM structure a novel 4×4 MIMO transmission-based technique called enhanced generalized LIM-OFDM is also drawing attention as in this method the real and imaginary parts of the complex time-domain OFDM signals are not estimated directly rather it follows a feasible way for the time frequency domain transformations[65]. Three conditions are considered in that research just varying the distance and alignment between transmitting and receiving device and the proposed scheme is adopted for the frequency selective VLC channels. This research claims that LIM-OFDM schemes have superior bit error ratio (BER) performances as compared with the reference optical MIMO transmission systems. The proposed method shows better power efficiency than NDC-OFDM, DCO-OFDM and ACO-OFDM for analytical channel for different constellation size (4,8,16) and spectral efficiency (2,3,4 bits/s/Hz). But among three physical channels, NDC-OFDM performs better in one and for the rest two, LIM-OFDM performs better with same constellation size and spectral efficiency considered for analytical channel.

2.2.3 Impairments in Pixelated Communication

For a pixelated system, various research works are done considering impairments to find out the best modulation schemes. It is shown that using CP and appropriate equalization technique spatial misalignment between transmitter and receiver can be mitigated [47]. In the presence of impairments like linear misalignment, defocus and vignetting degrade the performance of pixelated wireless system. Defocus blur is initiated because of out of focus receiver from the transmitter in a pixelated system. The received constellation points are to be attenuated because of defocus blur explained firmly in [48]. It is observed from MATLAB simulation that due to defocus blur SACO-OFDM exhibits less attenuation than SDCO-OFDM. Research work [49] also consider another major impairment that is the linear misalignment problem between the transmitter and receiver. Attenuation resulting from phase shift in constellation points is the effect of the LFM. If the fractional offset is half of the pixel the impact is even higher. Another research work [50] shows that the gradual fall-off in illumination at the edges of an image known as vignetting, has considerable impact on pixelated spatial OFDM system. Because of vignetting ICI is generated in frequency domain and attenuation arises which is agreed by both the theoretical and simulation analysis. For mitigation of the impairment, two methods are discussed. First method is, to reduce BER floor in SDCO system, the heavily affected higher subcarriers

must be kept null. The second method is, estimating the effect of vignetting and equalizing accordingly in receiver section. It is shown that, 4 QAM SDCO-OFDM exhibits less optical power efficiency than equalized 16 QAM SACO-OFDM. Another research work [51] investigated theoretically the joint effect of LFM, defocus, and vignetting. According to the analysis, as the impact of impairments are independent of each other, the joint effect of these impairments can be overcome by joining the techniques that are used to diminish these impairments individually. NCS-OFDM more power efficiency compared to SACO-OFDM and SDCO-OFDM in the presence of impairments like motion blur, defocus blur and spatial sampling frequency offset (SSFO). The research work based on theoretical model does not consider the effect of motion blur which is a prime impairment of pixelated communication system having tremendous effect on received image. It is yet to be analyzed.

Visual MIMO is communication using LED panel and the CMOS technology in OWC which increases the ranges from ten to hundred meters. Some challenges of visual MIMO and solutions are provided by one research work [84]. Characteristics of display appearance, detection of electronic display and recovering the signal from display are the main challenges of visual MIMO and to solve these problems image processing algorithms are suggested. Four operating modes for visual MIMO transmitter are defined in [85] just to mitigate the channel distortions like- lens blur ,visibility and perspective distortions. The constraints of implementing visual MIMO are considered in [86]. The message signal embedding at the display is a complex task as the message should be indistinguishable to the observer so that the original purpose of showing video or image is unrestricted. The geometric distortions of received images are the other constraints of visual MIMO. A real time message extraction algorithm with bitrate of 6222.2 bps and 94.6% of accuracy is presented in this paper. Due to mismatched frame rates and phase offset between transmitter and receiver, the problem of synchronization between screen camera link is originated and to resolve this problem rate less coding is introduced in [87]. The reason behind these unsynchronized frames depends on various conditions like camera capability, lighting conditions and system factors. For proper reception, the frame rate of transmitter should not be higher than half of the frame rate of receiver. Smartphone based pixelated communication is presented in [88]. Transmitting smartphone display the data carrying images and through camera the receiving smartphone captured the series of images. For detection of images at the receiver side with success rate up to 93%. Speeded Up Robust Features (SURF) scheme is used. Similar

type of work is also presented in [29]. Due to misplacement of transmitter and receiver, trapezoidal effect is found in received image and to recover this problem, projective transformation is implemented. To reduce ISI created from user mobility, a novel quantization process is also introduced in that paper. For short range using smartphones, the proposed system achieves 98% of success rate when a number of experiments are done considering various position displacement conditions. In screen to camera communication, the effect of angle and distance is modeled in [93] and it is shown that if preprocessing can be performed before displaying the image (which will be transmitted) then high throughput can be achieved in receiver section after decoding. It is shown that, 1kbps to more than 250kbps throughput can be achieved even the receiving camera angle is varied to 10 degree to 80 degree, respectively. Moreover, throughput will vary 275kbps to 10 kbps approximately if distance of transmitting screen and receiving camera is varied 40 cm to 225 cm, respectively.

2.2.4 Motion Blur

Previous section shows that, research works based on both theoretical model and experimental work do not take into account the prime impairment of pixelated systems termed as motion blur. As this thesis is concern about developing theoretical model of the effect of motion blur in context of pixelated communication system, it is necessary to explore about motion blur from previous research works.

During the camera exposure period, if the LCD screen of transmitter or the camera of receiver moves motion blur occurs. For the duration of the exposure time, the transmitted image frame moves to different area of the camera sensor photosensitive surface in case of motion blur [79]. Larger camera movements can make the whole image unintelligible though small movements soften the image and diminish the details [80]. When the exposure time is not so long, neither the transmitter screen nor the receiver camera movements are likely to become visible in the image. Image acquisition manner determines either this phenomena will occur or not. To collect enough photons to the sensor pixels in low light conditions, long exposure times are required. An automatic exposure algorithm can provide the decision of required exposure time. In [81], such kind of algorithm is proposed. Another research [80] shows the process of motion blur inspection along with the explanation of all types of motion blur. This research also propose a three-dimensional model which allows the camera to move around three different axes. Motion blur

can be linear (horizontal or vertical) as well as angular too. In [82], the exposure time is taken less than 0.125 seconds and linear motion blur is shown as this research considered only the linear motion of receiving camera. By using Wiener filtration, it is possible to correct the blur if the PSF is known, or it is possible to estimate [83].

The effect of motion blur can be understood by PSF of it. All the kernel values of PSF of motion blur are not same. The number of nonzero values of PSF components depends on motion length and direction. The values of nonzero term of PSF of motion blur are same [69,78]. In [69], motion blur is considered only for vertical and horizontal direction and simulation is carried out to find the best candidate of OFDM based modulation taking into account the motion blur. Most of the researches done on motion blur are in image processing context to detect motion blur and to estimate length and angle of motion blur and also for restoring blur-less image. In framework of a pixelated system, only simulation is done in account of motion blur but mathematical model is not developed yet to understand the effect of motion blur in received pixelated image frame and the impact of it on communication. The mathematical model is developed in next chapter to understand the impact both in spatial domain and spatial frequency domain.

2.3 Conclusion

From previous research works, the pixelated communication system based on different spatial OFDM modulations is discussed in this chapter. Besides that, the findings of experimental works are also mentioned. Some new OFDM based modulation techniques which show better results in VLC are also addressed in this chapter. From discussion of impairments related works it is clear that there is no work done which can explain the effect of motion blur mathematically and experimentally in context of pixelated communication.

CHAPTER THREE

SPATIAL OFDM BASED PIXELATED SYSTEMS

3.1 Overview

Using spatial OFDM data are transmitted in parallel by a series of time varying images in a pixelated system. Generally, VLC uses conventional OFDM whereas spatial OFDM is used in pixelated systems as a pixelated system has to encode data in 2D space domain. Spatial OFDM is nothing but the two dimensional spatial domain extension of conventional OFDM. To overcome the spatial distortions in a pixelated system, data are encoded in spatial frequency domain as subcarriers of spatial OFDM are in the spatial frequency domain. Earlier researches proposed three forms of spatial-OFDM scheme known as SDCO-OFDM, SACO-OFDM and SADO-OFDM as these methods are capable to produce real non negative value which is prime condition of a pixelated system. These methods are presented in this chapter.

Pixelated system and spatial OFDM are discussed in detailed in this chapter. A pixelated system is discussed along with transmitter, receiver and optical channel in **Section 3.2**. Before illustrating SDCO-OFDM, SACO-OFDM and SADO-OFDM, **Section 3.3** provides clear idea about the theory of spatial domain and spatial OFDM. Lastly, **Section 3.4** is for conclusion.

3.2 Pixelated System

For a high spectral efficiency gain pixelated system, which is a subsection of optical wireless communication has drawn significant attention recently [43-46,52,53,55, 57-59,66,70]. The pixelated system is based on very simple working principle. By implementing IM/DD, scheme an array of optical transmitter is used to convert electrical signal which carries information to sequence of encoded image frames varied with time. The time varying image frames are then received by an array of imaging receiver for detection. Before transmission data are organized and encoded in two dimensional space recognized as spatial domain. With comparison to single element systems, spatial domain provides high *signal to noise ratio* (SNR) with immense gain in spectral efficiency for short range optical wireless communications. In the electrical domain

spatial OFDM is used as modulation technique and it will be discussed in the coming sections of this chapter. Generally optical emitters can be an LCD or an LED panel with millions of pixels. One main advantage of these type of emitter is handheld devices and consumer products like cell phones, *personal digital assistant* (PDA) etc. have these type of emitters with various specifications and low cost[58, 59]. For short range high speed secure communication these devices are used for this prime advantage. Photo detector array produces an output electrical signal with the help of imaging lens from data carrying image frames in the receiver side. Some examples of imaging receivers are *complementary metal-oxide semiconductor* (CMOS) imagers and *Charge coupled device* (CCD) cameras.

Point to point or quasi diffuse links are two forms of pixelated systems. For point to point pixelated OWC, the transmitter should be placed in the FOV of the receiver, and *line of side* (LOS) should be maintained between the transmitter and the receiver for better communication [12]. Fig. 3.1 shows such an example. The condition of LOS is not mandatory for quasi diffuse links, as images are projected on the ceiling or walls of a room by transmitter and images are collected from the ceiling or walls [12, 51, 70] through receiver.

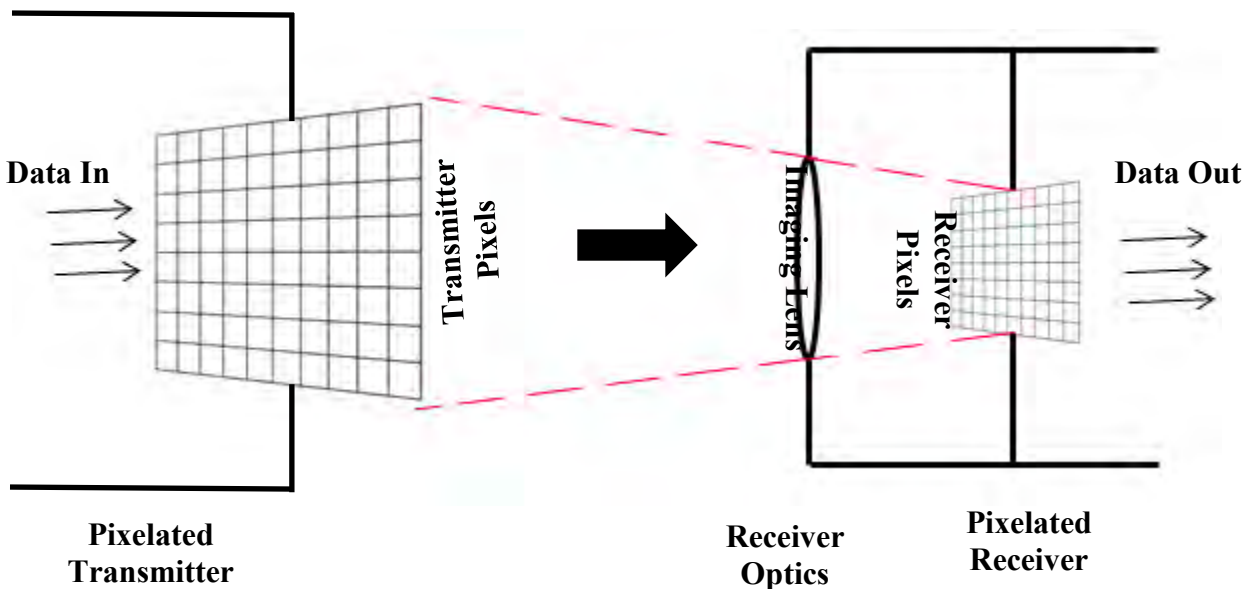


Fig. 3.1: A point to point pixelated system [43]

3.2.1 A Generalized Pixelated System

This section describes a generalized pixelated system. Fig. 3.2 and Fig. 3.3 show the schematic and block diagram of such a system, respectively. After encoding, the data are converted into 2D image frames shown in Fig. 3.2. In the following subsections, the transmitter, the receiver and the channel conditions of pixelated systems are discussed.

3.2.1.1 Transmitter

The combination of an electrical modulator and an optical modulator consist the transmitter part of a pixelated system. Electrical modulator modulates the entering electrical signal carrying information and generates a unipolar signal shown in Fig. 3.3. Techniques like On-Off Keying (OOK) or OFDM is used as electrical modulation. Next, an intensity modulator received that modulated electrical signal to form image frames. Smallest unit of the pixelated grids are known as transmitter pixels. The pixel intensity is determined by the optical modulator according to the values of the input signal [43]. No information is lost during electrical to optical conversion as only positive signals are provided at the input of optical modulator. Some examples of intensity modulator used in a pixelated system are pixelated grids of LED, plasma screens and LCD screens or panels.

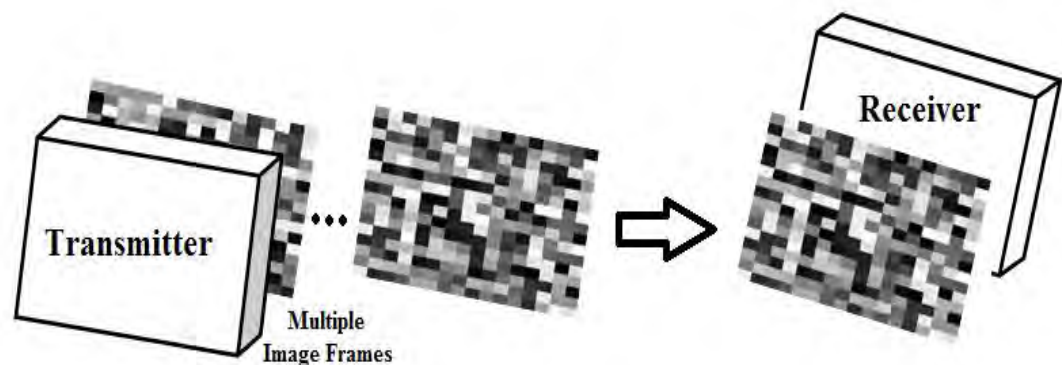


Fig. 3.2: Schematic of a pixelated OWC system[69]

Mapping of an OOK signal into pixel values using intensity modulation is shown in Fig. 3.4. Value 0 corresponds to black or dark pixel representing absence of light signal whereas value 1 is responsible for bright or white pixel representing the existence of light. The number of pixelated frames, number of pixels per frame and number of bits per pixels determines the total transmission rate in a pixelated system. The total transmission rate can be achieved using multiplication of these three terms. After optical modulation light signal is found which are transmitted to optical channel represents the intensities of the data carrying images. For simplicity the electrical to optical conversion efficiency is considered unity in this thesis.

3.2.1.2 Optical Channel

Intensity modulated direct detection channel is known as optical channel for a pixelated system. All types of data cannot be sent in this optical channel which is the prime constraint of this channel. For entire duration of transmission the information bearing optical intensities must remain non-negative. The signal may be corrupted by deterministic and random distortions during transmission. To develop signaling techniques for reliable transmission of signal with high data rate through this noisy and impaired channel is the main concern.

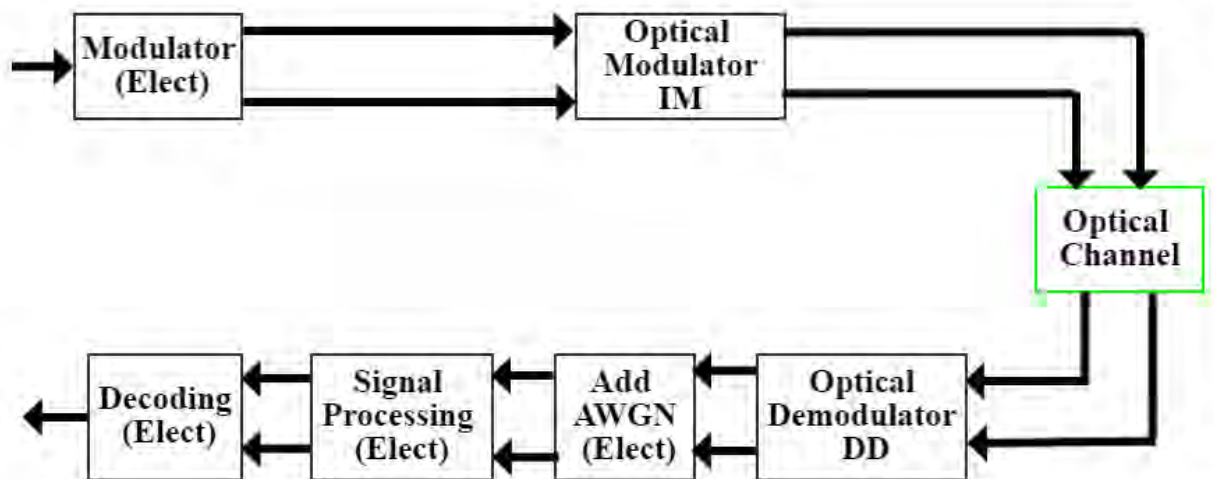


Fig. 3.3: Block diagram of a pixelated OWC system

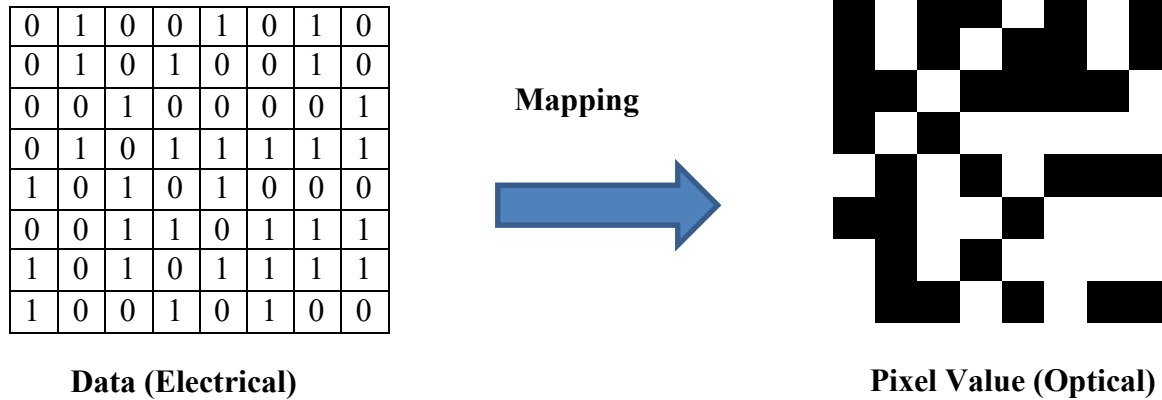


Fig. 3.4: Mapping of information to pixel values for 8×8 data set

A well-known problem in OWC is multipath propagation which causes temporal distortion. Though, the reason of lower channel delay spread and longer frame duration is the low frame rates resulting negligible temporal distortion in a pixelated system [43, 44, 58].

Receiver electronics leads to thermal noise [66] and ambient light leads to shot noise [44, 56, 66]. AWGN [9, 71] is modeled considering the shot noise and thermal noise for pixelated link in this thesis.

3.2.1.3 Receiver

Some well-known receivers used in direct detection is CCD cameras, CMOS imagers. The photo detector and an imaging lens constitute the receiver. Images on an array of receiver pixels is reproduced by photo detector pixels whereas imaging lens concentrates the incoming light to the photo detector. The photo detector converts the optical signals to electrical signals. The receiver pixel is nothing but the individual photodiode from a photodiode array or the individual pixel of the CCD/CMOS cameras. The transmitted images must be aggregated on the FOV of the receiver. It is compulsory to maintain the temporal synchronization between transmitter and receiver. Signal processing techniques are applied just after the receiver sampled the transmitted images in spatial domain. The encoded messages are determined from the received message with

the help of corner detection of received image. Then boundary of the image portion which is carrying information is extracted, decoded and recovered.

The convolution of transmitted pixel intensity and the *point spread function* (PSF) determined the intensity of the received pixels q_{l_1, l_2} as follow

$$q_{l_1, l_2} = p_{l_1, l_2} * h_{l_1, l_2} \quad (3.1)$$

Here, h_{l_1, l_2} is the PSF and p_{l_1, l_2} is the transmitted pixels. The channel gain and magnification parameter has been considered unity. Two dimensional linear convolution is presented by * sign.

The electrical signal y_{l_1, l_2} can be written as

$$y_{l_1, l_2} = q_{l_1, l_2} + z_{l_1, l_2} \quad (3.2)$$

$$\text{So, } y_{l_1, l_2} = (p_{l_1, l_2} * h_{l_1, l_2}) + z_{l_1, l_2} \quad (3.3)$$

$$\text{As, } p_{l_1, l_2} = s_{l_1, l_2} \quad (3.4)$$

$$y_{l_1, l_2} = (s_{l_1, l_2} * h_{l_1, l_2}) + z_{l_1, l_2} \quad (3.5)$$

Here, s_{l_1, l_2} and z_{l_1, l_2} represents the AWGN and transmitted electrical signal respectively. The responsivity of the photo detecting element has been considered unity in this thesis.

3.3 Spatial OFDM for Pixelated Systems

OFDM modulation scheme provide robustness against the temporal distortion in OWC. Unlike spatial distortion, temporal distortion can be disregarded in pixelated OWC system, as its effect is acceptable whereas spatial distortion affects severely on the system performance. By encoding data in spatial frequency domain, Spatial OFDM can overcome some of the spatial distortion.

3.3.1 Spatial Domain and Spatial Frequency Domain

The concept of spatial domain and spatial frequency domain is necessary to understand spatial OFDM. It is an important topic and has applications in signal processing and specifically in image processing [72-74]. As the information is encoded in 2D image space, the concept is also necessary for a pixelated system.

The spatial domain is nothing but the normal image space. 2D spatial domain means 2D image space. Any change in pixels of an image or change in position in the image space or directly projects change in real space. For representing the distance the number of pixels presented in an image is equivalent to the real distance. To represent the intensity variations with respect to pixels of an image this concept is used primarily.

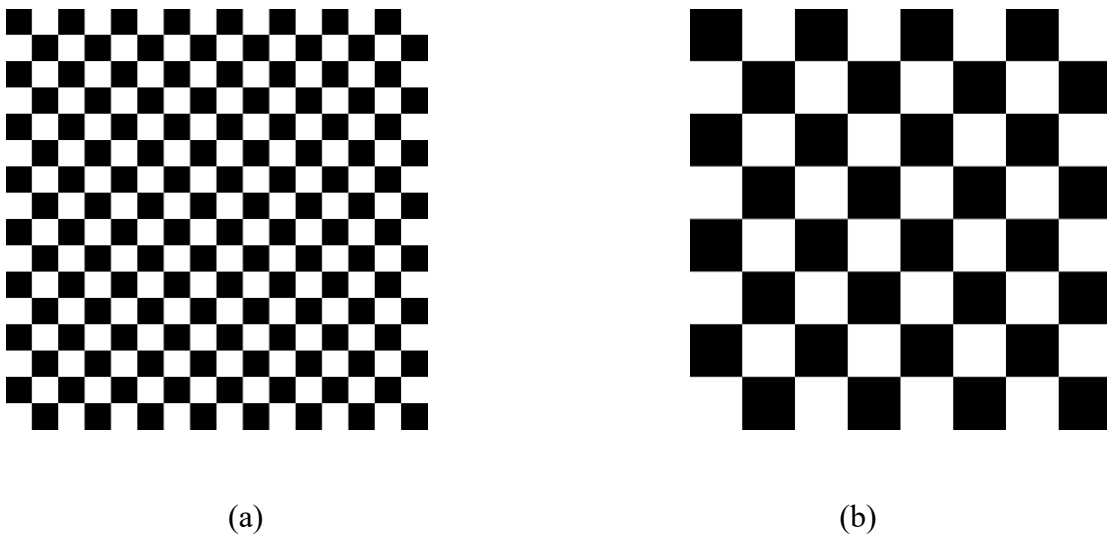


Fig. 3.5: (a) higher spatial frequency, (b) lower spatial frequency

Frequency representation of image space is known as spatial frequency. Spatial frequency refers the frequency equivalence of spatial domain. Moreover, over short image distances the periodicity of changing the intensity of pixels is actually represented by spatial frequency. With the change of real scene the pixel values of an image change. The rate by which the pixel values of an image changes in spatial domain is represented by spatial frequency domain whereas the

image is considered as it is in spatial domain. Rapid changes in intensity over short image distances make spatial frequency higher. Lower spatial frequency corresponds to slow changes and fast changes in pixel values over short image distance leads higher spatial frequency. The higher spatial frequency and lower spatial frequency depicted in Fig. 3.5 (a) and (b). High intensities and low intensities are represented as white and black square boxes respectively.

To convert the signal from spatial domain to spatial frequency domain in pixelated communication, a 2D Fourier transform is performed which is shown in equation (3.6).

$$X_{k_1, k_2} = \frac{1}{N_1 N_2} \sum_{l_1=0}^{N_1-1} \sum_{l_2=0}^{N_2-1} x_{l_1, l_2} \exp \left\{ \frac{-j2\pi k_1 l_1}{N_1} + \frac{-j2\pi k_2 l_2}{N_2} \right\} \quad (3.6)$$

3.3.2 OFDM and Spatial OFDM

In the previous chapter it has been mentioned that, OFDM provides robustness against temporal distortions resulting from dispersive optical channels for OWC system. For IM/DD system, with compared to other modulation schemes like OOK or PPM, OFDM provides better optical power efficiency. Spatial modulation is performed in a pixelated system for the reason of the features such as no requirement of synchronization between transmitter and receiver, and to avoid correlation between them while maintaining high spectral efficiency and avoiding ICI at the receiver input.

Over one symbol period data are transmitted by a number of mutually orthogonal subcarriers in OFDM. Due to this orthogonality closely spaced subcarriers do not create any interference so high transmission rate is achieved. Furthermore, at the receiver inclusion of *cyclic prefix* (CP) and longer duration provides simplified equalization [75, 76]. As OFDM creates bipolar signal it is mandatory to ensure unipolarity of the transmitted data for OWC.

Fig. 3.6 depicts a generalized block diagram of spatial OFDM system. Unlike conventional OFDM, serial to parallel conversion of data is not required in spatial OFDM. Fig. 3.7 shows that spatial OFDM frames are 2D array formed from mapping data. Based on the constellation used the information is mapped as complex numbers. Fig. 3.7 also indicates that to modulate a pixelated frame these spatial OFDM frames are used. To remove the negative values from the frame the spatial OFDM frame is passed through bipolar to unipolar conversion techniques before the modulation. The method of bipolar to unipolar conversion is different for SDCO-OFDM, SACO-OFDM and SADO-OFDM.

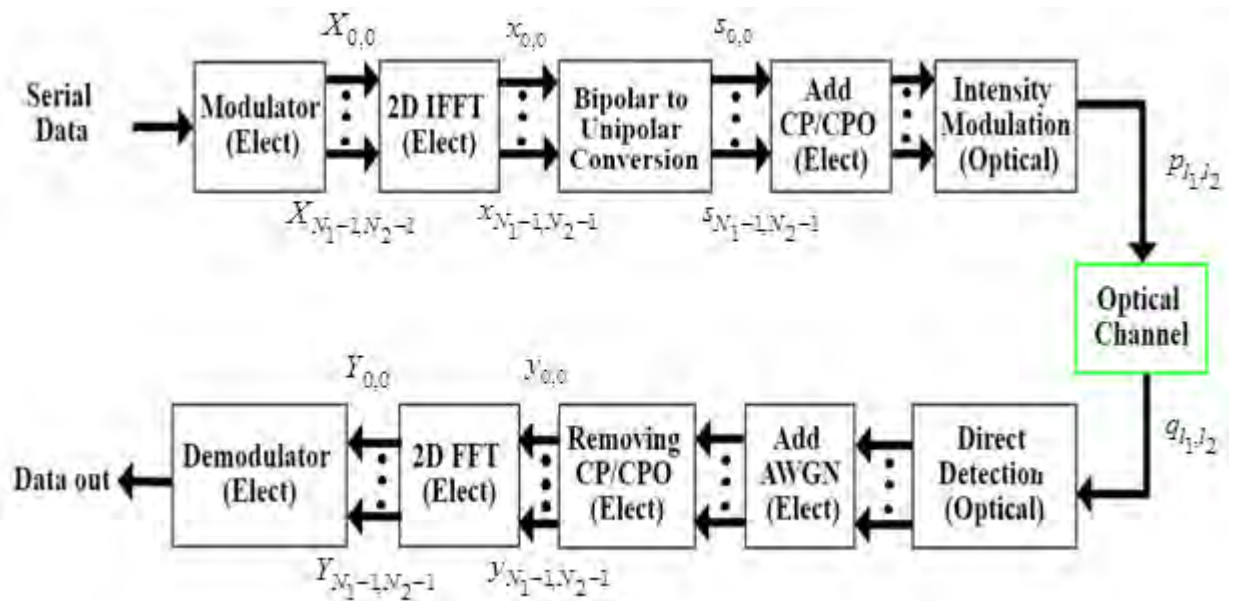


Fig. 3.6: Block diagram of a spatial OFDM system[51]

By using optical modulators data are mapped to the pixelated image frames, once the polarity conversion is completed. Through spatial frequency selective optical channels the pixelated image frame is transmitted. Data are mapped in number of bits for each pixel and several groups of pixels constitute an image frame. Consequently, by multiplying the number of pixels per frame with the number of bits per pixel can provide the total number of data which can be send by an image frame. If multiple numbers of frames are transmitted at the same time instead of transmitting single image frame the transmission rate will be much higher. To extract the original information the exact opposite of the transmitter side happens at the receiver.

0	0.38	0.68	0.89	0.11	0.88
0.91	0.31	0.45	0	1	0.67
0.7	0.83	0.33	0.19	0.45	0.77
0	0.31	0.45	0.55	1	0.37
0.33	0.88	0.22	1	0.81	0
0.91	0.41	0.75	0.77	0.88	0.67

Spatial OFDM Frame

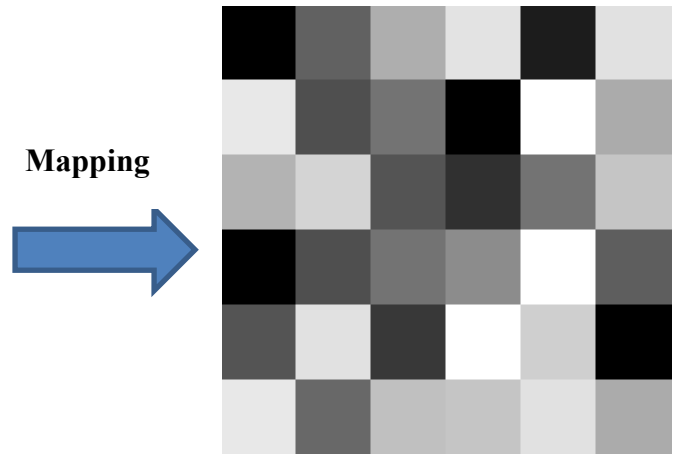


Fig. 3.7: Mapping of spatial OFDM frame to pixelated image frame

Before the mapping of electrical data to the optical images, the addition of *cyclic prefix* (CP) and *cyclic postfix* (CPo) to the spatial frame is an important feature of spatial OFDM. To combat ISI, the last part of the symbol is copied to the front of the OFDM symbol as CP in conventional OFDM. When spatial OFDM is considered, cyclic extension is attached to the edges of the transmitted frame. The right few columns of the frame are copied to the most left and left few columns are copied to the most right of the frame. Similarly first few rows are copied and attached at the bottom of the frame and last few rows are copied and attached at the top of the frame. CP is the attached extra rows at the bottom and columns at the left whereas CPo is the attached extra rows at the top and columns at the right. Fig. 3.8 presents the CP and CPo. Single tap equalization at the receiver is possible for this extension.

The received signal:
$$Y_{k_1, k_2} = S_{k_1, k_2} H_{k_1, k_2} + Z_{k_1, k_2} \quad (3.7)$$

Here, S_{k_1, k_2} , H_{k_1, k_2} and Z_{k_1, k_2} are the transmitted signal, the PSF and the AWGN in spatial frequency domain respectively.

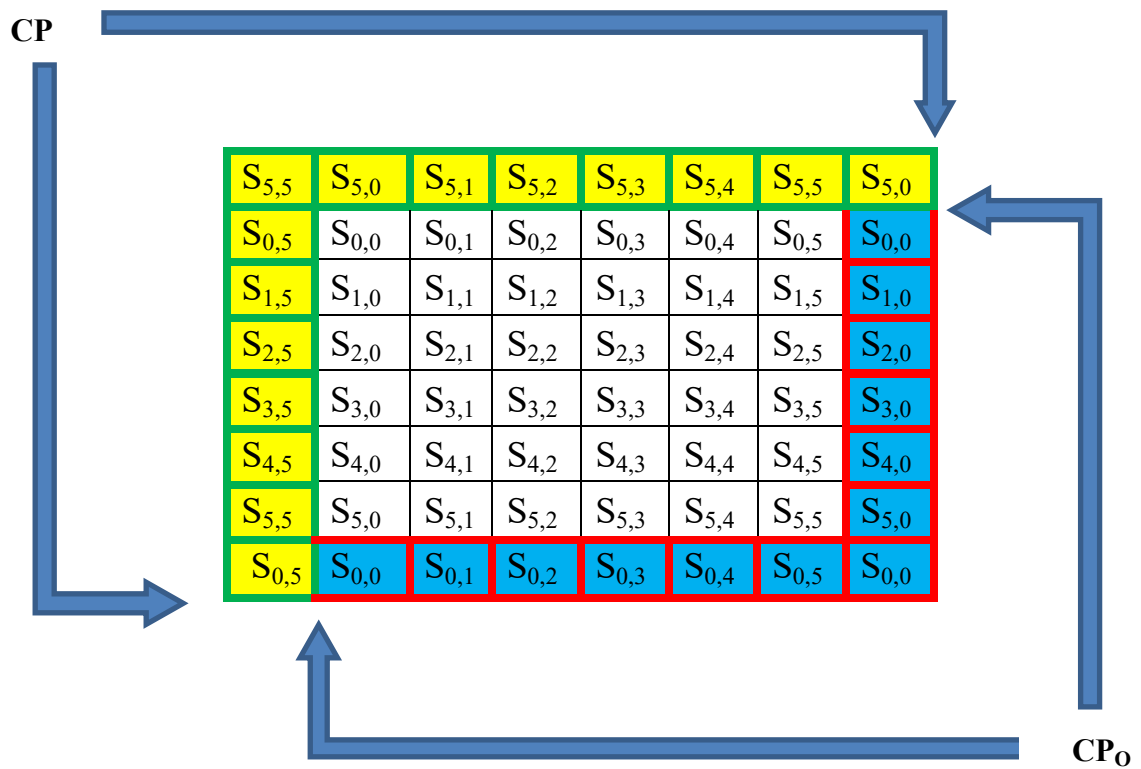


Fig. 3.8: Addition of cyclic prefix (CP) and cyclic postfix (CPo)

3.3.3 Unipolar Optical OFDM system

Three basic unipolar optical OFDM systems are SDCO-OFDM, SACO-OFDM and SADO-OFDM. These are unipolar optical OFDM systems because these systems have their own way of converting bipolar signal to unipolar. These systems are described in this section.

2.3.3.1 SDCO-OFDM system

SDCO-OFDM [43, 51] uses a DC bias to generate unipolar signal from bipolar OFDM. The block diagram of SDCO-OFDM is shown in Fig. 3.9.

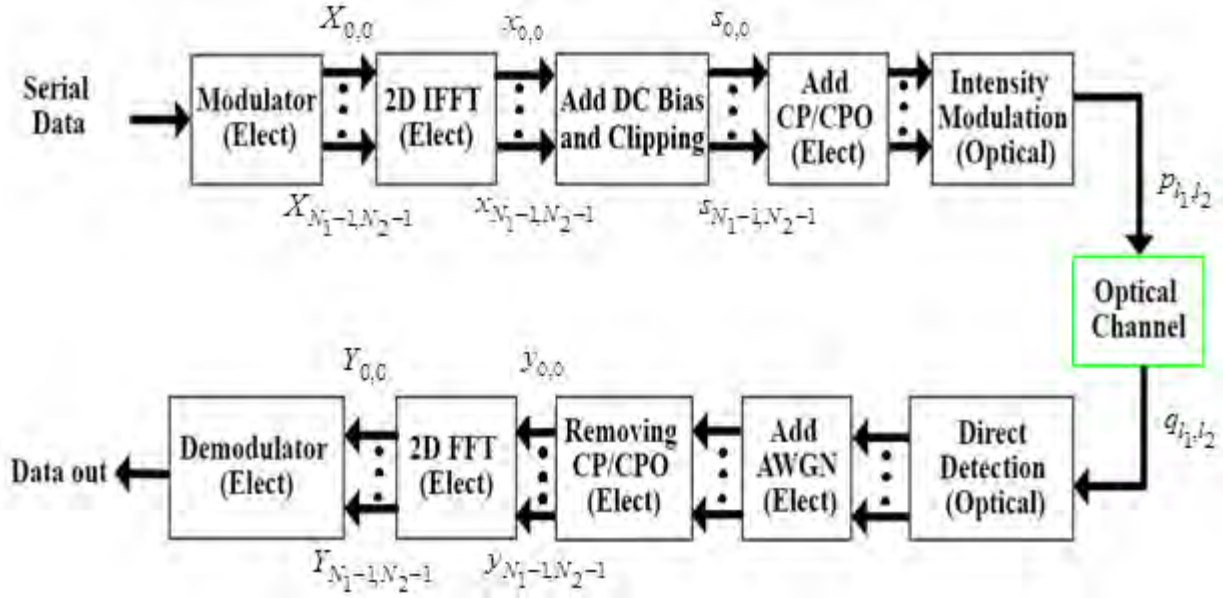


Fig. 3.9: Block diagram of an SDCO-OFDM based pixelated system [51]

Block diagram clearly indicates that data are first modulated using any digital modulation technique of specific any like 4 or 16 array *quadrature amplitude modulation* (QAM). and after modulation spatial frequency domain signal x is found which has $N_1 \times N_2$ elements. The number of elements of x depends on the constellation size of the modulation.

As optical signal can't represent complex number, Hermitian symmetry is applied on x to make it real valued. Assumed that both N_1 and N_2 are even integers Hermitian symmetry is applied on x .

$$X_{k_1, k_2} = X_{N_1 - k_1, N_2 - k_2}^* \quad (3.8)$$

The complex conjugate operator is represented by „*“ sign. Later, a bipolar 2D spatial domain signal x_{i_1, i_2} is found by performing 2D *inverse fast Fourier transform* (IFFT) operation on X_{k_1, k_2} .

After that a DC bias is added to the spatial domain signal x_{l_1, l_2} to make it unipolar so that it can be easily converted to light in IM/DD system. Due to the characteristics of Gaussian distribution of the bipolar signal, large DC bias is also incapable to remove all negative components. Therefore clipping the negative components is treated as solution of this problem. But, Due to clipping an unwanted noise is introduced which is known as clipping noise. High level of DC bias can eradicate this noise at a cost of using high level of power. In contrast, a Low power usage cannot remove clipping noise. To mitigate this problem an optimum DC bias should be chosen so that minimum power usage can remove clipping noise at great extent.

DC bias can be expressed as:

$$b_{DC} = \mu\sigma_x \quad (3.9)$$

Where, σ_x is the standard deviation of x_{l_1, l_2} and μ is the proportionality constant. s_{l_1, l_2} is the DC biased signal can be expressed as:

$$s_{l_1, l_2} = x_{l_1, l_2} + b_{DC} \quad (3.10)$$

To remove the remaining negative components s_{l_1, l_2} is further clipped at the zero amplitude level. Next, CP and CPo is appended before fed the signal into intensity modulator block. Finally, intensity modulator converts electrical signal s_{l_1, l_2} to pixel intensity p_{l_1, l_2} and send it through optical channel. By using direct detection block the received pixels intensity q_{l_1, l_2} are converted back to an electrical signal and then the CP and CPo are removed in the receiver. The received signal q_{l_1, l_2} and the AWGN noise z_{l_1, l_2} determine the value of resultant electrical signal y_{l_1, l_2} . To demodulate and to recover the data, a 2D *fast Fourier transform* (FFT) is performed on y_{l_1, l_2} to generate a spatial frequency domain signal Y_{k_1, k_2} .

3.3.3.2 SACO-OFDM system

Unlike SDCO-OFDM, in SACO-OFDM all subcarriers are not used to map data and there is no requirement of DC bias addition to remove negative components. In this case, odd and even subcarriers mean the odd index columns and the even index columns of x , respectively [47, 69]. There is no requirement of DC bias addition here because only using odd subcarriers in data mapping ensures no clipping noise and information loss in negative section clipping. SACO-OFDM and SDCO-OFDM followed the same method to convert complex modulated data into real valued data and that is done with the help of Hermitian symmetry. As a result, x_{l_1, l_2} is generated from 2D-IFFT of the real valued bipolar signal x . Then, unipolar signal s_{l_1, l_2} is produced by asymmetrical clipping of the negative region of x_{l_1, l_2} .

$$s_{l_1, l_2} = \begin{cases} 0, & \text{if } x_{l_1, l_2} < 0 \\ x_{l_1, l_2}, & \text{if } x_{l_1, l_2} \geq 0 \end{cases} \quad (3.11)$$

Before feeding the resultant signal s_{l_1, l_2} to intensity modulator to produce light intensity P_{l_1, l_2} a CP and a CPo is added. Like SDCO-OFDM, in receiver SACO-OFDM perform the inverse operation of transmitter and there demodulation and decoding is applicable only for odd subcarriers as even subcarriers are set to zero in transmitter.

3.3.3.2 SADO-OFDM System

SADO-OFDM is the spatial domain version of ADO-OFDM [67,77] is a method where the concepts of both SDCO-OFDM and SACO-OFDM are used. Like SDCO-OFDM and SACO-OFDM, the electrical signal is modulated first using M-ary modulation where M determines the constellation size and the number of the element of complex modulated signal x . After that Hermitian symmetry is applied on x to ensure that all values of x are real number using equation (2.11). Now, according to the index number x is divided into odd and even components termed as X_{odd} and X_{even} respectively.

After applying of 2D IFFT on X_{odd} and X_{even} , x_{odd} and x_{even} is generated respectively. Like SACO-OFDM, asymmetric clipping is done with x_{odd} to make it unipolar.

$$s_{odd} = \begin{cases} 0, & \text{if } x_{odd} < 0 \\ x_{odd}, & \text{if } x_{odd} \geq 0 \end{cases} \quad (3.12)$$

On the other hand, an optimum DC bias according to equation (2.11) is added to X_{even} to remove the negative portion of that signal.

The DC biased even index signal is:

$$s_{SDCO} = x_{even} + b_{DC} \quad (3.13)$$

Further clipping is applied on s_{SDCO} to remove the remaining negative portion of the signal.

Next, s_{odd} and s_{even} constitute the resultant signal.

$$s_{even} = \begin{cases} 0, & \text{if } s_{SDCO} < 0 \\ s_{SDCO}, & \text{if } s_{SDCO} \geq 0 \end{cases} \quad (3.14)$$

$$s_{SADO} = s_{odd} + s_{even} \quad (3.15)$$

Finally, CP and CPo are added and intensity modulator emits light intensity p_{l_1, l_2} from CP and CPo added s_{SADO} .

In receiver, y_{SADO} is found after direct detection of q_{l_1, l_2} . y_{SADO} is dependent on received pixel intensity q_{l_1, l_2} and AWGN z_{l_1, l_2} . Then, Y_{SADO} is generated by removing CP, CPo and performing 2D FFT of y_{SADO} . After equalization of Y_{SADO} , all odd subcarriers termed Y_{odd} are separated.

Y_{even} is recovered in different way as the even subcarriers are not treated like odd subcarriers in SADO-OFDM.

Again 2D FFT is performed on Y_{SADO} to produce y_{SADO} and estimator is used to estimate the interfering SACO-OFDM signal y_{SACO} . Next, y_{even} is found by subtracting the combined signal y_{SADO} and the estimated signal y_{SACO} . Lastly, Y_{even} is recovered by applying 2D IFFT to y_{even} .

$$y_{even} = y_{SADO} - y_{SACO}(Estimated) \quad (3.16)$$

To generate and demodulate Y , Y_{odd} and Y_{even} must be combined.

$$Y = Y_{odd} + Y_{even} \quad (3.17)$$

3.4 Conclusion

Pixelated systems are discussed in detail in this chapter. This chapter also illustrates the difference between spatial domain and spatial frequency domain. The necessity of spatial OFDM and the relation between conventional OFDM with spatial OFDM is also discussed. Three general methods named SDCO-OFDM, SACO-OFDM and SADO-OFDM are described here for better understanding of unipolar spatial optical OFDM methods.

CHAPTER FOUR

MATHEMATICAL MODEL

4.1 Introduction

A number of issues are responsible for degrading the performance of pixelated communication system which are known as channel impairments. The major constraints of pixelated communication system are spatial impairments, for which the performance of the communication degrade drastically. The major spatial impairments are: motion blur, defocus blur, LFM, vignetting and channel noise.

The most prominent spatial impairment is motion blur. When transmitting device is not static or receiving device is movable then motion blur affects the communication performance. If anyone or both between LCD screen of transmitting device or camera of receiving device are movable then the camera of receiving device captures blurred images due to motion blur. As the images of pixelated communication system carry data due to motion blur, huge data cannot be estimated correctly in receiver section. Defocus blur is common in practical pixelated communication system. If the distance between transmitting device and receiving device is not fixed then defocus blur is occurred as receiving device is out of focus.

Another major impairment is LFM. Practically perfect alignment between transmitting device's screen and receiving device's camera is not possible which results in misalignment of received images. Due to misalignment, some portion of images is not captured by receiving device's camera causing high bit error rate (BER). Vignetting is gradual fall-off illumination from the center to corner of the received images. This is also a cause of incorrect data recovery.

This chapter shows the effect of linear and angular motion blur in **Section 4.2**. The joint effect of defocus and motion blur is derived mathematically in **Section 4.3**. In **Section 4.4**, the effect of all spatial impairments like motion blur, defocus blur, LFM, vignetting and channel noise are

modeled to understand the practical worst scenario when all impairments are present. Finally, **Section 4.5** summarizes the findings of the chapter.

4.2 Modelling the Effect of Motion Blur

To understand the effect of motion blur, first it is necessary to explore the PSF of motion blur. From [78], the PSF of motion blur is expressed as:

$$h_{u,v} = \begin{cases} \frac{1}{C}, & \text{if } \sqrt{u^2+v^2} \leq \frac{C}{2} \text{ and } \frac{u}{v} = -\tan \theta \\ 0, & \text{otherwise} \end{cases} \quad (4.1)$$

Where, C is the motion length and θ is the motion angle.

$h_{-1,-1}$	$h_{-1,0}$	$h_{-1,1}$
$h_{0,-1}$	$h_{0,0}$	$h_{0,1}$
$h_{1,-1}$	$h_{1,0}$	$h_{1,1}$

Fig. 4.1: PSF for motion blur

If motion length is 3, and 9 element PSF is considered then for vertical (90°) motion blur according to (4.1),

$$h_{-1,0} = h_{0,0} = h_{1,0} = \frac{1}{3} \text{ and } h_{-1,-1} = h_{0,-1} = h_{1,-1} = h_{0,1} = h_{-1,1} = h_{1,1} = 0$$

For horizontal (0°) motion blur,

$$h_{0,-1} = h_{0,0} = h_{0,1} = \frac{1}{3} \text{ and } h_{-1,-1} = h_{-1,0} = h_{-1,1} = h_{1,-1} = h_{1,0} = h_{1,1} = 0$$

Similarly for angular (45^0) motion blur,

$$h_{-1,-1} = h_{0,0} = h_{1,1} = \frac{1}{3} \text{ and } h_{-1,0} = h_{-1,1} = h_{0,1} = h_{0,-1} = h_{1,-1} = h_{1,0} = 0$$

And for angular (135^0) motion blur,

$$h_{-1,1} = h_{0,0} = h_{1,-1} = \frac{1}{3} \text{ and } h_{-1,0} = h_{-1,-1} = h_{0,-1} = h_{1,0} = h_{1,1} = h_{0,1} = 0$$

In Chapter 2, the spatial OFDM system is explained with mathematical equation. From equation (2.1) of Chapter 2, the relation between received spatial OFDM signal and transmitted pixel intensity is clearly understood. So, in presence of motion blur, when $(2P+1) \times (2P+1)$ number of pixels are transmitted it can be written that:

For vertical motion blur,
$$q_{l_1,l_2} = \sum_{m=-p}^p h_{m,0} \cdot p_{l_1+m,l_2} \quad (4.2)$$

For horizontal motion blur,
$$q_{l_1,l_2} = \sum_{m=-p}^p h_{0,m} \cdot p_{l_1,l_2+m} \quad (4.3)$$

For (135^0) angular motion blur,
$$q_{l_1,l_2} = \sum_{m=-p}^p h_{m,-m} \cdot p_{l_1+m,l_2-m} \quad (4.4)$$

For (45^0) angular motion blur,
$$q_{l_1,l_2} = \sum_{m=-p}^p h_{m,m} \cdot p_{l_1+m,l_2+m} \quad (4.5)$$

In case of vertical motion blur, using (2.2), (4.2) can be modified as:

$$y_{l_1,l_2} = \sum_{m=-p}^p h_{m,0} \cdot s_{l_1+m,l_2} + z_{l_1,l_2} \quad (4.6)$$

Where z_{l_1,l_2} is the noise in electrical domain.

Using the formula for 2D IFFT, the transmitted signal s_{l_1+m,l_2} can be determined by:

$$s_{l_1+m,l_2} = \frac{1}{N_1 N_2} \sum_{k_1=0}^{N_1-1} \sum_{k_2=0}^{N_2-1} s_{k_1,k_2} \exp \left\{ \frac{j2\pi k_1 (l_1 + m)}{N_1} + \frac{j2\pi k_2 l_2}{N_2} \right\} \quad (4.7)$$

Now, substituting the value of s_{l_1+m, l_2} from equation 4.7 into equation 4.6,

$$y_{l_1, l_2} = \frac{1}{N_1 N_2} \sum_{k_1=0}^{N_1-1} \sum_{k_2=0}^{N_2-1} s_{k_1, k_2} \exp\left\{ \frac{j2\pi k_1 l_1}{N_1} + \frac{j2\pi k_2 l_2}{N_2} \right\} \left\{ \sum_{m=-p}^p h_{m,0} \exp\left(\frac{j2\pi k_1 m}{N_1} \right) \right\} + z_{l_1, l_2} \quad (4.8)$$

So,

$$y_{l_1, l_2} = \frac{1}{N_1 N_2} \sum_{k_1=0}^{N_1-1} \sum_{k_2=0}^{N_2-1} s_{k_1, k_2} H_{k_1, k_2}^m \exp\left\{ \frac{j2\pi k_1 l_1}{N_1} + \frac{j2\pi k_2 l_2}{N_2} \right\} + z_{l_1, l_2} \quad (4.9)$$

Where, $H_{k_1, k_2}^m = \sum_{m=-p}^p h_{m,0} \exp\left(\frac{j2\pi k_1 m}{N_1} \right)$

Now for vertical motion blur,

$$H_{k_1, k_2}^{Vm} = \sum_{m=-p}^p h_{m,0} \exp\left(\frac{j2\pi k_1 m}{N_1} \right) \quad (4.10)$$

Similarly,

For horizontal motion blur,

$$H_{k_1, k_2}^{Hm} = \sum_{m=-p}^p h_{0,m} \exp\left(\frac{j2\pi k_2 m}{N_2} \right) \quad (4.11)$$

For (135°) angular motion blur,

$$H_{k_1, k_2}^{Am(135)} = \sum_{m=-p}^p h_{m,-m} \exp\left(\frac{j2\pi k_1 m}{N_1} - \frac{j2\pi k_2 m}{N_2} \right) \quad (4.12)$$

For (45°) angular motion blur,

$$H_{k_1, k_2}^{Am(45)} = \sum_{m=-p}^p h_{m,m} \exp\left(\frac{j2\pi k_1 m}{N_1} + \frac{j2\pi k_2 m}{N_2} \right) \quad (4.13)$$

From equation (4.10),(4.11),(4.12) and (4.13) it is clear that the transfer function of motion blur(vertical, horizontal and angular) is a function of PSF of motion blur and subcarrier index.

The effect of angular (45^0 or 135^0 or 225^0 or 315^0) motion blur can be found from equation (4.12) and (4.13),

$$H_{k_1,k_2}^{Am} = \sum_{m=-p}^p h_{m\sqrt{2}\sin\theta,m\sqrt{2}\cos\theta} \exp\left(\frac{j2\pi k_1 m\sqrt{2}\sin\theta}{N_1} + \frac{j2\pi k_2 m\sqrt{2}\cos\theta}{N_2}\right) \quad (4.14)$$

If motion length is 3 then for vertical motion,

$$\begin{aligned} H_{k_1,k_2}^{Vm(3)} &= h_{-1,0} \exp\left(\frac{-j2\pi k_1}{N_1}\right) + h_{0,0} + h_{1,0} \exp\left(\frac{j2\pi k_1}{N_1}\right) \\ &= h_{0,0} + h_{1,0} \left[\exp\left(\frac{-j2\pi k_1}{N_1}\right) + \exp\left(\frac{j2\pi k_1}{N_1}\right) \right] \\ &= h_{0,0} + 2h_{1,0} \cos \frac{j2\pi k_1}{N_1} \end{aligned}$$

Using equation (4.1), it can be further simplified as:

$$H_{k_1,k_2}^{Vm(3)} = \frac{1}{3} \exp\left(\frac{-j2\pi k_1}{N_1}\right) + \frac{1}{3} + \frac{1}{3} \exp\left(\frac{j2\pi k_1}{N_1}\right) = \frac{1}{3} \sum_{m=-1}^1 \exp\left(\frac{j2\pi k_1 m}{N_1}\right)$$

So equation (4.10) can be rewritten as,

$$H_{k_1,k_2}^{Vm} = \frac{1}{C} \sum_{m=-p}^p \exp\left(\frac{j2\pi k_1 m}{N_1}\right) \quad (4.15)$$

Where, C is the motion length.

Similarly equation (4.11) can be rewritten as,

$$H_{k_1,k_2}^{Hm} = \frac{1}{C} \sum_{m=-p}^p \exp\left(\frac{j2\pi k_2 m}{N_2}\right) \quad (4.16)$$

In a similar way equation (4.14) can be written as:

$$H_{k_1, k_2}^{Am} = \frac{1}{C} \sum_{m=-p}^p \exp\left(\frac{j2\pi k_1 m \sqrt{2} \sin \theta}{N_1} + \frac{j2\pi k_2 m \sqrt{2} \cos \theta}{N_2}\right) \quad (4.17)$$

The equation of (4.15), (4.16) and (4.17) represent the effect of vertical, horizontal and angular motion blur respectively in pixelated communication system. Now, it can be said that the effect of vertical, horizontal and angular motion blur mainly dependent on motion length and subcarrier index which indicates that the effect of motion blur at different subcarrier index is not same.

4.3 Modelling the Joint Effect of Motion and Defocus Blur

The expression of PSF of motion blur is given in previous section. Before going to investigate the joint impact of motion and defocus blur, knowing the expression of PSF of defocus blur is important. The PSF of defocus blur is modelled as Gaussian distribution as given in [51]:

$$h_{l_1, l_2} = h_{0,0} \exp\left(\frac{-l_1^2 - l_2^2}{2\sigma^2}\right) \quad (4.18)$$

Where, $h_{0,0}$ = The maximum amplitude of the distribution.

When $(2P+1) \times (2P+1)$ number of pixels are transmitted, the summation of the intensity of the transmitted pixels weighted by the corresponding PSF elements determines the intensity of each of the received pixels.

When vertical motion and defocus blur are present then the expression of q_{l_1, l_2} can be modified as:

$$q_{l_1, l_2} = \sum_{u=-p}^p \sum_{v=-p}^p \sum_{m=-p}^p \frac{1}{C} h_{u,v} \cdot p_{l_1+u, l_2+v} \quad (4.19)$$

If horizontal motion and defocus blur is present then the expression of q_{l_1, l_2} can be modified as:

$$q_{l_1, l_2} = \sum_{u=-p}^p \sum_{v=-p}^p \sum_{m=-p}^p \frac{1}{C} h_{u,v} \cdot p_{l_1+u, l_2+v+m} \quad (4.20)$$

Similarly in case of joint presence of angular motion and defocus blur,

$$q_{l_1, l_2} = \sum_{u=-p}^p \sum_{v=-p}^p \sum_{m=-p}^p \frac{1}{C} h_{u,v} \cdot P_{l_1+u+m\sqrt{2}\sin\theta, l_2+v+m\sqrt{2}\cos\theta} \quad (4.21)$$

For vertical motion and defocus blur the equation (2.4) in **Chapter 2** can be modified as:

$$P_{l_1+u+m, l_2+v} = S_{l_1+u+m, l_2+v}$$

$$S_{l_1+u+m, l_2+v} = \frac{1}{C N_1 N_2} \sum_{m=-p}^p \sum_{k_1=0}^{N_1-1} \sum_{k_2=0}^{N_2-1} s_{k_1, k_2} \exp\left\{ \frac{j2\pi k_1(l_1 + u + m)}{N_1} + \frac{j2\pi k_2(l_2 + v)}{N_2} \right\} \quad (4.22)$$

Now, substituting the value of s_{l_1+u+m, l_2+v} from equation (4.22) into equation (4.6) the value y_{l_1, l_2} of can be found as:

$$y_{l_1, l_2} = \frac{1}{N_1 N_2} \sum_{k_1=0}^{N_1-1} \sum_{k_2=0}^{N_2-1} s_{k_1, k_2} \exp\left\{ \frac{j2\pi k_1 l_1}{N_1} + \frac{j2\pi k_2 l_2}{N_2} \right\} \times \left\{ \sum_{u=-p}^p \sum_{v=-p}^p h_{u,v} \exp\left(\frac{j2\pi k_1 u}{N_1} + \frac{j2\pi k_2 v}{N_2} \right) \right\}$$

$$\times \left\{ \frac{1}{C} \sum_{m=-p}^p \exp\left(\frac{j2\pi k_1 m}{N_1} \right) \right\} + z_{l_1, l_2}$$

So,

$$y_{l_1, l_2} = \frac{1}{N_1 N_2} \sum_{k_1=0}^{N_1-1} \sum_{k_2=0}^{N_2-1} S_{k_1, k_2} H_{k_1, k_2}^d H_{k_1, k_2}^{Vm} \exp\left(\frac{j2\pi k_1 l_1}{N_1} + \frac{j2\pi k_2 l_2}{N_2} \right) + z_{l_1, l_2} \quad (4.23)$$

Where,

$$H_{k_1, k_2}^d = \sum_{u=-p}^p \sum_{v=-p}^p h_{u,v} \exp\left(\frac{j2\pi k_1 u}{N_1} + \frac{j2\pi k_2 v}{N_2} \right) \quad (4.24)$$

$$H_{k_1, k_2}^{Vm} = \frac{1}{C} \sum_{m=-p}^p \exp\left(\frac{j2\pi k_1 m}{N_1} \right) \quad (4.25)$$

In joint presence of horizontal motion and defocus blur, H_{k_1, k_2}^{Vm} of equation (4.23) will be replaced by H_{k_1, k_2}^{Hm} where,

$$H_{k_1, k_2}^{Hm} = \frac{1}{C} \sum_{m=-p}^p \exp\left(\frac{j2\pi k_2 m}{N_2}\right) \quad (4.26)$$

Similarly, in joint presence of angular motion and defocus blur,

$$H_{k_1, k_2}^{Am} = \frac{1}{C} \sum_{m=-p}^p \exp\left(\frac{j2\pi k_1 m \sqrt{2} \sin \theta}{N_1} + \frac{j2\pi k_2 m \sqrt{2} \cos \theta}{N_2}\right) \quad (4.27)$$

From equation (4.23) it is seen that the spatial domain signal q_{l_1, l_2} is a function of 2D IFFT version of spatial frequency domain signal S_{k_1, k_2} , transfer function of defocus blur, transfer function of motion blur and electrical noise. The transfer function of defocus blur is shown in (4.24) which indicates that the attenuation due to defocus blur depends on PSF of defocus blur and the subcarrier index. That means the attenuation changes as the subcarrier index. The transfer function of vertical, horizontal angular motion blur are shown in equation (4.25), (4.26) and (4.27) which are agreed with equation (4.15), (4.16) and (4.17) of previous section respectively. Moreover, (4.27) indicates that the motion blur in the spatial frequency domain is a function of subcarrier index, motion length and motion angle.

4.4 Modelling the Effect of All Impairments

The difference between transmitted frame and received frame is shown in Fig 4.2 when received image is affected with all spatial impairments. The area of PSF region marked in red and green arrow lines contributes to received pixel q_{l_1, l_2} . The term q_{l_1, l_2} is the summation of the intensities of the transmitted pixels weighted by segment areas depending on LFM, PSF elements of motion blur, PSF elements of defocus blur and vignetting function.

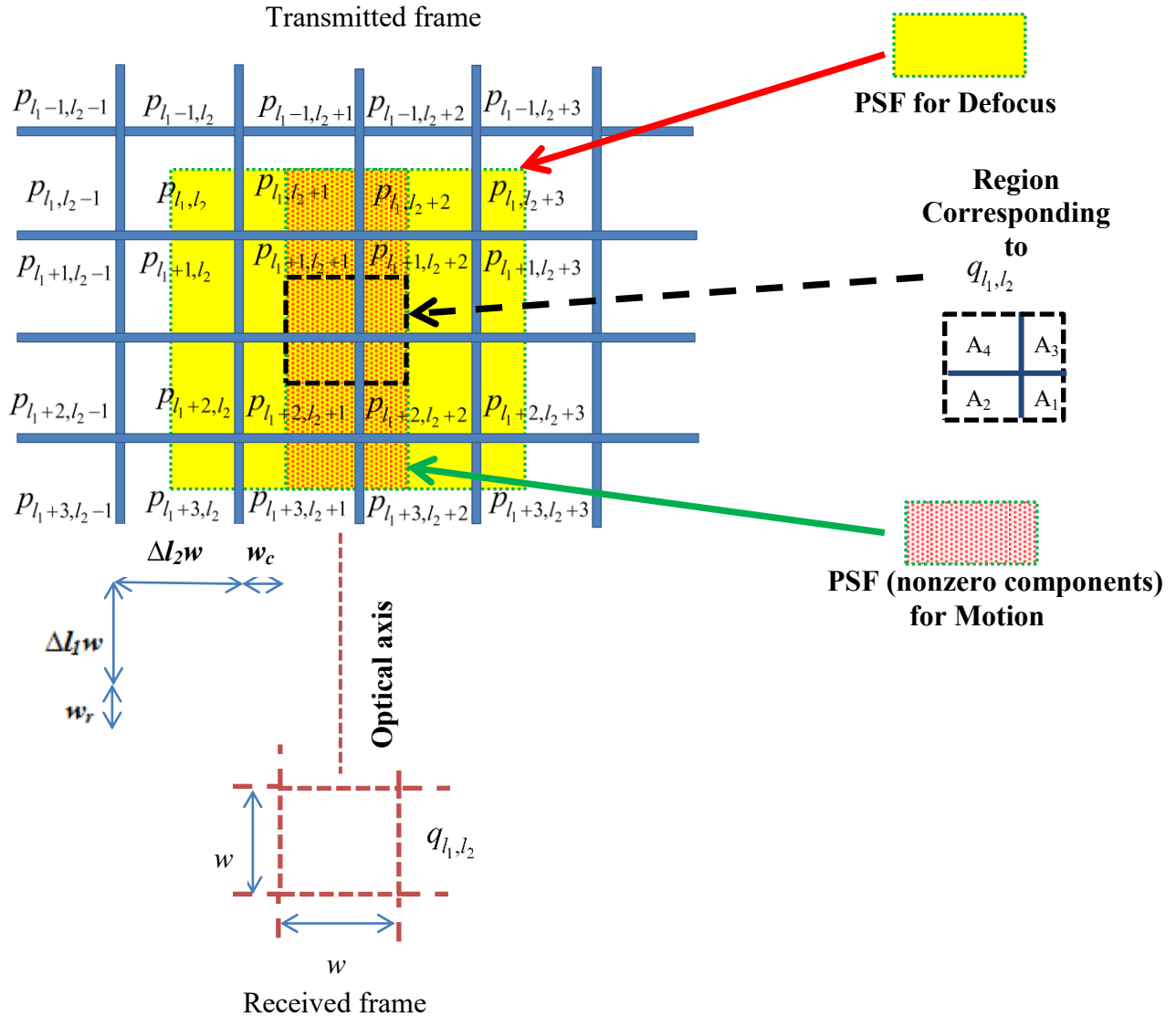


Fig. 4.2: The difference between transmitted and received frames in joint presence of all spatial impairments [51]

w is considered as the length of square-shape pixel. To represent LFM, w_r and w_c are used to denote the fractional offsets in 2-D and l_1 and l_2 are used to represent the lengths of misalignment in terms of number of full pixels. For simplicity, $\Delta l_1 = \Delta l_2 = 1$ and $p = 1$ is considered. q_{l_1, l_2} depends on a number of transmitted pixels because of motion blur LFM and defocus blur. The received pixel q_{l_1, l_2} corresponds to the weighted sum of four transmitted pixels, p_{l_1+1, l_2+1} , p_{l_1+2, l_2+1} , p_{l_1+1, l_2+2} and p_{l_1+2, l_2+2} . Due to LFM, the received pixel q_{l_1, l_2} have four

areas denoted by as A_1 , A_2 , A_3 and A_4 . When vertical motion length of 3 present with other impairments then the term q_{l_1, l_2} can be written in the following format using the vignetting function, $\cos^4 \theta_{l_1, l_2}$ [50] as:

$$q_{l_1, l_2} = \frac{1}{3} q_1 + \frac{1}{3} q_2 + \frac{1}{3} q_3 \quad (4.28)$$

Where,

$$q_1 = \left[\begin{aligned} &(A_4 p_{l_1, l_2} + A_3 p_{l_1, l_2+1} + A_2 p_{l_1+1, l_2} + A_1 p_{l_1+1, l_2+1}) h_{-1, -1} \cos^4 \theta_{l_1-1, l_2-1} \\ &+ (A_4 p_{l_1, l_2+1} + A_3 p_{l_1, l_2+2} + A_2 p_{l_1+1, l_2+1} + A_1 p_{l_1+1, l_2+2}) h_{-1, 0} \cos^4 \theta_{l_1-1, l_2} \\ &+ (A_4 p_{l_1, l_2+2} + A_3 p_{l_1, l_2+3} + A_2 p_{l_1+1, l_2+2} + A_1 p_{l_1+1, l_2+3}) h_{-1, 1} \cos^4 \theta_{l_1-1, l_2+1} \\ &+ (A_4 p_{l_1+1, l_2} + A_3 p_{l_1+1, l_2+1} + A_2 p_{l_1+2, l_2} + A_1 p_{l_1+2, l_2+1}) h_{0, -1} \cos^4 \theta_{l_1, l_2-1} \\ &+ (A_4 p_{l_1+1, l_2+1} + A_3 p_{l_1+1, l_2+2} + A_2 p_{l_1+2, l_2+1} + A_1 p_{l_1+2, l_2+2}) h_{0, 0} \cos^4 \theta_{l_1, l_2} \\ &+ (A_4 p_{l_1+1, l_2+2} + A_3 p_{l_1+1, l_2+3} + A_2 p_{l_1+2, l_2+2} + A_1 p_{l_1+2, l_2+3}) h_{0, 1} \cos^4 \theta_{l_1, l_2+1} \\ &+ (A_4 p_{l_1+2, l_2+2} + A_3 p_{l_1+2, l_2+1} + A_2 p_{l_1+3, l_2} + A_1 p_{l_1+3, l_2+1}) h_{1, -1} \cos^4 \theta_{l_1+1, l_2-1} \\ &+ (A_4 p_{l_1+2, l_2+1} + A_3 p_{l_1+2, l_2+2} + A_2 p_{l_1+3, l_2+1} + A_1 p_{l_1+3, l_2+2}) h_{1, 0} \cos^4 \theta_{l_1+1, l_2} \\ &+ (A_4 p_{l_1+2, l_2+2} + A_3 p_{l_1+2, l_2+3} + A_2 p_{l_1+3, l_2+2} + A_1 p_{l_1+3, l_2+3}) h_{1, 1} \cos^4 \theta_{l_1+1, l_2+1} \end{aligned} \right]$$

$$q_2 = \left[\begin{aligned} &(A_4 p_{l_1-1, l_2} + A_3 p_{l_1-1, l_2+1} + A_2 p_{l_1, l_2} + A_1 p_{l_1, l_2+1}) h_{-1, -1} \cos^4 \theta_{l_1-2, l_2-1} \\ &+ (A_4 p_{l_1-1, l_2+1} + A_3 p_{l_1-1, l_2+2} + A_2 p_{l_1, l_2+1} + A_1 p_{l_1, l_2+2}) h_{-1, 0} \cos^4 \theta_{l_1-2, l_2} \\ &+ (A_4 p_{l_1-1, l_2+2} + A_3 p_{l_1-1, l_2+3} + A_2 p_{l_1, l_2+2} + A_1 p_{l_1, l_2+3}) h_{-1, 1} \cos^4 \theta_{l_1-2, l_2+1} \\ &+ (A_4 p_{l_1, l_2} + A_3 p_{l_1, l_2+1} + A_2 p_{l_1+1, l_2} + A_1 p_{l_1+1, l_2+1}) h_{0, -1} \cos^4 \theta_{l_1-1, l_2-1} \\ &+ (A_4 p_{l_1, l_2+1} + A_3 p_{l_1, l_2+2} + A_2 p_{l_1+1, l_2+1} + A_1 p_{l_1+1, l_2+2}) h_{0, 0} \cos^4 \theta_{l_1-1, l_2} \\ &+ (A_4 p_{l_1, l_2+2} + A_3 p_{l_1, l_2+3} + A_2 p_{l_1+1, l_2+2} + A_1 p_{l_1+1, l_2+3}) h_{0, 1} \cos^4 \theta_{l_1-1, l_2+1} \\ &+ (A_4 p_{l_1+1, l_2+2} + A_3 p_{l_1+1, l_2+1} + A_2 p_{l_1+2, l_2} + A_1 p_{l_1+2, l_2+1}) h_{1, -1} \cos^4 \theta_{l_1, l_2-1} \\ &+ (A_4 p_{l_1+1, l_2+1} + A_3 p_{l_1+1, l_2+2} + A_2 p_{l_1+2, l_2+1} + A_1 p_{l_1+2, l_2+2}) h_{1, 0} \cos^4 \theta_{l_1, l_2} \\ &+ (A_4 p_{l_1+1, l_2+2} + A_3 p_{l_1+1, l_2+3} + A_2 p_{l_1+2, l_2+2} + A_1 p_{l_1+2, l_2+3}) h_{1, 1} \cos^4 \theta_{l_1, l_2+1} \end{aligned} \right]$$

And

$$\begin{aligned}
 q_3 = & \left[\begin{aligned}
 & (A_4 p_{l_1+1, l_2} + A_3 p_{l_1+1, l_2+1} + A_2 p_{l_1+2, l_2} + A_1 p_{l_1+2, l_2+1}) h_{-1, -1} \cos^4 \theta_{l_1, l_2-1} \\
 & + (A_4 p_{l_1+1, l_2+1} + A_3 p_{l_1+1, l_2+2} + A_2 p_{l_1+2, l_2+1} + A_1 p_{l_1+2, l_2+2}) h_{-1, 0} \cos^4 \theta_{l_1, l_2} \\
 & + (A_4 p_{l_1+1, l_2+2} + A_3 p_{l_1+1, l_2+3} + A_2 p_{l_1+2, l_2+2} + A_1 p_{l_1+2, l_2+3}) h_{-1, 1} \cos^4 \theta_{l_1, l_2+1} \\
 & + (A_4 p_{l_1+2, l_2} + A_3 p_{l_1+2, l_2+1} + A_2 p_{l_1+3, l_2} + A_1 p_{l_1+3, l_2+1}) h_{0, -1} \cos^4 \theta_{l_1+1, l_2-1} \\
 & + (A_4 p_{l_1+2, l_2+1} + A_3 p_{l_1+2, l_2+2} + A_2 p_{l_1+3, l_2+1} + A_1 p_{l_1+3, l_2+2}) h_{0, 0} \cos^4 \theta_{l_1+1, l_2} \\
 & + (A_4 p_{l_1+2, l_2+2} + A_3 p_{l_1+2, l_2+3} + A_2 p_{l_1+3, l_2+2} + A_1 p_{l_1+3, l_2+3}) h_{0, -1} \cos^4 \theta_{l_1+1, l_2+1} \\
 & + (A_4 p_{l_1+3, l_2+2} + A_3 p_{l_1+3, l_2+1} + A_2 p_{l_1+4, l_2} + A_1 p_{l_1+4, l_2+1}) h_{1, -1} \cos^4 \theta_{l_1+2, l_2-1} \\
 & + (A_4 p_{l_1+3, l_2+1} + A_3 p_{l_1+3, l_2+2} + A_2 p_{l_1+4, l_2+1} + A_1 p_{l_1+4, l_2+2}) h_{1, 0} \cos^4 \theta_{l_1+2, l_2} \\
 & + (A_4 p_{l_1+3, l_2+2} + A_3 p_{l_1+3, l_2+3} + A_2 p_{l_1+4, l_2+2} + A_1 p_{l_1+4, l_2+3}) h_{1, 1} \cos^4 \theta_{l_1+2, l_2+1}
 \end{aligned} \right]
 \end{aligned}$$

In equation (4.28) general case is not considered. Just considering general case of LFM, equation (4.28) can be modified by one full pixel component by Δl_1 and Δl_2 numbers of full pixels in 2D as shown in Equation (4.29).

$$q_{l_1, l_2} = \frac{1}{3} q_1' + \frac{1}{3} q_2' + \frac{1}{3} q_3' \quad (4.29)$$

The expressions of q_1' , q_2' and q_3' are shown in following pages.

$$\begin{aligned}
q_1 = & \left[\begin{aligned}
& A_4 (p_{l_1+\Delta l_1-1, l_2+\Delta l_2-1} h_{-1,-1} \cos^4 \theta_{l_1-1, l_2-1} + p_{l_1+\Delta l_1-1, l_2+\Delta l_2} h_{-1,0} \cos^4 \theta_{l_1-1, l_2} \\
& + p_{l_1+\Delta l_1-1, l_2+\Delta l_2+1} h_{-1,1} \cos^4 \theta_{l_1-1, l_2+1} + p_{l_1+\Delta l_1, l_2+\Delta l_2-1} h_{0,-1} \cos^4 \theta_{l_1, l_2-1} \\
& + p_{l_1+\Delta l_1, l_2+\Delta l_2} h_{0,0} \cos^4 \theta_{l_1, l_2} + p_{l_1+\Delta l_1, l_2+\Delta l_2+1} h_{0,1} \cos^4 \theta_{l_1, l_2+1} \\
& + p_{l_1+\Delta l_1+1, l_2+\Delta l_2+1} h_{1,-1} \cos^4 \theta_{l_1+1, l_2-1} + p_{l_1+\Delta l_1+1, l_2+\Delta l_2} h_{1,0} \cos^4 \theta_{l_1+1, l_2} \\
& + p_{l_1+\Delta l_1+1, l_2+\Delta l_2+1} h_{1,1} \cos^4 \theta_{l_1+1, l_2+1}) + A_3 (p_{l_1+\Delta l_1-1, l_2+\Delta l_2} h_{-1,-1} \cos^4 \theta_{l_1-1, l_2-1} \\
& + p_{l_1+\Delta l_1-1, l_2+\Delta l_2+1} h_{-1,0} \cos^4 \theta_{l_1-1, l_2} + p_{l_1+\Delta l_1-1, l_2+\Delta l_2+2} h_{-1,1} \cos^4 \theta_{l_1-1, l_2+1} \\
& + p_{l_1+\Delta l_1, l_2+\Delta l_2} h_{0,-1} \cos^4 \theta_{l_1, l_2-1} + p_{l_1+\Delta l_1, l_2+\Delta l_2+1} h_{0,0} \cos^4 \theta_{l_1, l_2} \\
& + p_{l_1+\Delta l_1, l_2+\Delta l_2+2} h_{0,1} \cos^4 \theta_{l_1, l_2+1} + p_{l_1+\Delta l_1+1, l_2+\Delta l_2} h_{1,-1} \cos^4 \theta_{l_1+1, l_2-1} \\
& + p_{l_1+\Delta l_1+1, l_2+\Delta l_2+1} h_{1,0} \cos^4 \theta_{l_1+1, l_2} + p_{l_1+\Delta l_1+1, l_2+\Delta l_2+2} h_{1,1} \cos^4 \theta_{l_1+1, l_2+1}) \\
& + A_2 (p_{l_1+\Delta l_1, l_2+\Delta l_2-1} h_{-1,-1} \cos^4 \theta_{l_1-1, l_2-1} + p_{l_1+\Delta l_1, l_2+\Delta l_2} h_{-1,0} \cos^4 \theta_{l_1-1, l_2} \\
& + p_{l_1+\Delta l_1, l_2+\Delta l_2+1} h_{-1,1} \cos^4 \theta_{l_1-1, l_2+1} + p_{l_1+\Delta l_1+1, l_2+\Delta l_2-1} h_{0,-1} \cos^4 \theta_{l_1, l_2-1} \\
& + p_{l_1+\Delta l_1+1, l_2+\Delta l_2} h_{0,0} \cos^4 \theta_{l_1, l_2} + p_{l_1+\Delta l_1+1, l_2+\Delta l_2+1} h_{0,1} \cos^4 \theta_{l_1, l_2+1} \\
& + p_{l_1+\Delta l_1+2, l_2+\Delta l_2-1} h_{1,-1} \cos^4 \theta_{l_1+1, l_2-1} + p_{l_1+\Delta l_1+2, l_2+\Delta l_2} h_{1,0} \cos^4 \theta_{l_1+1, l_2} \\
& + p_{l_1+\Delta l_1+2, l_2+\Delta l_2+1} h_{1,1} \cos^4 \theta_{l_1+1, l_2+1}) + A_1 (p_{l_1+\Delta l_1, l_2+\Delta l_2} h_{-1,-1} \cos^4 \theta_{l_1-1, l_2-1} \\
& + p_{l_1+\Delta l_1, l_2+\Delta l_2+1} h_{-1,0} \cos^4 \theta_{l_1-1, l_2} + p_{l_1+\Delta l_1, l_2+\Delta l_2+2} h_{-1,1} \cos^4 \theta_{l_1-1, l_2+1} \\
& + p_{l_1+\Delta l_1+1, l_2+\Delta l_2} h_{0,-1} \cos^4 \theta_{l_1, l_2-1} + p_{l_1+\Delta l_1+1, l_2+\Delta l_2+1} h_{0,0} \cos^4 \theta_{l_1, l_2} \\
& + p_{l_1+\Delta l_1+1, l_2+\Delta l_2+2} h_{0,1} \cos^4 \theta_{l_1, l_2+1} + p_{l_1+\Delta l_1+2, l_2+\Delta l_2} h_{1,-1} \cos^4 \theta_{l_1+1, l_2-1} \\
& + p_{l_1+\Delta l_1+2, l_2+\Delta l_2+1} h_{1,0} \cos^4 \theta_{l_1+1, l_2} + p_{l_1+\Delta l_1+2, l_2+\Delta l_2+2} h_{1,1} \cos^4 \theta_{l_1+1, l_2+1})
\end{aligned} \right]
\end{aligned}$$

$$\begin{aligned}
q_2 = & \left[\begin{aligned}
& A_4 (p_{l_1+\Delta l_1-2, l_2+\Delta l_2-1} h_{-1,-1} \cos^4 \theta_{l_1-1, l_2-1} + p_{l_1+\Delta l_1-2, l_2+\Delta l_2} h_{-1,0} \cos^4 \theta_{l_1-1, l_2} \\
& + p_{l_1+\Delta l_1-2, l_2+\Delta l_2+1} h_{-1,1} \cos^4 \theta_{l_1-1, l_2+1} + p_{l_1+\Delta l_1-1, l_2+\Delta l_2-1} h_{0,-1} \cos^4 \theta_{l_1, l_2-1} \\
& + p_{l_1+\Delta l_1-1, l_2+\Delta l_2} h_{0,0} \cos^4 \theta_{l_1, l_2} + p_{l_1+\Delta l_1-1, l_2+\Delta l_2+1} h_{0,1} \cos^4 \theta_{l_1, l_2+1} \\
& + p_{l_1+\Delta l_1, l_2+\Delta l_2+1} h_{1,-1} \cos^4 \theta_{l_1+1, l_2-1} + p_{l_1+\Delta l_1, l_2+\Delta l_2} h_{1,0} \cos^4 \theta_{l_1+1, l_2} \\
& + p_{l_1+\Delta l_1, l_2+\Delta l_2+1} h_{1,1} \cos^4 \theta_{l_1+1, l_2+1}) + A_3 (p_{l_1+\Delta l_1-2, l_2+\Delta l_2} h_{-1,-1} \cos^4 \theta_{l_1-1, l_2-1} \\
& + p_{l_1+\Delta l_1-2, l_2+\Delta l_2+1} h_{-1,0} \cos^4 \theta_{l_1-1, l_2} + p_{l_1+\Delta l_1-2, l_2+\Delta l_2+2} h_{-1,1} \cos^4 \theta_{l_1-1, l_2+1} \\
& + p_{l_1+\Delta l_1-1, l_2+\Delta l_2} h_{0,-1} \cos^4 \theta_{l_1, l_2-1} + p_{l_1+\Delta l_1-1, l_2+\Delta l_2+1} h_{0,0} \cos^4 \theta_{l_1, l_2} \\
& + p_{l_1+\Delta l_1-1, l_2+\Delta l_2+2} h_{0,1} \cos^4 \theta_{l_1, l_2+1} + p_{l_1+\Delta l_1, l_2+\Delta l_2} h_{1,-1} \cos^4 \theta_{l_1+1, l_2-1} \\
& + p_{l_1+\Delta l_1, l_2+\Delta l_2+1} h_{1,0} \cos^4 \theta_{l_1+1, l_2} + p_{l_1+\Delta l_1, l_2+\Delta l_2+2} h_{1,1} \cos^4 \theta_{l_1+1, l_2+1}) \\
& + A_2 (p_{l_1+\Delta l_1-1, l_2+\Delta l_2-1} h_{-1,-1} \cos^4 \theta_{l_1-1, l_2-1} + p_{l_1+\Delta l_1-1, l_2+\Delta l_2} h_{-1,0} \cos^4 \theta_{l_1-1, l_2} \\
& + p_{l_1+\Delta l_1-1, l_2+\Delta l_2+1} h_{-1,1} \cos^4 \theta_{l_1-1, l_2+1} + p_{l_1+\Delta l_1, l_2+\Delta l_2-1} h_{0,-1} \cos^4 \theta_{l_1, l_2-1} \\
& + p_{l_1+\Delta l_1, l_2+\Delta l_2} h_{0,0} \cos^4 \theta_{l_1, l_2} + p_{l_1+\Delta l_1, l_2+\Delta l_2+1} h_{0,1} \cos^4 \theta_{l_1, l_2+1} \\
& + p_{l_1+\Delta l_1+1, l_2+\Delta l_2-1} h_{1,-1} \cos^4 \theta_{l_1+1, l_2-1} + p_{l_1+\Delta l_1+1, l_2+\Delta l_2} h_{1,0} \cos^4 \theta_{l_1+1, l_2} \\
& + p_{l_1+\Delta l_1+1, l_2+\Delta l_2+1} h_{1,1} \cos^4 \theta_{l_1+1, l_2+1}) + A_1 (p_{l_1+\Delta l_1-1, l_2+\Delta l_2} h_{-1,-1} \cos^4 \theta_{l_1-1, l_2-1} \\
& + p_{l_1+\Delta l_1-1, l_2+\Delta l_2+1} h_{-1,0} \cos^4 \theta_{l_1-1, l_2} + p_{l_1+\Delta l_1-1, l_2+\Delta l_2+2} h_{-1,1} \cos^4 \theta_{l_1-1, l_2+1} \\
& + p_{l_1+\Delta l_1, l_2+\Delta l_2} h_{0,-1} \cos^4 \theta_{l_1, l_2-1} + p_{l_1+\Delta l_1, l_2+\Delta l_2+1} h_{0,0} \cos^4 \theta_{l_1, l_2} \\
& + p_{l_1+\Delta l_1, l_2+\Delta l_2+2} h_{0,1} \cos^4 \theta_{l_1, l_2+1} + p_{l_1+\Delta l_1+1, l_2+\Delta l_2} h_{1,-1} \cos^4 \theta_{l_1+1, l_2-1} \\
& + p_{l_1+\Delta l_1+1, l_2+\Delta l_2+1} h_{1,0} \cos^4 \theta_{l_1+1, l_2} + p_{l_1+\Delta l_1+1, l_2+\Delta l_2+2} h_{1,1} \cos^4 \theta_{l_1+1, l_2+1})
\end{aligned} \right]
\end{aligned}$$

$$\begin{aligned}
& A_4 (p_{l_1+\Delta l_1, l_2+\Delta l_2-1} h_{-1,-1} \cos^4 \theta_{l_1-1, l_2-1} + p_{l_1+\Delta l_1, l_2+\Delta l_2} h_{-1,0} \cos^4 \theta_{l_1-1, l_2} \\
& + p_{l_1+\Delta l_1, l_2+\Delta l_2+1} h_{-1,1} \cos^4 \theta_{l_1-1, l_2+1} + p_{l_1+\Delta l_1+1, l_2+\Delta l_2-1} h_{0,-1} \cos^4 \theta_{l_1, l_2-1} \\
& + p_{l_1+\Delta l_1+1, l_2+\Delta l_2} h_{0,0} \cos^4 \theta_{l_1, l_2} + p_{l_1+\Delta l_1+1, l_2+\Delta l_2+1} h_{0,1} \cos^4 \theta_{l_1, l_2+1} \\
& + p_{l_1+\Delta l_1+2, l_2+\Delta l_2+1} h_{1,-1} \cos^4 \theta_{l_1+1, l_2-1} + p_{l_1+\Delta l_1+2, l_2+\Delta l_2} h_{1,0} \cos^4 \theta_{l_1+1, l_2} \\
& + p_{l_1+\Delta l_1+2, l_2+\Delta l_2+1} h_{1,1} \cos^4 \theta_{l_1+1, l_2+1}) + A_3 (p_{l_1+\Delta l_1, l_2+\Delta l_2} h_{-1,-1} \cos^4 \theta_{l_1-1, l_2-1} \\
& + p_{l_1+\Delta l_1, l_2+\Delta l_2+1} h_{-1,0} \cos^4 \theta_{l_1-1, l_2} + p_{l_1+\Delta l_1, l_2+\Delta l_2+2} h_{-1,1} \cos^4 \theta_{l_1-1, l_2+1} \\
& + p_{l_1+\Delta l_1+1, l_2+\Delta l_2} h_{0,-1} \cos^4 \theta_{l_1, l_2-1} + p_{l_1+\Delta l_1+1, l_2+\Delta l_2+1} h_{0,0} \cos^4 \theta_{l_1, l_2} \\
& + p_{l_1+\Delta l_1+1, l_2+\Delta l_2+2} h_{0,1} \cos^4 \theta_{l_1, l_2+1} + p_{l_1+\Delta l_1+2, l_2+\Delta l_2} h_{1,-1} \cos^4 \theta_{l_1+1, l_2-1} \\
& + p_{l_1+\Delta l_1+2, l_2+\Delta l_2+1} h_{1,0} \cos^4 \theta_{l_1+1, l_2} + p_{l_1+\Delta l_1+2, l_2+\Delta l_2+2} h_{1,1} \cos^4 \theta_{l_1+1, l_2+1}) \\
q_3 = & + A_2 (p_{l_1+\Delta l_1+1, l_2+\Delta l_2-1} h_{-1,-1} \cos^4 \theta_{l_1-1, l_2-1} + p_{l_1+\Delta l_1+1, l_2+\Delta l_2} h_{-1,0} \cos^4 \theta_{l_1-1, l_2} \\
& + p_{l_1+\Delta l_1+1, l_2+\Delta l_2+1} h_{-1,1} \cos^4 \theta_{l_1-1, l_2+1} + p_{l_1+\Delta l_1+2, l_2+\Delta l_2-1} h_{0,-1} \cos^4 \theta_{l_1, l_2-1} \\
& + p_{l_1+\Delta l_1+2, l_2+\Delta l_2} h_{0,0} \cos^4 \theta_{l_1, l_2} + p_{l_1+\Delta l_1+2, l_2+\Delta l_2+1} h_{0,1} \cos^4 \theta_{l_1, l_2+1} \\
& + p_{l_1+\Delta l_1+3, l_2+\Delta l_2-1} h_{1,-1} \cos^4 \theta_{l_1+1, l_2-1} + p_{l_1+\Delta l_1+3, l_2+\Delta l_2} h_{1,0} \cos^4 \theta_{l_1+1, l_2} \\
& + p_{l_1+\Delta l_1+3, l_2+\Delta l_2+1} h_{1,1} \cos^4 \theta_{l_1+1, l_2+1}) + A_1 (p_{l_1+\Delta l_1+1, l_2+\Delta l_2} h_{-1,-1} \cos^4 \theta_{l_1-1, l_2-1} \\
& + p_{l_1+\Delta l_1+1, l_2+\Delta l_2+1} h_{-1,0} \cos^4 \theta_{l_1-1, l_2} + p_{l_1+\Delta l_1+1, l_2+\Delta l_2+2} h_{-1,1} \cos^4 \theta_{l_1-1, l_2+1} \\
& + p_{l_1+\Delta l_1+2, l_2+\Delta l_2} h_{0,-1} \cos^4 \theta_{l_1, l_2-1} + p_{l_1+\Delta l_1+2, l_2+\Delta l_2+1} h_{0,0} \cos^4 \theta_{l_1, l_2} \\
& + p_{l_1+\Delta l_1+2, l_2+\Delta l_2+2} h_{0,1} \cos^4 \theta_{l_1, l_2+1} + p_{l_1+\Delta l_1+3, l_2+\Delta l_2} h_{1,-1} \cos^4 \theta_{l_1+1, l_2-1} \\
& + p_{l_1+\Delta l_1+3, l_2+\Delta l_2+1} h_{1,0} \cos^4 \theta_{l_1+1, l_2} + p_{l_1+\Delta l_1+3, l_2+\Delta l_2+2} h_{1,1} \cos^4 \theta_{l_1+1, l_2+1})
\end{aligned}$$

The equation (4.29) can be simplified as follows:

$$q_{l_1, l_2} = \sum_{u=-1}^1 \sum_{v=-1}^1 \sum_{m=-1}^1 \left[\frac{1}{3} h_{u,v} \cdot \cos^4 \theta_{(l_1+u+m), (l_2+v)} \right] \times \left\{ \begin{aligned} & A_4 P_{(l_1+\Delta l_1+u+m), (l_2+\Delta l_2+v)} + A_3 P_{(l_1+\Delta l_1+u+m), (l_2+\Delta l_2+1+v)} \\ & + A_2 P_{(l_1+\Delta l_1+u+1+m), (l_2+\Delta l_2+v)} + A_1 P_{(l_1+\Delta l_1+u+1+m), (l_2+\Delta l_2+1+v)} \end{aligned} \right\}$$

For $(2p+1) \times (2p+1)$ PSE this equation becomes:

$$q_{l_1, l_2} = \sum_{u=-p}^1 \sum_{v=-p}^1 \sum_{m=-p}^1 \left[\frac{1}{C} h_{u,v} \cdot \cos^4 \theta_{(l_1+u+m), (l_2+v)} \right. \\ \left. \times \left\{ \begin{aligned} &A_4 P_{(l_1+\Delta l_1+u+m), (l_2+\Delta l_2+v)} + A_3 P_{(l_1+\Delta l_1+u+m), (l_2+\Delta l_2+1+v)} \\ &+ A_2 P_{(l_1+\Delta l_1+u+1+m), (l_2+\Delta l_2+v)} + A_1 P_{(l_1+\Delta l_1+u+1+m), (l_2+\Delta l_2+1+v)} \end{aligned} \right\} \right]$$

Where, $C=2p+1$

From equation (2.2), $y_{l_1, l_2} = q_{l_1, l_2} + z_{l_1, l_2}$

$$\text{so, } y_{l_1, l_2} = \sum_{u=-p}^1 \sum_{v=-p}^1 \sum_{m=-p}^1 \left[\frac{1}{C} h_{u,v} \cdot \cos^4 \theta_{(l_1+u+m), (l_2+v)} \right. \\ \left. \times \left\{ \begin{aligned} &A_4 P_{(l_1+\Delta l_1+u+m), (l_2+\Delta l_2+v)} + A_3 P_{(l_1+\Delta l_1+u+m), (l_2+\Delta l_2+1+v)} \\ &+ A_2 P_{(l_1+\Delta l_1+u+1+m), (l_2+\Delta l_2+v)} + A_1 P_{(l_1+\Delta l_1+u+1+m), (l_2+\Delta l_2+1+v)} \end{aligned} \right\} \right] + z_{l_1, l_2}$$

This equation can be further simplified as:

$$y_{l_1, l_2} = \sum_{u=-p}^1 \sum_{v=-p}^1 \sum_{m=-p}^1 \left[\frac{1}{C} h_{u,v} \cdot s''_{(l_1+u+m), (l_2+v)} \right] + z_{l_1, l_2} \quad (4.30)$$

Where, $s''_{l_1, l_2} = s'_{l_1, l_2} \cos^4 \theta_{l_1, l_2}$ and $s'_{l_1, l_2} = \left\{ \begin{aligned} &A_4 P_{(l_1+\Delta l_1), (l_2+\Delta l_2)} + A_3 P_{(l_1+\Delta l_1), (l_2+\Delta l_2+1)} \\ &+ A_2 P_{(l_1+\Delta l_1+1), (l_2+\Delta l_2)} + A_1 P_{(l_1+\Delta l_1+1), (l_2+\Delta l_2+1)} \end{aligned} \right\}$

Equation (4.30) is valid for vertical motion blur along with other impairments.

For horizontal motion blur this equation will be:

$$y_{l_1, l_2} = \sum_{u=-p}^1 \sum_{v=-p}^1 \sum_{m=-p}^1 \left[\frac{1}{C} h_{u,v} \cdot s''_{(l_1+u), (l_2+v+m)} \right] + z_{l_1, l_2}$$

Similarly for (45°) angular motion blur,

$$y_{l_1, l_2} = \sum_{u=-p}^1 \sum_{v=-p}^1 \sum_{m=-p}^1 \left[\frac{1}{C} h_{u,v} \cdot s''_{(l_1+u+m), (l_2+v+m)} \right] + z_{l_1, l_2}$$

And for (135^0) angular motion blur,

$$y_{l_1, l_2} = \sum_{u=-p}^1 \sum_{v=-p}^1 \sum_{m=-p}^1 \left[\frac{1}{C} h_{u,v} \cdot S''_{(l_1+u+m), (l_2+v-m)} \right] + z_{l_1, l_2}$$

Now, for angular motion blur and others impairments,

$$y_{l_1, l_2} = \sum_{u=-p}^1 \sum_{v=-p}^1 \sum_{m=-p}^1 \left[\frac{1}{C} h_{u,v} \cdot S''_{(l_1+u+m\sqrt{2}\sin\theta), (l_2+v-m\sqrt{2}\cos\theta)} \right] + z_{l_1, l_2}$$

Applying 2D FFT spatial frequency domain data will be found.

$$Y_{k_1, k_2} = S''_{k_1, k_2} \cdot H_{k_1, k_2}^{dm} + Z_{k_1, k_2} \quad (4.31)$$

Where, S'_{l_1, l_2} is the spatial domain correspondence of S''_{k_1, k_2} . Now, with the help of S'_{k_1, k_2} , S''_{k_1, k_2} will be expressed and then S'_{k_1, k_2} will be shown as a function of S_{k_1, k_2} . S''_{k_1, k_2} can be represented in term of vignetting attenuation H_{k_1, k_2}^v and inter carrier interference (ICI) I'_{k_1, k_2} . ICI, I'_{k_1, k_2} is responsible for interference on a transmitted subcarrier S'_{k_1, k_2} from all other subcarriers $S'_{k'_1, k'_2}$ [50]: It is noted that, $k'_1, k'_2 \neq k_1, k_2$

$$\begin{aligned} S''_{k_1, k_2} &= S'_{k_1, k_2} H_{k_1, k_2}^v + I'_{k_1, k_2} \\ &= S'_{k_1, k_2} H_{k_1, k_2}^v + \sum_{k'_1=0}^{N_1-1} \sum_{k'_2=0}^{N_2-1} S'_{k'_1, k'_2} F_{k'_1-k, k'_2-k} \end{aligned} \quad (4.32)$$

Where,

$$H_{k_1, k_2}^v = \frac{1}{N_1 N_2} \sum_{l_1=0}^{N_1-1} \sum_{l_2=0}^{N_2-1} \cos^4 \theta_{l_1, l_2} \exp \left\{ \frac{j2\pi(k'_1 - k_1)l_1}{N_1} \right\} \exp \left\{ \frac{j2\pi(k'_2 - k_2)l_2}{N_2} \right\}$$

Here, $k'_1 - k_1, k'_2 - k_2 \neq 0$

According to [49], it can be written as:

$$S'_{k_1, k_2} = S_{k_1, k_2} \cdot H_{k_1, k_2}^a \cdot H_{k_1, k_2}^p \quad (4.33)$$

Where, H_{k_1, k_2}^a is the attenuation and H_{k_1, k_2}^p is the phase rotation caused by LFM. Now using (4.31) and (4.32) it can be written as:

$$S''_{k_1, k_2} = S_{k_1, k_2} \cdot H_{k_1, k_2}^a \cdot H_{k_1, k_2}^p \cdot H_{k_1, k_2}^v + I_{k_1, k_2} \quad (4.34)$$

Where, $I_{k_1, k_2} = \sum_{k'_1=0}^{N_1-1} \sum_{k'_2=0}^{N_2-1} H_{k'_1, k'_2}^a \cdot H_{k'_1, k'_2}^p \cdot S'_{k'_1, k'_2} \cdot F_{k'_1-k, k'_2-k}$ is interference on subcarriers.

As, $S_{k_1, k_2} = X_{k_1, k_2}$, so using equation (4.32), equation (4.29) can be modified as:

$$Y_{k_1, k_2} = X_{k_1, k_2} \cdot H_{k_1, k_2}^{dm} \cdot H_{k_1, k_2}^a \cdot H_{k_1, k_2}^p \cdot H_{k_1, k_2}^v + I_{k_1, k_2} \cdot H_{k_1, k_2}^{dm} + Z_{k_1, k_2} \quad (4.35)$$

It is clear from (4.35) that the before received transmitted subcarrier faces attenuation and phase rotation for LFM and vignetting and also faces degradation for defocus and motion blur along with AWGN noise. The defocus and motion blur not only affect the transmitted subcarriers but also leave impact on the inter carrier interference. So, the combined effect is the joint attenuation due to motion, defocus blur, vignetting, and LFM.

4.5 Conclusion

The effect of joint presence of all impairments is mathematically derived to realize the difference of single impairment effect and the effect of joint presence of all impairments. It is observed that, the joint effects are the combination of the individual effects and the impairments are largely independent of each other.

CHAPTER FIVE

SPATIAL LIM AND SPATIAL NDC

5.1 Introduction

One of the major requirement of optical communication is the data which will be transmitted must be real and non-negative. But, in OFDM the data may be complex and negative. To mitigate this shortfall, various techniques are followed in different optical OFDM methods. As mentioned in the literature review, unlike DCO-OFDM where a DC bias is used, spatial LIM OFDM transmits positive, negative, real and complex data separately. In contrast, NDC-OFDM follows Hermetian symmetry to ensure that all data are real, and sends positive and negative part of data symbol distinctly.

In this chapter, in the presence of spatial impairments, NDC-OFDM and LIM-OFDM are considered in the context of pixelated systems. LIM-OFDM and NDC-OFDM are extended to spatial domain to form spatial LIM-OFDM (SLIM-OFDM) and spatial NDC-OFDM (SNDC-OFDM) for pixelated communication systems.

At first, the electrical and optical power efficiency of SLIM-OFDM, SNDC-OFDM along with other optical spatial OFDM methods are compared considering only AWGN channel noise. After that, in the joint presence of vignetting, LFM, defocus blur and channel noise both the electrical and optical power efficiency of SLIM-OFDM, SNDC-OFDM, SDCO-OFDM, SACO-OFDM and SADO-OFDM for pixelated systems are compared.

In case of electrical and optical power efficiency, comparative analysis between spatial LIM and spatial NDC is presented in this chapter. **Section 5.2** and **Section 5.3** show the concept of spatial LED index modulation and spatial NDC-OFDM in the context of pixelated communication systems, respectively. The next section provides performance analysis of spatial LED index modulation and spatial NDC-OFDM over other different OFDM forms for pixelated OWC. Lastly concluding remarks are provided in **Section 5.4**.

5.2 Spatial LED Index Modulation (Spatial LIM)

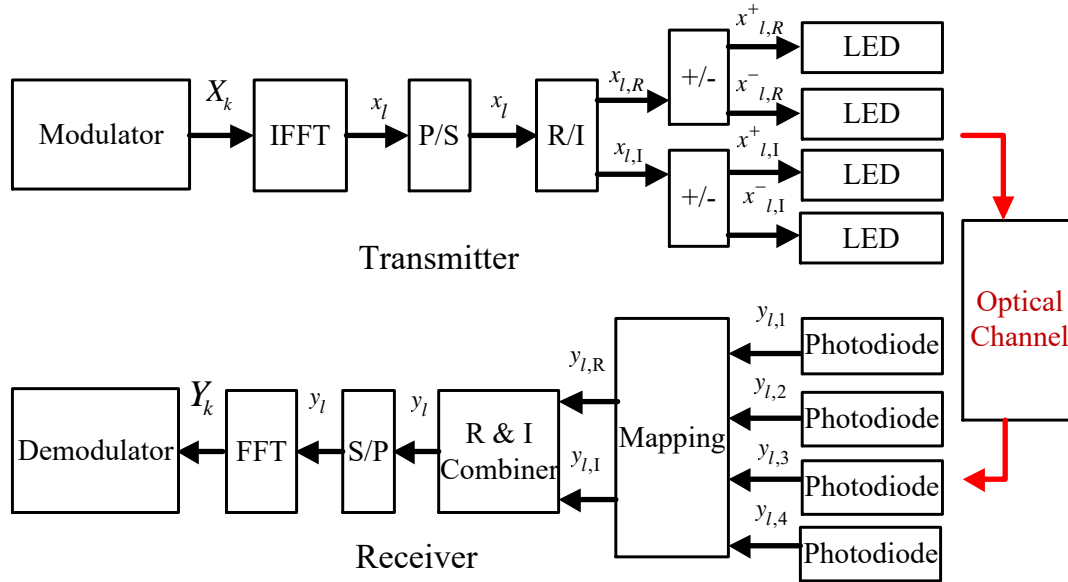


Fig. 5.1: Block diagram of LED index modulation for pixelated communication[65].

The block diagram of LIM-OFDM is shown in Fig. 5.1[65]. It is noted that Hermitian symmetry is required to make OFDM symbol real valued as conventional OFDM signal is complex in nature. Consequently, to achieve compatibility to IM/DD systems complexity increases. Like other OFDM formats, Hermitian symmetry is not required in LIM-OFDM. In the beginning, message data bits are modulated using the modulation block. M-array QAM method is used where M is the modulation order. Using N point inverse fast Fourier transform (IFFT) frequency domain signal X_k is converted to time domain signal x_l after modulation. x can be expressed as:

$$x = [x_0, x_1, x_2, \dots, x_{N-1}] \quad (5.1)$$

Where N is the data size.

Each complex symbol x_l is obtained after parallel to serial conversion.

where $l = [0, 1, 2, \dots, N-1]$.

Afterward, the real and imaginary parts of the complex OFDM signal are separated. Next the sign of those real and imaginary components is checked. In LIM-OFDM [65], at least four LEDs are required where the first two LEDs are responsible to transmit real part, and the other two are responsible to transmit imaginary part for a single OFDM complex symbol. If the real part of complex symbol is positive then the first LED will be in „on state, and in that case the second LED will be in „off state“. But if the real part of complex symbol is negative then the reverse case will happen. In the same way, if the imaginary part of complex OFDM symbol is positive then the third LED will be in „on state“ and in that case the fourth LED will be in „off state“. Similarly, if the imaginary part is negative then the reverse case will happen. As the real or imaginary part of a complex symbol cannot be bipolar at a time two LEDs will be in off state in any circumstances.

In pixelated communication, a pixel within an image is the smallest transmitting unit. For spatial LIM-OFDM, four different image frames are required to represent the symbols in pixelated communication. Among four frames, two frames are required to send real valued positive and real-valued negative where others two frames are used to send imaginary-valued positive and imaginary-valued negative. It is considered that, the real ($x_{l,R}$) and imaginary ($x_{l,I}$) parts are separated from OFDM symbol x_l such that, $x = x_{l,R} + jx_{l,I}$. For both real and imaginary parts the polarity is then checked as the sign information of symbols is modulated by image index. $x_{l,R}^+$ and $x_{l,R}^-$ are used to express the positive and negative portions of $x_{l,R}$ respectively, as shown below:

$$x_{l,R}^+ = \begin{cases} x_{l,R}, & \text{if } x_{l,R} > 0 \\ 0, & \text{if } x_{l,R} < 0 \end{cases} \quad (5.2)$$

$$x_{l,R}^- = \begin{cases} 0, & \text{if } x_{l,R} > 0 \\ -x_{l,R}, & \text{if } x_{l,R} < 0 \end{cases} \quad (5.3)$$

In the same way, $x_{l,I}^+$ and $x_{l,I}^-$ are used to express the positive and negative portions of $x_{l,I}$ respectively, as shown below:

$$x_{l,I}^+ = \begin{cases} x_{l,I}, & \text{if } x_{l,I} > 0 \\ 0, & \text{if } x_{l,I} < 0 \end{cases} \quad (5.4)$$

$$x_{l,I}^- = \begin{cases} 0, & \text{if } x_{l,I} > 0 \\ -x_{l,I}, & \text{if } x_{l,I} < 0 \end{cases} \quad (5.5)$$

Then, four different pixels of four different images are illuminated for the four components of x_l . In Spatial LIM-OFDM four image frames are found in case of single OFDM image frame. LCD screen of transmitter is used to transmit these four image frames sequentially. Camera of the receiver section is used to capture these images and it is considered that there is no synchronization error in the receiver. CMOS sensor of camera provides the electrical domain data from optical domain. Channel noise in the electrical domain is modelled as AWGN to keep consistency with the literature [77]. The mapping block is used to map the four components of the noisy electrical signal and to estimate the real, $y_{l,R}$ and imaginary portion, $y_{l,I}$. In receiver, y_l which is the complex time domain signal can be expressed as bellow:

$$y_l = \pm y_{l,R} \pm jy_{l,I} \quad (5.6)$$

The frequency domain signal Y_k is obtained after serial to parallel conversion and FFT operation. Lastly, demodulation is performed for data recovery.

5.3 Spatial Non-DC Biased Modulation (Spatial NDC)

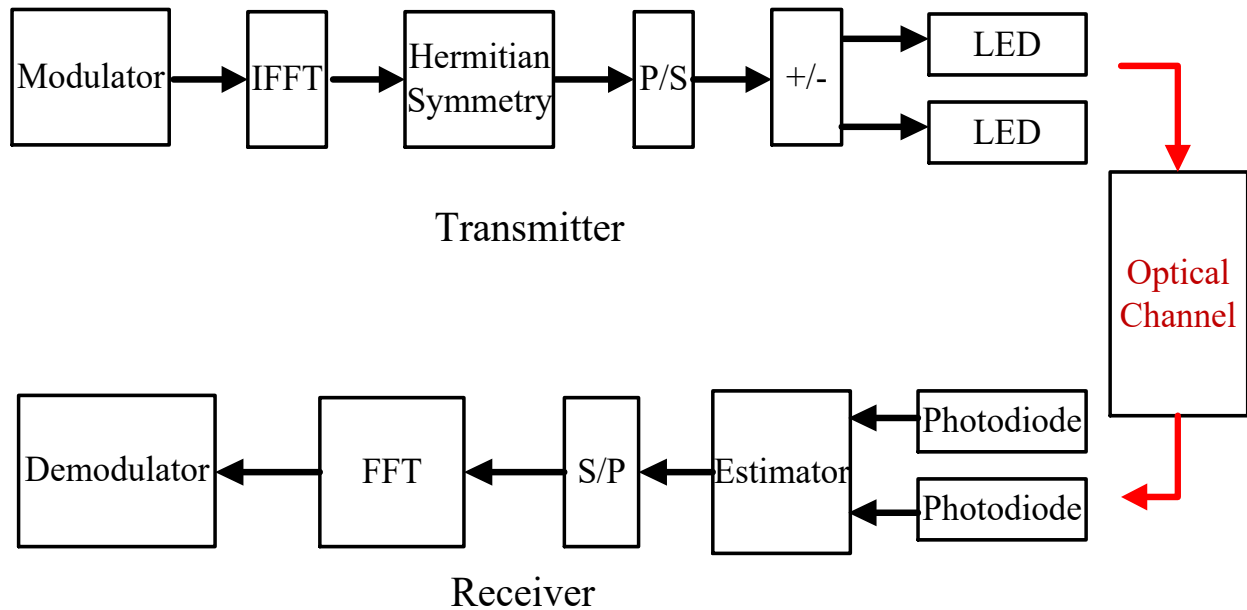


Fig. 5.2: Block diagram of non-DC biased modulation for pixelated communication[64].

The system architecture of NDC-OFDM is shown in Fig. 5.2 [64]. SNDC-OFDM uses Hermitian symmetry block which converts complex number into real and that's why SNDC-OFDM does not need real and imaginary separator blocks. This is the main difference between SLIM-OFDM and SNDC-OFDM. In NDC-OFDM [64], the positive and negative valued symbols are responsible to illuminate two different LEDs. But in SNDC-OFDM, positive and negative valued symbols are carried by two different image frames. The sign and magnitude of the symbols are estimated by an estimator in the receiver section. With comparison to SLIM-OFDM and SNDC-OFDM, both LIM-OFDM and NDC-OFDM need higher infrastructure cost as these are taking advantage of the spatial domain by using multiple LEDs.

5.4 Simulation Results

The BER performances of different OFDM forms are investigated in this section. For the evaluation of BER performance, both average electrical and average optical power are considered in this work. The power efficiency metric for average electrical power limited channels is not the same as metric for average optical power. The average optical power and average electrical power will depend on $E\{s_l\}$ and $E\{s_l^2\}$ respectively if the electrical signal is s_l , where $E\{\bullet\}$ is the expectation operator. A modulation scheme with high electrical to optical power ratio $E\{s_l^2\}/E\{s_l\}$ is required for a fixed $E\{s_l\}$ to obtain a better BER. Alternatively it can be said that, if a system transform optical power to electrical power efficiently only then better BER can be expected. Here $E_{b(opt)}/N_0$ is the received optical energy per bit to single sided noise spectral density and $E_{b(elec)}/N_0$ is the received electrical energy per bit to single sided noise spectral density. As $E_{b(opt)}/N_0$ takes into account the optical to electrical conversion efficiency, so it is more useful performance metric. Both are taken as metrics in this work.

Both a channel with spatial impairments and an AWGN channel are modeled in case of pixelated communication system. MATLAB tool is used to obtain simulation results. A CP of 10 %, 4-ary and 16-ary quadrature amplitude modulation (QAM) constellations and 256 number of OFDM subcarriers are considered for simulations.

An important fact is that, using only the odd subcarriers, data are modulated in case of SACO-OFDM, though both the odd and even subcarriers are used to modulate data in SLIM-OFDM, SNDC-OFDM, SDCO-OFDM and SADO-OFDM. With the aim of yielding this difference in the spectral efficiency of various modulation forms the total transmitted optical power is normalized to unity.

The power level on ACO-OFDM and DCO-OFDM elements govern the BER performance of ADO-OFDM.

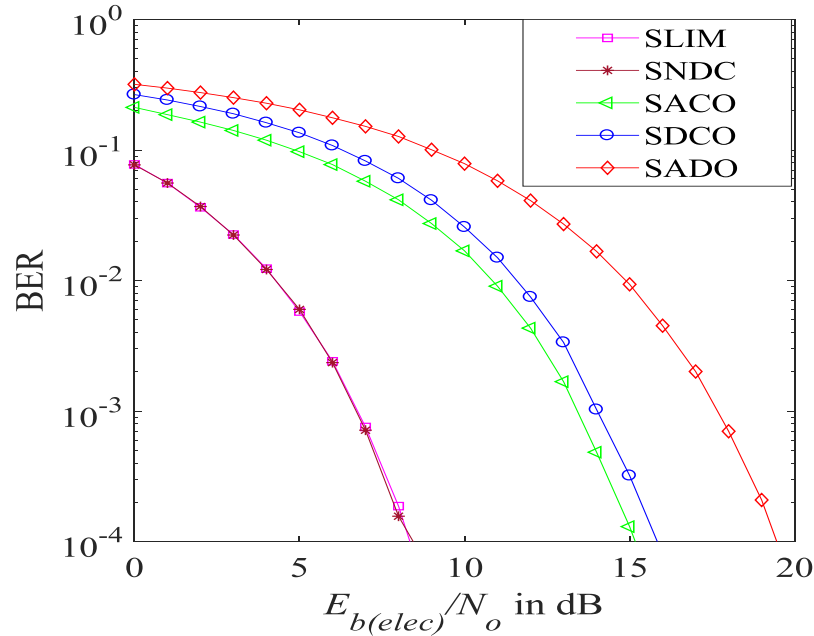


Fig. 5.3: BER vs. $E_{b(elec)}/N_0$ curve in pixelated systems for stand-alone AWGN channels.

In this section, the BER performance of SLIM-OFDM modulation is compared with SNDC-OFDM, SDCO-OFDM, SACO-OFDM and SADO-OFDM. 16-QAM SACO-OFDM has to be compared with 4-QAM SLIM-OFDM, 4-QAM SNDC-OFDM, 4-QAM SDCO-OFDM and 4-QAM SADO-OFDM as only the odd subcarriers are used in SACO-OFDM. The BER performance of SADO-OFDM depends on the levels of power on SACO-OFDM and SDCO-OFDM elements within SADO-OFDM. When SADO-OFDM is considered in the simulations, it is assumed that 70% power is on SACO-OFDM element and 30% power is on SDCO-OFDM component.

Fig. 5.3 shows the plots of BER versus $E_{b(elec)}/N_0$ for AWGN channel for pixelated systems. It is seen from the plot that, the BER performance of both

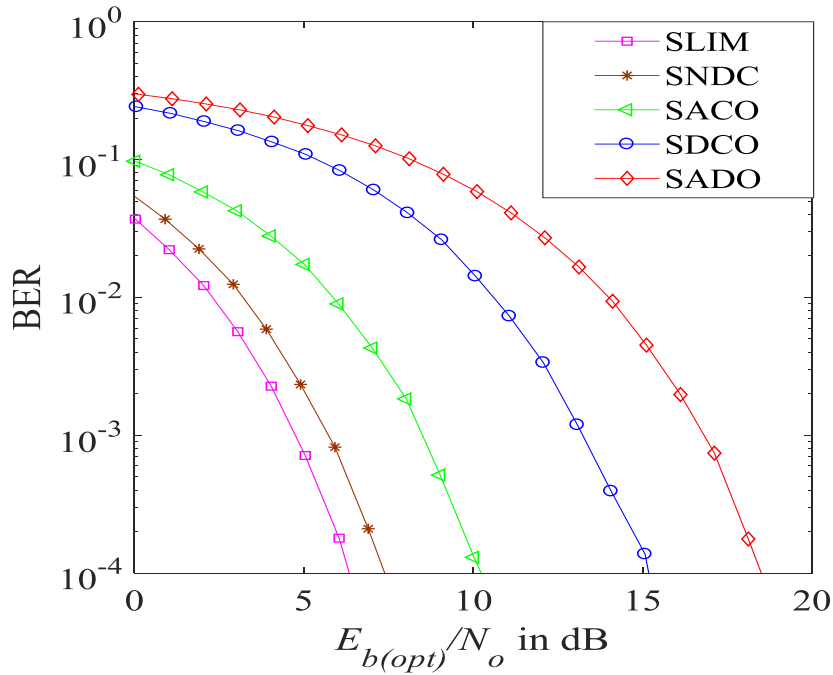


Fig. 5.4: BER vs. $E_{b(opt)}/N_0$ curve for pixelated systems for stand-alone AWGN channels

SLIM-OFDM and SNDC-OFDM are 7 dB better than 16-QAM SACO-OFDM for a target BER of 10^{-4} . In addition, SNDC-OFDM and SLIM-OFDM are 5 dB and 8 dB better than SACO-OFDM and 4-QAM SDCO-OFDM respectively. Now, in terms of electrical power efficiency SLIM-OFDM is very close to SNDC-OFDM.

Next, Fig. 5.4 shows the plots of BER versus $E_{b(opt)}/N_0$ for AWGN channels for pixelated systems. It is seen that, the BER performance of SNDC-OFDM is 2 dB and 7 dB superior to 4-QAM DCO-OFDM and 16-QAM ACO-OFDM respectively. However, for a given BER of 10^{-4} , 4-QAM LIM-OFDM is 1.3 dB better than SNDC-OFDM. Furthermore, 4-QAM SNDC-OFDM is almost 11 dB more optically power efficient than 4-QAM SADO-OFDM. So, it is clearly seen from Fig. 5.4 that SLIM-OFDM provides higher electrical to optical power ratio than SNDC-OFDM.

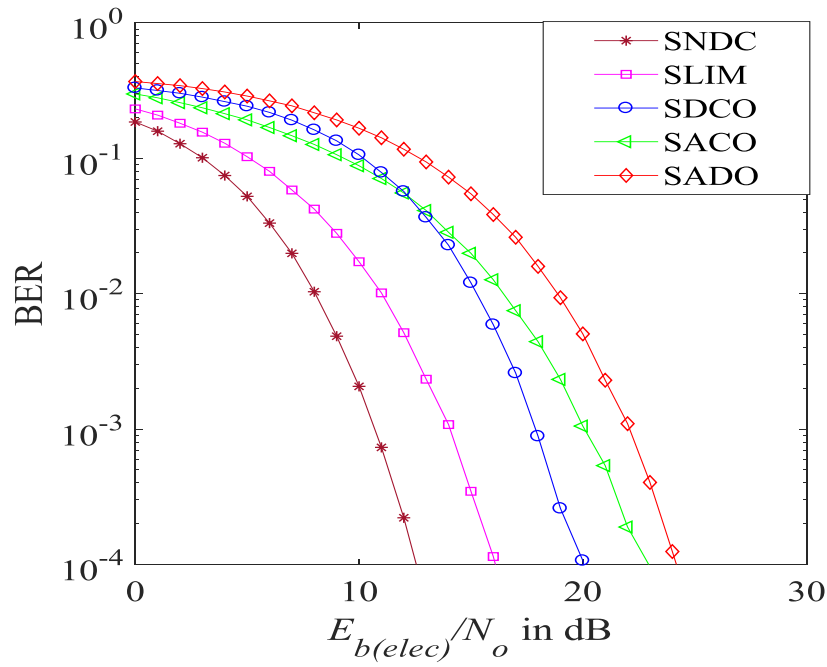


Fig. 5.5: BER vs. $E_{b(elec)}/N_o$ curve for pixelated systems with different impairments

Then, with presence of spatial impairments in case of pixelated communication system the BER performances are evaluated for different optical spatial OFDM schemes. AWGN channel with the concurrent presence of LFM, defocus, vignetting is considered for all the plots.

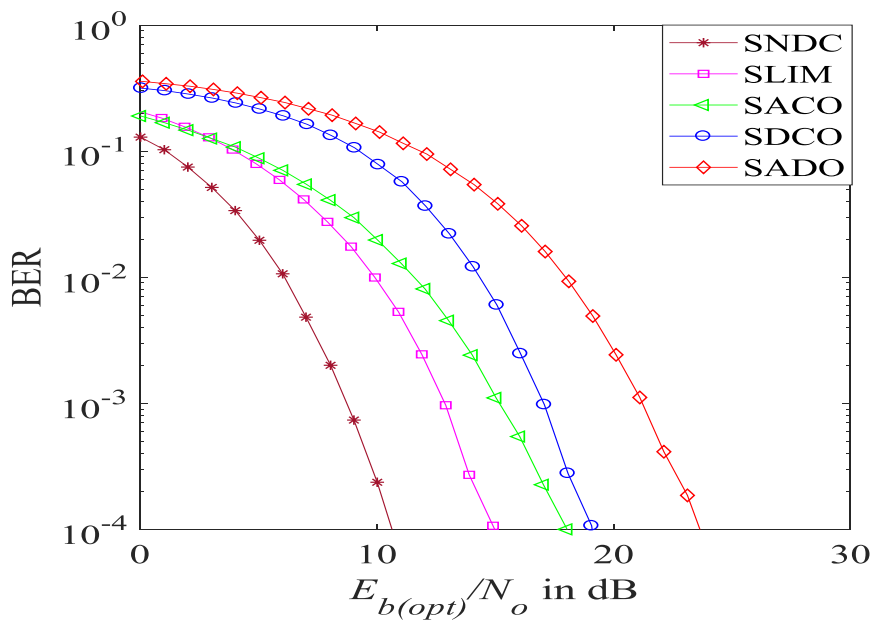


Fig. 5.6: BER vs. $E_{b(opt)}/N_o$ curve for pixelated systems with different impairments

Higher subcarriers are kept null and the received signal is equalized in order to overcome defocus. In terms of electrical power efficiency SNDC-OFDM provides better performance than SLIM-OFDM shown in Fig. 5.5. The difference between them is 3dB. To achieve a BER of 10^{-4} , the required $E_{b(elec)}/N_0$ for SNDC-OFDM, SLIM-OFDM, SACO-OFDM, SDCO-OFDM and SADO-OFDM are 12 dB, 16 dB, 20dB 23 dB and 24 dB, respectively.

For a pixelated system with impairments the BER versus $E_{b(opt)}/N_0$ curve is shown in Fig 5.6. From Fig. 5.6 it is clear that, with comparison to 4-QAM SLIM-OFDM, 4-QAM SNDC-OFDM is approximately 4 dB more optical power efficient.

5.4 Conclusion

SLIM and SNDC are explained with block diagrams in this chapter. Later, simulation results are incorporated to realize which one is more electrical and optical power efficient between SLIM and SNDC. From the BER curves, it is clear that SNDC performs better than SLIM, SACO and SDCO if channel is modeled with different spatial impairments like motion blur, LFM, vignetting along with channel noise.

On the other hand, when channel is modeled only with AWGN, SLIM shows better optical power efficiency than SNDC. But, though SLIM and SNDC both show better electrical and optical power efficiency than SDCO and SACO in every case, the data rate of SLIM and SNDC is lower than SDCO and SACO because SLIM and SNDC take the advantage of temporal domain by using multiple image frame to encode a single spatial OFDM frame. In simulation, target BER of 10^{-4} is considered as no channel coding is used. By using channel coding it can be further reduced to 10^{-9} .

CHAPTER SIX

PRACTICAL EXPERIMENT

6.1 Overview

In this chapter, procedure of practical experiment is explained along with BER calculation from recovered data. Data is recovered from images which are received from practical experiments. Three different experiments are done for motion blur, rotational misalignment and for perspective distortion respectively. For each case, SDCO and 4QAM modulation are performed on random generated data before image creation and transmission. After receiving, original data is recovered from received impaired images.

This chapter is organized as follows: the following section will describe the process of practical experiment including set up of practical a pixelated system, block diagram of transmitter and receiver. The next section will explain procedure of capturing angular misaligned images from practical experiment and data recovery from it. Similarly, next two sections will deal with BER calculation from captured images with perspective distortion impairment and motion blur impaired images respectively.

6.2 Experimental Set-up

A schematic diagram of a practical pixelated system has been presented in Fig. 6.1. The LCD screen of a Laptop is used as the transmitter and the camera of a webcam is used as the receiver. Using MATLAB tool, random binary data of specific matrix size is generated in the laptop. Next, the data matrix is converted into image frame for transmission and displayed in LCD screen of laptop. The camera of webcam is used to capture that transmitted image. Data cable is used to connect the webcam to another laptop in order to transfer the image frame to receiver Laptop. Decoding is performed using MATLAB software in receiver Laptop. A series of images are transferred according to this process when BER is calculated in case of practical impaired images explained later in this chapter.



Fig. 6.1: Schematic diagram of practical pixelated communication system

6.2.1 Transmitter

Fig. 6.2 represents the block diagram of transmitter of practical experiment of pixelated communication. In his experiment, the transmitter is the LCD screen of a Laptop with resolution of 1366×768 pixels. Using MATLAB software a 20×20 matrix containing random binary data is generated for modulation. This random data matrix is then modulated following 4QAM technique. After that, inverse fast Fourier transform, Hermetian symmetry and dc bias adding are performed to complete SDCO operation. The SDCO encoded data matrix is then used to create a gray scale image using MATLAB. This created image has 20×20 cells where each cell is represented by a group of pixels. Four corner points of image is marked red using MATLAB to make easier detection of corner point in receiver.

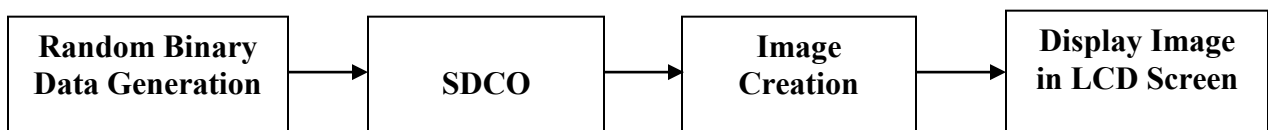


Fig. 6.2: Transmitter block diagram of pixelated systems

6.2.2 Receiver

Fig. 6.3 shows the block diagram of receiver portion of practical experiment of pixelated communication. After capturing the image, the data is transferred to a personal computer or

laptop for decoding the image for recovery of the transmitted data. From each image frame, the region of interest (ROI) is segmented by detecting four corner points which are marked as red in grey scale image before transmission. After segmenting, the main challenge of receiver is to regenerate the original image. As the resolution of LCD screen of transmitter Laptop and the camera of receiver is not same, it is not known to receiver that how many pixels are representing a single cell in received image.

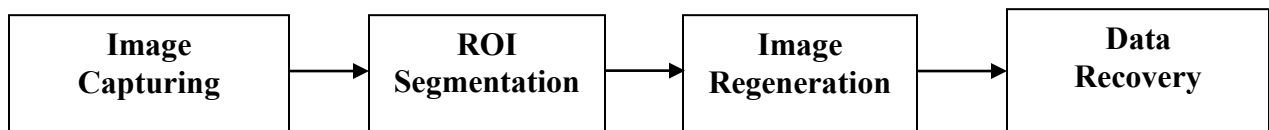


Fig. 6.3: Receiver block diagram of a pixelated system

In receiver laptop, the segmented image is divided into 20×20 cells and all pixel values of each cell are averaged to estimate the original value of the pixel. This has to be done as in transmitted image a group of pixel representing the same value of a single data. Finally, data is recovered for regenerated image using fast Fourier transform and QAM demodulation. The transmitted image, received image, segmented *region of interest* (ROI) and decoded images are shown in Fig. 6.4(a), (b), (c) and (d), respectively.

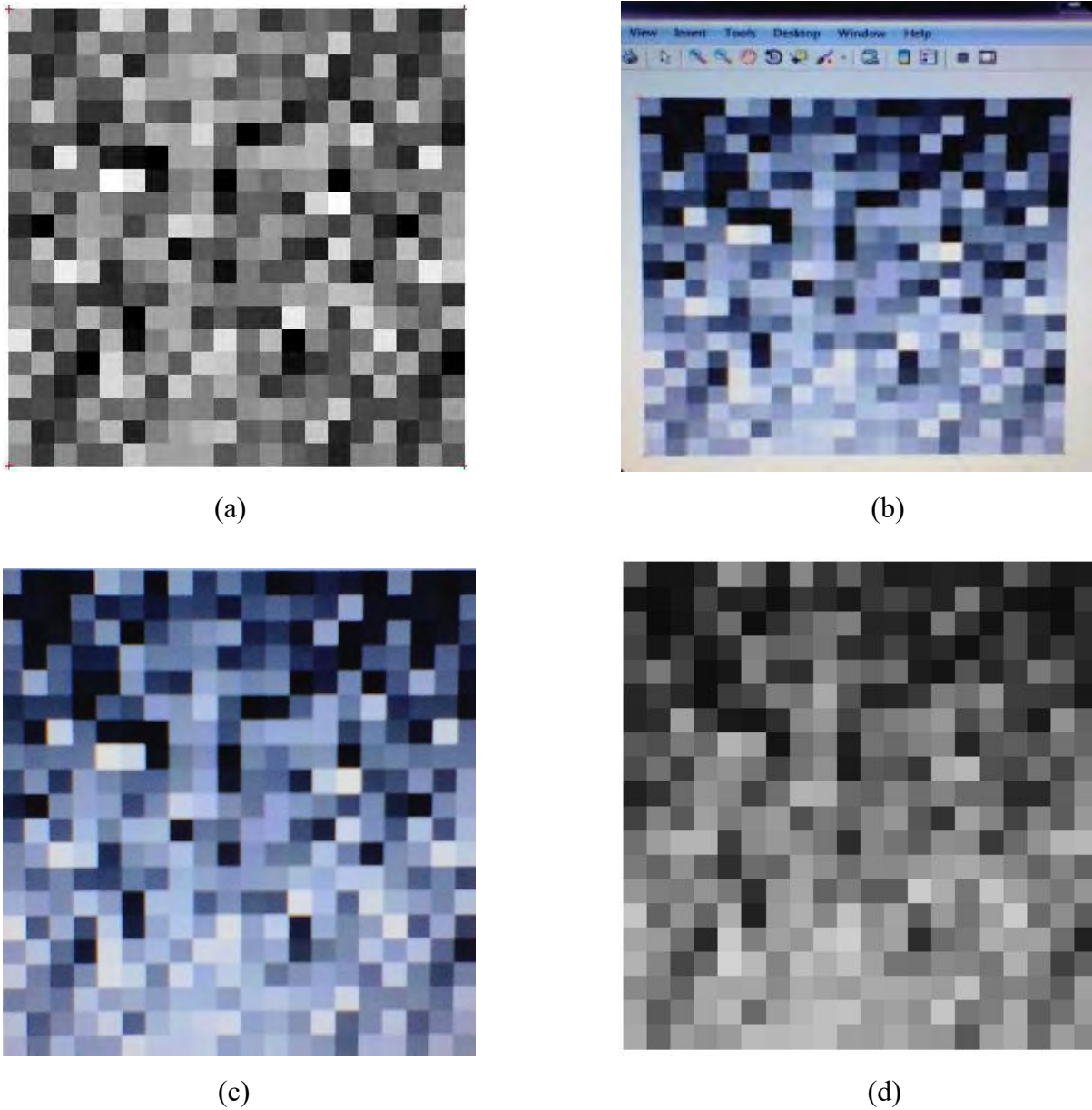


Fig 6.4: (a) Transmitted image, (b) Received image, (c) Segmented ROI, (d) Decoded image

6.3 Angle Correction of Rotational Misaligned Image

An important impairment is rotational misalignment which causes angular separation between transmitted and received images. In this experiment, rotational misaligned images are found because receiving camera is tilted at an angle with respect to transmitting screen. Pixel coordinate of received image now is not same as transmitted one because during image capturing, receiving device is not angularly aligned with transmitted device and the angle separation is

unknown to receiving device. In that case, to regenerate the original bit stream from received image, corner detection of the information bearing image portion and angular alignment with respect to transmitted image is necessary. Without corner detection, region of interest (ROI) cannot be identified. Moreover, for automatic segmentation of ROI, angular alignment is also important. During transmission, transmitting device marks four corners of the images with specific color so that receiving device can easily detect the corner points. After detecting the corner points, angular misalignment is removed using this simple algorithm in MATLAB. Finally ROI is segmented for demodulation and decoding. The steps of the algorithm are:

- Read the coordinate value of at least two corner points of reference image.
- Read the coordinate value of the respective corner points of received image.
- Calculate the transformation matrix from these two pair of points.
- Determine the new coordinate value of all points of received image by multiplying existing coordinate value and transformation matrix.
- Relocate the pixel value of every point of received image according to new coordinate values so that the angular distance becomes zero.

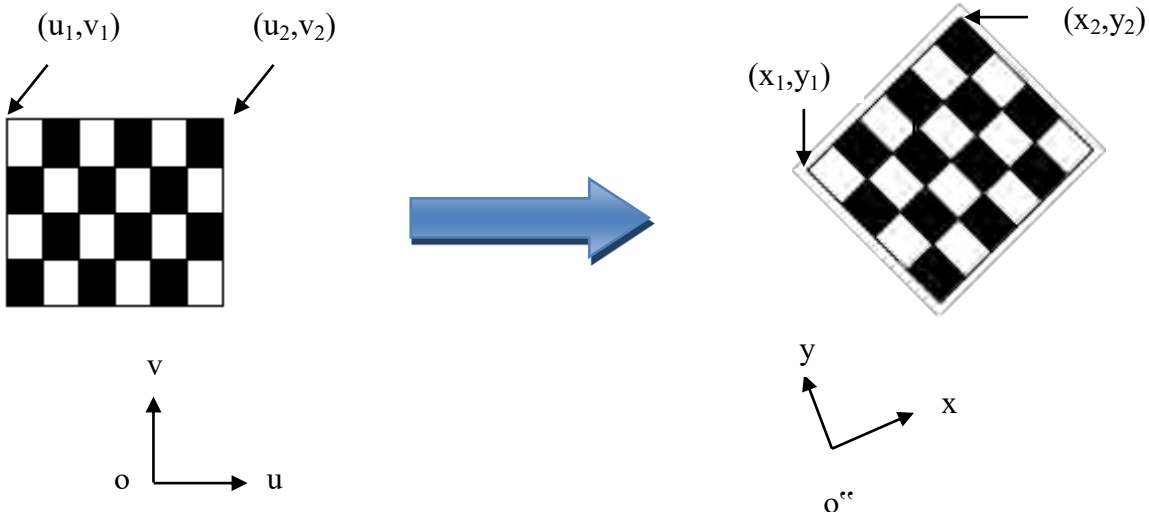


Fig. 6.5: Coordinate changing for image rotation

Fig. 6.5 shows that rotation of image causes coordinate changing of pixel intensity values. If the relation between these two coordinates can be determined then it will be easy to minimize the

angular separation to zero degree. In order to determine the relation between these two coordinate, 3×2 transformation matrix is calculated. The transformation matrix [92] is:

$$T = \begin{bmatrix} t_1 & -t_2 \\ t_2 & t_1 \\ t_3 & t_4 \end{bmatrix} \quad (6.1)$$

If the coordinates of transmitted and received images are uv and $o'xy$, respectively, then the relation [92] between these two coordinate is:

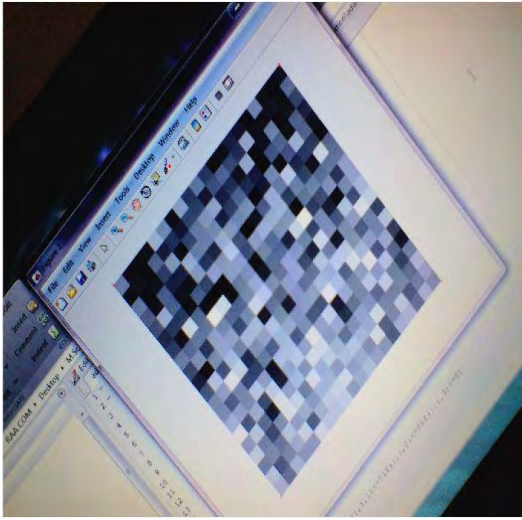
$$\begin{bmatrix} u & v \end{bmatrix} = \begin{bmatrix} x & y & 1 \end{bmatrix} T \quad (6.2)$$

From (6.1) and (6.2), two homogeneous equations can be found;

$$u = t_1x + t_2y + t_3 \quad (6.3)$$

$$v = -t_2x + t_1y + t_4 \quad (6.4)$$

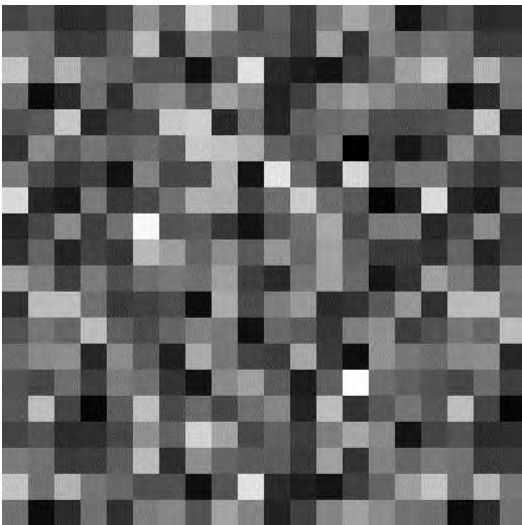
Where, t_1, t_2, t_3, t_4 are the coefficients of transformation matrix. It is clear that without information of transmitted image coordinates the coefficients of transformation matrix cannot be calculated. As a reference image is prior known to receiver, the coordinate information of transmitted image is extracted from it. At least two pair of points is necessary to solve Equation (6.3) and (6.4). In receiver, four corner points are detected to segment ROI. Now the coordinate values of any two corner points of received image along with corresponding coordinate values of reference image are used to calculate the coefficients of transformation matrix. Once the coefficients of transformation matrix is calculated then using Equation (6.3), coordinate of received image can be transformed to coordinate of transmitted image so that the angular separation between these two images become zero. Fig. 6.6 (a) shows rotational misaligned image from practical experiment where Fig. 6.6(b) shows alignment corrected image. For this process required reference image is shown in Fig. 6.6(c) and segmented ROI is shown in Fig. 6.6(d).



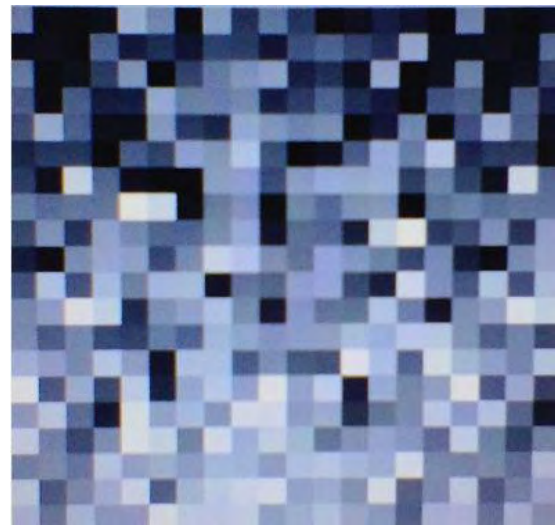
(a)



(b)



(c)



(d)

Fig. 6.6: (a) Rotational misaligned image, (b) Rotational alignment corrected image, (c) Reference Image, (d) Segmented ROI

BER is not calculated for this impairment because using this method received image can be turned into same as transmitted image if transmitted image is only impaired by rotational misalignment.

6.4 BER Calculation from Perspective Distorted Images

When images are captured if the receiver is moving, perspective distortion is inevitable, as all portions of the image are not at the same distance from the camera lens of the receiving device. To understand the effect of perspective distortion on BER performance, perspective distorted images should be captured first, and then data should be recovered from them. In this experiment, perspective distorted images are received because the receiving camera is nearer to the upper portion of the LCD display of the laptop than the lower portion. As a result, distorted images are captured by the camera. Projective transformation can be used to correct this distortion. According to this method, the size of the transmitted image should be known to the receiver previously. The receiver creates a reference image from random data which has a size the same as the transmitted one.

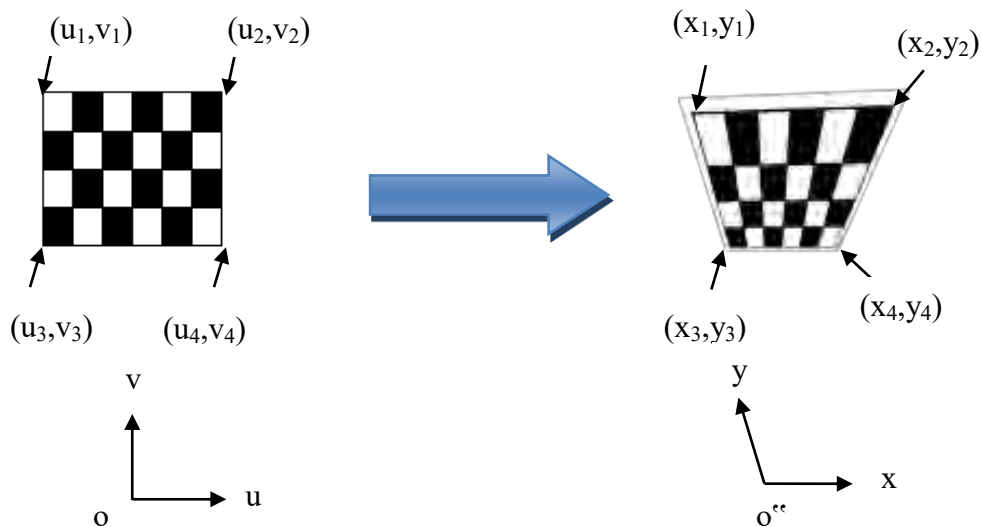


Fig. 6.7: Geometric transformation for perspective distortion

When the camera is closer to one portion of the transmitted image than the rest of the part of the image, perspective distortion occurs. It is shown in Fig. 6.7 that the upper portion is expanded more than the lower part due to perspective distortion, and the coordinates of the received image are not the same as those of the transmitted one. If the coordinates of the received image can be transformed into the coordinates of the transmitted one, this distortion can be minimized.

So the 3×3 transformation matrix [92] T which relates these two coordinates is:

$$T = \begin{bmatrix} t_1 & t_4 & t_7 \\ t_2 & t_5 & t_8 \\ t_3 & t_6 & t_9 \end{bmatrix} \quad (6.5)$$

Where, $t_1, t_2, t_3, t_4, t_5, t_6, t_7, t_8, t_9$ are the coefficients of transformation matrix. If the coordinates of transmitted and received image are $ou\upsilon$ and $o'x'y$ respectively then the relation between these two coordinates [92] is defined by coefficients of transformation matrix as follows:

$$u = \frac{t_1x + t_2y + t_3}{t_7x + t_8y + t_9} \quad (6.6)$$

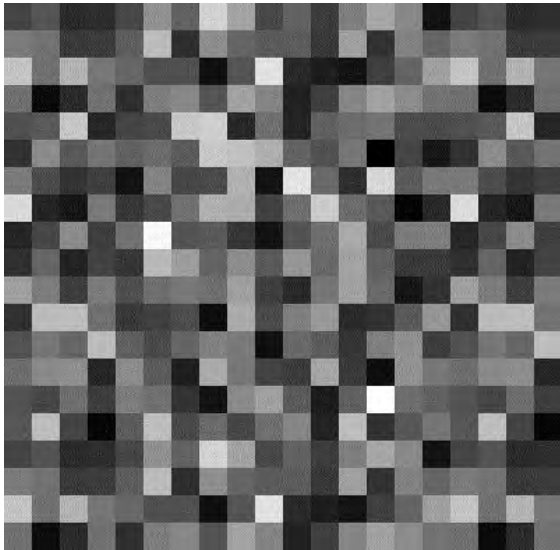
$$v = \frac{t_4x + t_5y + t_6}{t_7x + t_8y + t_9} \quad (6.7)$$

To find out the coefficients of transformation matrix at least four corresponding point pairs from reference image and received image is necessary. As four corner points are needed to detect to segment ROI, in this experiment four corner points are used to determine the coefficients of transformation matrix. After that, coordinate of received image is transformed into coordinate of transmitted image using Equation (6.6) and (6.7) for all pixel. This whole process is called projective transformation which is performed by MATLAB software. In brief projective transformation can be explained by the following steps:

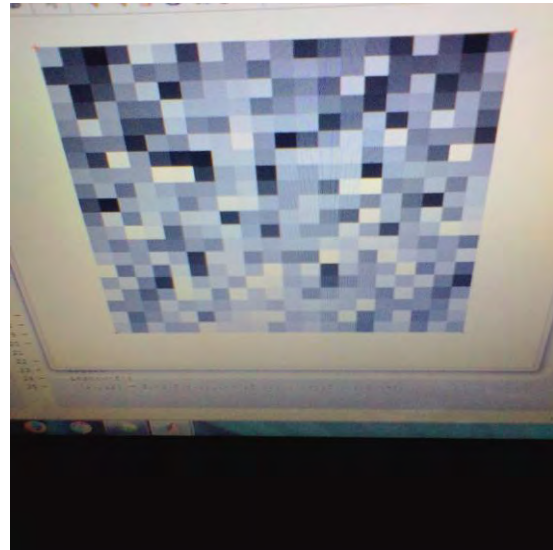
- a) Consider at least four set of point correspondences between reference image and distorted image.
- b) Compute transformation matrix from four pair corresponding points of reference and received image.
- c) Correct the distorted image using the transformation matrix.

A series of 20 images are transmitted and processed after reception to understand the effect of perspective distortion and projective transformation for real time pixelated communication.

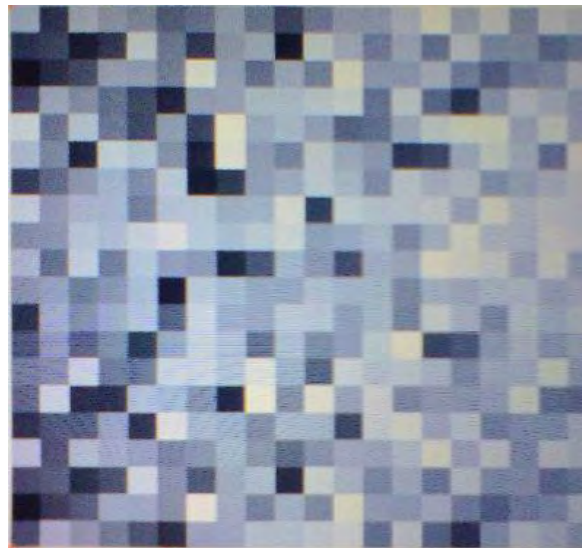
Reference image frame is shown in Fig. 6.8(a). Fig. 6.8(b) shows the perspective distorted received image and after projective transformation corrected image is shown in Fig. 6.8(c). Fig. 6.9 and 6.10 are representing BER curve for distorted images and projective transformed images respectively. For using projective transformation the performance of communication is improved showed in Fig. 6.10.



(a)



(b)



(c)

Fig. 6.8: (a) Reference image, (b) Received distorted image,
(c) Image after projective transformation

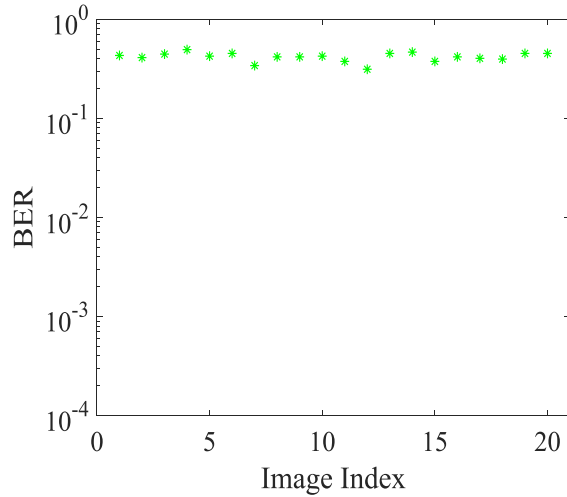


Fig. 6.9:

BER curve (distorted images)

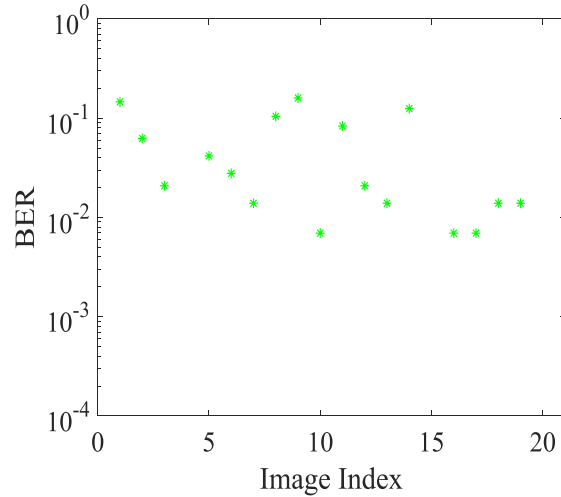


Fig. 6.10:

BER curve (projective transformed images)

The amount of prospective distortion is not same for 20 images. Also there are others noise too for every received image which are not considered in case of decoding. As a result the BER curve of Fig. 6.10 shows random pattern.

6.5 BER Calculation from Motion Blurred Images

Motion blur is a common impairment in pixelated communication system. In this experiment, LCD screen of Laptop shows encoded image having no high frequency component at first. During image capturing, camera is not immobile which results motion blur in the received image. After capturing all images by camera, Laptop screen is used to show images having high frequency component. One sample of image having higher frequency is shown in Fig. 6.11 and Fig. 6.12 represents another image having no higher frequency. For both type of image transmission corner points are marked as red color so that these points can be detected in receiver. In this experiment, room is remained dark so that no ambient light can affect the performance of communication. As the camera is not static during transmission both angular misalignment and perspective distortion is found along with motion blur in received images. For first 20 images having high frequency component, the algorithms of angular misalignment correction and projective transformation described in previous two sections are applied first. Then ROI is segmented and decoded for data recovery. Similar process is followed for second 20

images having no high frequency components for data recovery and to understand the effect of motion blur on low frequency components. In receiver, using MATLAB tool better bit error rate performance is found for image containing no high frequency component with respect to having high frequency component. 20×20 bit data is modulated and encoded for transmission as image shown in Fig. 6.13. Fig. 6.14 and 6.15 show received image and segmented image respectively. Recovered image is shown in Fig. 6.16. For almost same amount of blur, better bit error rate performance is found at second time shown in Fig. 6.17 and 6.18 which proves that motion blur affects higher subcarrier much more than lower subcarriers. So, for motion blur impaired channel, BER can be made lower in expense of lower spectral efficiency.

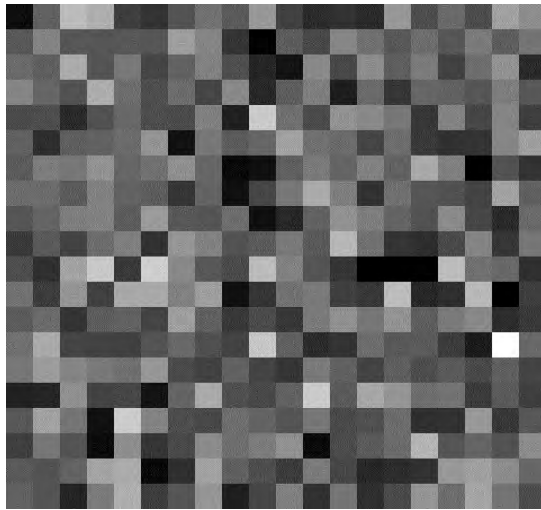


Fig. 6.11: Image with higher frequency

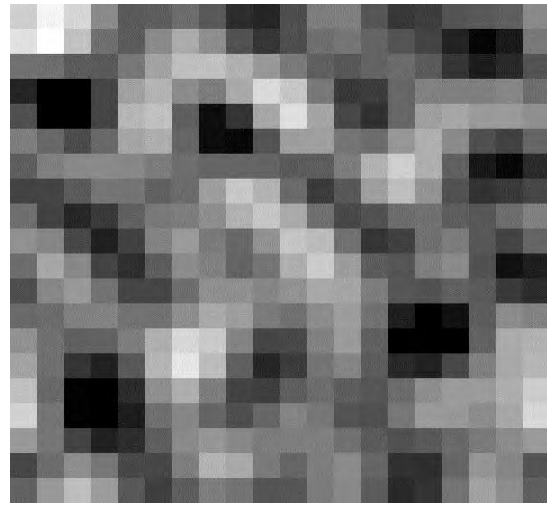


Fig. 6.12: Image without higher frequency

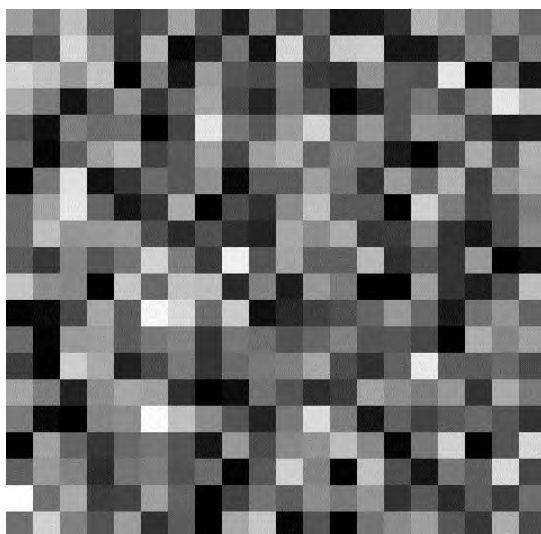


Fig. 6.13: Transmitted image

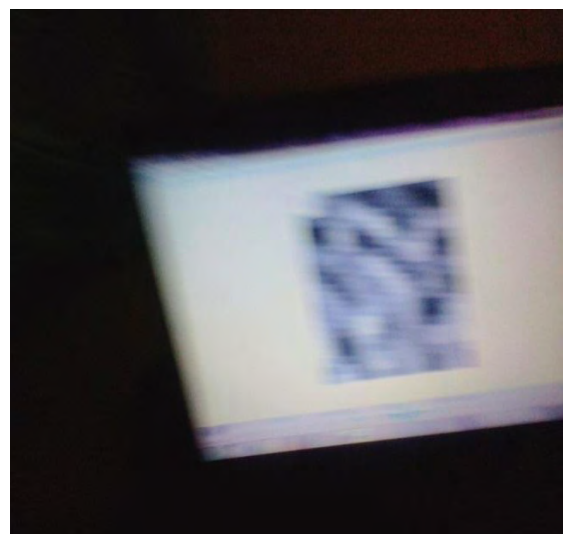


Fig. 6.14: Received motion blurred image

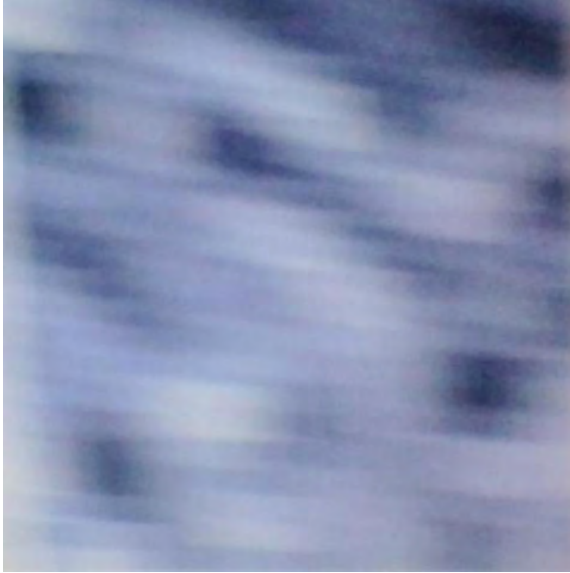


Fig. 6.15: Segmented ROI

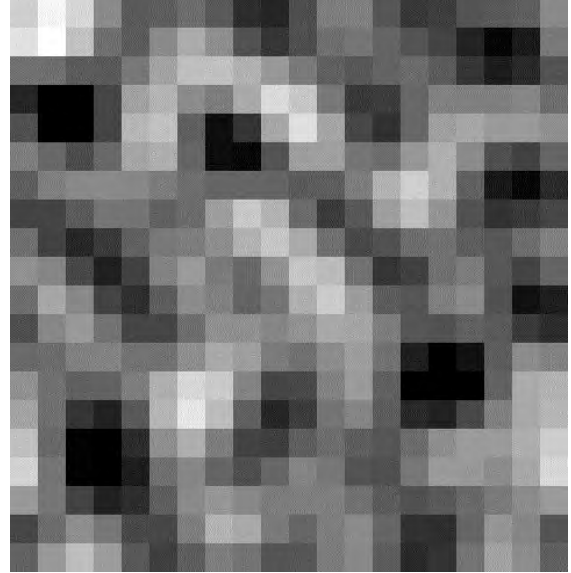


Fig. 6.16: Recovered image

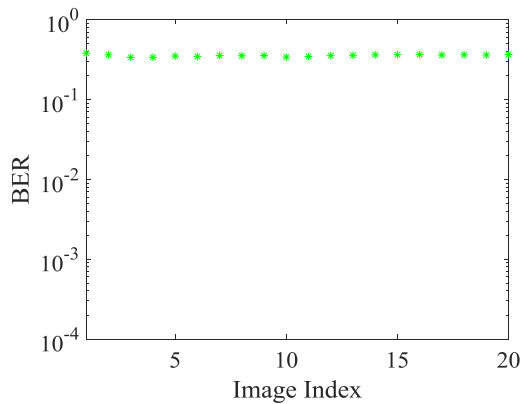


Fig. 6.17: BER using higher frequency

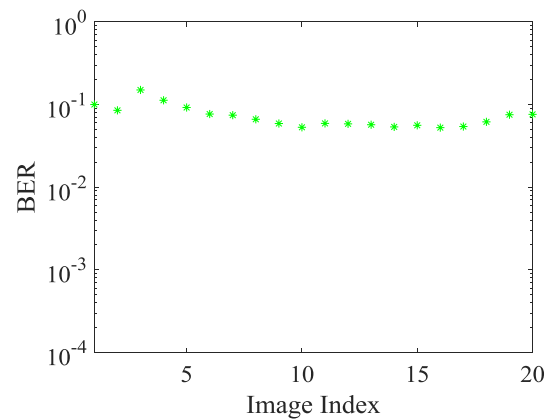


Fig. 6.18: BER without using higher frequency

6.6 Conclusion

In this chapter, a set up of practical experiment is shown with necessary diagrams. A pathway is explained how to deal with received image to decode data from it. A process is explained to mitigate rotational misalignment of received image where the rotational angle and direction is unknown to receiver. Finally, the BER performance is presented which clearly indicates the effect of motion blur and perspective distortion in practical pixelated communication. In all the experiments, SDCO encoded images are used to understand the effect of impairments in practical

communication. From these experiments, it can be said that these impairments will also affect the performance of practical pixelated communication if other spatial optical OFDM methods are used instead of SDCO.

CHAPTER SEVEN

CONCLUSION

7.1 Introduction

In this thesis, the effect of motion blur on pixelated image due to lateral or angular motion is modeled mathematically. The joined effect of motion blur and defocus blur as well as the combined effects of LFM, vignetting, defocus and motion are also investigated. Five different spatial optical OFDM methods are applied on a pixelated system to find out the best candidate in terms of electrical and optical power efficiency. Only AWGN channel is modeled first and then another channel is considered which represents not only AWGN channel but also all impairments like LFM, vignetting, defocus and motion blur. Practical experiments are also carried out to understand the difference of simulation and practical environment. Some techniques are also applied to mitigate real time problem faced in practical experiments.

7.2 Contributions

The contributions of this thesis are the following:

- i. For the first time, the effects of linear (vertical or horizontal) and angular (45^0 or 135^0 or 225^0 or 315^0) motion are derived for any length of motion mathematically in the context of pixelated communication system in **Chapter 4**. As the joint effects of defocus and motion (linear and angular) are derived, the effect on each subcarrier for two types of blur becomes clear. Most complex scenario occurs when all impairments remain present. This scenario is also considered and mathematically a complex model is derived which concludes that individual impairments are independent.
- ii. Two new optical OFDM methods are extended to spatial domain for pixelated communication system termed as SLIM-OFDM and SNDC-OFDM with detailed descriptions in **Chapter 5**. These two methods are compared with three basic optical

OFDM methods to find out the best candidate in presence of channel noise and impairments. SNDC-OFDM provides more electrical and as well as optical power efficiency than all other modulation methods when all impairments are present along with channel noise though SLIM-OFDM shows better result in terms of optical power efficiency when only AWGN is present in channel.

- iii. Practical experiment is conducted to understand real time scenario. For motion blur, angular misalignment and perspective distortion; separate experiments are done for each case and from received group of images the BER is calculated. Some techniques are described in **Chapter 6** to mitigate the impact of practical impairments experienced in practical demonstration. After applying these techniques again, the BER is calculated and this time the results improve from previous.

7.3 Recommendations

Some recommendations for possible future research are:

- i) In case of mathematical model derivation, the effects of motion, defocus, LFM and vignetting are considered. Angular misalignment and perspective distortion are not considered, as a result this model is unable to indicate the impact of these two impairments. To find mathematically the individual effect and also the joint effect of these two impairments along with others impairments can be a research direction in future. During analyzing analytically, channel can be modeled with considering the all kinds of noise along with AWGN and impairments.
- ii) The proposed two spatial OFDM methods can be compared with other existing methods with considering different constellation size and position of transmitter and receiver, with modeling the channel of noise caused by ambient light may lead different result as these parameters may have impact on system performance.
- iii) In case of practical experiment, some techniques are elaborated to deal with motion, angular misalignment and vignetting. In case of motion blur generation only receiving device is used to shake while the transmitting one is fixed in its position. So by shaking both devices, the effect of relative motion can be analyzed from performance curve which will be more

realistic. LFM and LIM are not considered for practical experiments. So, removing or reducing the effects of LFM and LIM from practical pixelated images can be the future challenge.

REFERENCES

- [1] O'Brien, D., Turnbull, R., Minh, H. L., Faulkner, G., Bouchet, O., Porcon, P., Tabach, M. E., Gueutier, E., Wolf, M., Grobe, L., and Li, J., "High-speed optical wireless demonstrators: conclusions and future directions," *J. Lightw. Technol.*, vol. 30, pp. 2181-2187, 2012.
- [2] Bandara, K. and Chung, Y.-H., "Novel colour-clustered multiuser visible light communication," *Transactions on Emerging Telecommunications Technologies*, vol. 25, pp. 579-590, 2014.
- [3] Borah, D. K., Boucouvalas, A. C., Davis, C. C., Hranilovic, S., and Yiannopoulos, K., "A review of communication-oriented optical wireless systems," *EURASIP Journal on Wireless Communications and Networking*, vol. 2012, p. 91, 2012.
- [4] Li, T., Ni, Q., Malone, D., Leith, D., Xiao, Y., and Turletti, T., "Aggregation with fragment retransmission for very high-speed WLANs," *IEEE/ACM Trans. Netw.*, vol. 17, pp. 591-604, Apr. 2009.
- [5] Abichar, Z. and Chang, J. M., "Group-Based medium access control for IEEE 802.11n wireless LANs," *IEEE Trans. Mobile Comput.*, vol. 12, pp. 304-317, Feb. 2013.
- [6] Eldin, S. S., Nasr, M., Khamees, S., Sourour, E., and Elbanna, M., "LDPC coded MIMO OFDM-based IEEE 802.11n wireless LAN," in *IFIP International Conference on Wireless and Optical Communication Networks (WOCN)*, Cairo, Egypt, Apr. 2009.
- [7] Uysal, M. and Nouri, H., "Optical wireless communications_An emerging technology," in *Proc. Int. Conf. Transp. Opt. Netw.*, Jul. 2014, pp. 1_7.
- [8] Elgala, H., Mesleh, R., and Haas, H., "Indoor optical wireless communication: potential and state-of-the-art," *IEEE Commun. Mag.*, vol. 49, pp. 56-62, Sep. 2011.
- [9] Kahn, J. and Barry J., "Wireless infrared communications," in *Proc. IEEE*, vol. 85, pp. 265-298, 1997.
- [10] O'Brien, D., Katz, M., Wang, P., Kalliojarvi, K., Arnon, S., Matsumoto, M., Green, R., and Jivkova, S., "Short-range optical wireless communications," in *Technologies for the Wireless Future: Wireless World Research Forum (WWRF)*, vol. 2, pp. 277-296, 2006.
- [11] Green, R. J., Joshi, H., Higgins, M. D., and Leeson, M. S., "Recent developments in indoor optical wireless systems," *IET Communications*, vol. 2, pp. 3-10, 2008.
- [12] Hranilovic, S., *Wireless optical communication systems*: New York: Springer, 2004.
- [13] Feldman, M. R., Esener, S. C. , Guest, C. C., and Lee, S. H., "Comparison between optical and electrical interconnects based on power and speed considerations," *Appl. Opt.*, vol. 27, no. 9, pp. 1742_1751, Sep. 1998.
- [14] Miller, D. A. B., "Rationale and challenges for optical interconnects to electronic chips," *Proc. IEEE*, vol. 88, no. 6, pp. 728_749, Jun. 2000.

- [15] Kachris, C. , and Tomkos, I. , "A survey on optical interconnects for data centers," *IEEE Commun. Surveys Tuts.*, vol. 14, no. 4, pp. 1021_1036, 4th Quart., 2012.
- [16] Taubenblatt, M. A., "Optical interconnects for high-performance computing," *J. Lightw. Technol.*, vol. 30, no. 4, pp. 448_457, Feb. 15, 2012.
- [17] Khalighi, M. A., and Uysal, M., "Survey on free space optical communication:A communication theory perspective," *IEEE Commun. Surveys Tuts.*,vol. 16, no. 4, pp. 2231_2258, 4th Quart., 2014.
- [18] Hanson, F., and Radic, S., "High bandwidth underwater optical communication," *Appl. Opt.*, vol. 47, no. 2, pp. 277_283, 2008.
- [19] Gabriel, C.,Khalighi, M. A., Bourennane, S., Leon, P., and Rigaud, V., "Monte-Carlo-based channel characterization for underwater optical communication systems," *IEEE/OSA J. Opt. Commun. Netw.*, vol. 5, no. 1, pp. 1_12, Jan. 2013.
- [20] *IEEE Standard for Local and Metropolitan Area Networks_Part 15.7: Short-Range Wireless Optical Communication Using Visible Light*, IEEE Standard 802.15.7-2011, Sep. 2011, pp. 1_309.
- [21] Hemmati, H., *Deep Space Optical Communications*. Hoboken, NJ, USA: Wiley, 2006.
- [22] Chan, V. W. S., "Optical satellite networks," *J. Lightw. Technol.*, vol. 21, no. 11, pp. 2811_2827, Nov. 2003.
- [23] Kahn, J. M., and Barry, J. R. , "Wireless infrared communications," *Proc.IEEE*, vol. 85, no. 2, pp. 265_298, Feb. 1997.
- [24] Gfeller, F. R., and Bapst, U., "Wireless in-house data communication via diffuse infrared radiation," *Proc. IEEE*, vol. 67, no. 11, pp. 1474_1486, Nov. 1979.
- [25] Sichitiu, M. L., and Kihl, M., "Inter-vehicle communication systems: A survey," *IEEE Commun. Surveys Tuts.*, vol. 10, no. 2, pp. 88_105, 2nd Quart., 2008.
- [26] Wang, T. Q., Sekercioglu, Y. A., and Armstrong, J., "Hemispherical lens based imaging receiver for MIMO optical wireless communications," in *IEEE Globecom OWC workshop*, USA, Dec. 2012.
- [27] Elgala, H., Mesleh, R., and Haas, H., "Indoor Broadcasting via White LEDs and OFDM," *IEEE Trans. on Consumer Electron.*, vol. 55, no. 3, pp. 1127-1134, Aug. 2009.
- [28] O'Brien, D., Zeng, L., Hoa, L.M., Faulkner, G., Walewski, J. W., and Randel,S., "Visible light communications: Challenges and possibilities," in *Personal, Indoor and Mobile Radio Communications, 2008. PIMRC 2008. IEEE 19th International Symposium on*, 2008, pp. 1-5.
- [29] Boubezari, R., Minh, H. L., Ghassemlooy, Z., and Bouridane, A., "Smartphone camera based visible light communication," *J. Lightw. Technol.*, vol. 34, no. 17, pp. 41204126, Sep. 1, 2016.
- [30] Karunatilaka, D., Zafar, F., Kalavally, V., and Parthiban, R., "LED based indoor visible light communications: State of the art," *IEEE Commun. Surveys Tuts.*, vol. 17, no. 3, pp. 16491678, 3rd Quart., 2015.

- [31] Ghassemlooy, Z., Luo, P., and Zvanovec, S., "Optical camera communications," in *Optical Wireless Communications*. Cham, Switzerland: Springer, Aug. 2016, pp. 547-568.
- [32] NASA. (2017). An Introduction to National Aeronautics and Space. Administration Spectrum Management. [Online]. Available: https://www.nasa.gov/sites/default/files/atoms/files/spectrum_101.pdf
- [33] Komine, T., and Nakagawa, M., "Fundamental analysis for visible light communication system using LED lights," *IEEE Trans. Consum. Electron.*, vol. 50, no. 1, pp. 100-107, Feb. 2004.
- [34] O'Brien, D. C., Zeng, L., Le-Minh, H., Faulkner, G., Walewski, J. W., and Randel, S., "Visible light communications: Challenges and possibilities," in *Proc. Int. Symp. Pers., Indoor Mobile Radio Commun.*, Cannes, France, Sep. 2008, pp. 1-5.
- [35] Liu, H., Darabi, H., Banerjee, P., and Liu, J., "Survey of wireless indoor positioning techniques and systems," *IEEE Trans. Syst., Man, Cybern. C, Appl. Rev.*, vol. 37, no. 6, pp. 1067-1080, Nov. 2007.
- [36] Tsonev, D., Videv, S., and Haas, H., "Towards a 100 Gb/s visible light wireless access network," *Opt. Exp.*, vol. 23, no. 2, pp. 1627-1637, Jan. 2015.
- [37] Zafar, F., Bakaul, M., and Parthiban, R., "Laser-diode-based visible light communication: Toward gigabit class communication," *IEEE Commun. Mag.*, vol. 55, no. 2, pp. 144-151, Feb. 2017.
- [38] Azhar, A. H., Tran, T., and O'Brien, D. C., "Demonstration of high-speed data transmission using MIMO-OFDM visible light communications," in *IEEE Globecom OWC workshop* Dec. 2010.
- [39] Dambul, K. D., O'Brien, D. C., and Faulkner, G., "Indoor optical wireless MIMO system with an imaging receiver," *IEEE Photon Technol Lett.*, pp. 97-99, 2011.
- [40] Ramirez-Iniguez, R. and Green, R. J., "Optical antenna design for indoor optical wireless communication systems," *International Journal of Communication Systems*, pp. 229-245, 2005.
- [41] Mesleh, R., Elgala, H., Hammouda, M., Stefan, I., and Haas, H., "Optical spatial modulation with transmitter-receiver alignments," in *2011 16th European Conference on Networks and Optical Communications (NOC)*, 2011, pp. 1-4.
- [42] Zeng, L., O'Brien, D., Minh, H., Faulkner, G., Lee, K., Jung, D., Oh, Y., and Won, E. T., "High data rate multiple input multiple output (MIMO) optical wireless communications using white LED lighting," *IEEE J. Sel. Areas Commun.*, vol. 27, pp. 1654-1662, 2009.
- [43] Hranilovic, S. and Kschischang, F. R., "A pixelated MIMO wireless optical communication system," *IEEE J. Sel. Topics Quantum Electron.*, vol. 12, pp. 859-874, 2006.
- [44] Hranilovic, S. and Kschischang, F. R., "Short-range wireless optical communication using pixelated transmitters and imaging receivers," in *IEEE Int. Conf. Commun.*, 2004, pp. 891-895.

- [45] Mohamed, M. D. A. and Hranilovic, S., "Two-dimensional binary halftoned optical intensity channels," *IET Communications, Special Issue on Optical Wireless Communication Systems*, vol. 2, pp. 11–17, 2008.
- [46] Mohamed, M. D. A., Dabbo, A., and Hranilovic, S., "MIMO optical wireless channels using halftoning," in *IEEE International Conference on Communications 2008*, Beijing, China, May 2008.
- [47] Mondal, M. R. H., Panta, K. R., and Armstrong, J., "Performance of two dimensional asymmetrically clipped optical OFDM," presented at *the IEEE Globecom Workshops (GC'10)*, Piscataway, NJ, USA, Dec. 2010.
- [48] Mondal, M. R. H. and Armstrong, J., "The effect of defocus blur on a spatial OFDM optical wireless communication system," in *14th International Conference on Transparent Optical Networks (ICTON)*, Coventry, England, UK, 2-5 Jul. 2012.
- [49] Mondal, M. R. H. and Armstrong, J., "Impact of linear misalignment on a spatial OFDM based pixelated system," presented at the *Asia Pacific Conference on Communications (APCC)*, Jeju Island, South Korea, 15-17 Oct. 2012.
- [50] Mondal, M. R. H. and Armstrong, J., "Analysis of the effect of vignetting on MIMO optical wireless systems using spatial OFDM," *J. Lightw. Technol.*, vol. 32, pp. 922-929, 2014.
- [51] Mondal, M. R. H. and Panta, K., "Performance analysis of spatial OFDM for pixelated optical wireless systems," *Transactions on Emerging Telecommunications Technologies (ETT)*, pp. n/a-n/a, 2015.
- [52] Wook, H. B. C., Komine, T., Haruyama, S., and Nakagawa, M., "Visible light communication with LED-based traffic lights using 2-dimensional image sensor," presented at the *IEEE Consumer Communications and Networking Conference (CCNC)*, 8-10 Jan. 2006.
- [53] Ashok, A., Gruteser, M., Mandayam, N. B., Silva, J., Varga, M., and Dana, K. J., "Challenge: mobile optical networks through visual MIMO," presented at the *International Conference on Mobile Computing and Networking (Mobicom)*, Chicago, Illinois, USA, 20-24 Sep. 2010.
- [54] Ashok, A., Jain, S., Gruteser, M., Mandayam, N., Yuan, W., and Dana, K., "Capacity of pervasive camera based communication under perspective distortions," presented at the *IEEE International Conference on Pervasive Computing and Communications*, Budapest, Hungary, Mar. 2014.
- [55] Hao, T., Zhou, R., and Xing, G., "COBRA: color barcode streaming for smartphone systems," presented at the *International Conference on Mobile Systems, Applications and Services (MobiSys)*, Lake District, UK, 25-29 Jun. 2012.
- [56] Arai, S., Mase, S., Yamazato, T., Yendo, T., Fujii, T., Tanimoto, M., and Kimura, Y., "Feasible study of road-to-vehicle communication system using LED array and high-speed camera," presented at the *15th World Congress on ITS*, USA, Nov. 2008.
- [57] Pei, C., Zhang, Z., and Zhang, S., "SoftOC: Real-time Projector-wall-camera Communication System," presented at the *IEEE International Conference on Consumer Electronics (ICCE)*, Las Vegas, NV, USA, 11-14 Jan. 2013.

- [58] Perli, S. D., Ahmed, N., and Katabi, D., "PixNet: interference-free wireless links using LCD-camera pairs," in *International Conference on Mobile Computing and Networking (Mobicom)*, Chicago, Illinois, USA, Sep. 20-24 2010.
- [59] Perli, S. D., Ahmed, N., and Katabi, D., "PixNet : LCD-Camera pairs as communication links," in *Special Interest Group on Data Communication (SIGCOMM)*, New Delhi, India, Aug. 2010.
- [60] Aggarwal, M., Hua, H., and Ahuja, N., "On Cosine-fourth and Vignetting Effects in Real Lenses," in *International Conference On Computer Vision (ICCV)*, Vancouver, British Columbia, Canada, 7-14 Jul. 2001.
- [61] Mahajan, V. N., *Optical Imaging and Aberrations: Part I. Ray Geometrical Optics*: SPIE press book, Jul. 1998.
- [62] Horn, B. K. P., *Robot Vision*: Cambridge, Mass. : MIT Press, 1986.
- [63] Zheng, Y., "Single-image vignetting correction," *IEEE Trans. Pattern Anal. Mach. Intell.*, vol. 31, pp. 2243-2256, 2009.
- [64] Li, Y. , Tsonev , D., Haas, H. . "Non-DC-biased OFDM with optical spatial modulation." *2013 IEEE 24th Annual International Symposium on Personal, Indoor, and Mobile Radio Communications (PIMRC)*, IEEE, pp. 486-490 London, UK, ieeexplore.ieee.org/document/6666185/. Sept. 2013.
- [65] Yesilkaya, A., Basar, E. , Miramirkhani, F., Panayirci , E., Uysal, M. , Haas, H. "Optical MIMO-OFDM with generalized LED index modulation." *IEEE Transactions on Communications*, IEEE, Vol 65, pp. 3429-3441,N/A, ieeexplore.ieee.org/document/7915761/. (2017).
- [66] Dabbo, A. and Hranilovic, S., "Receiver design for wireless optical MIMO channels with magnification," presented at the *10th International Conference on Telecommunications*, Zagreb, Croatia, 8-10 Jun. 2009.
- [67] Wu, N., Bar-Ness, Y., "A novel power-efficient scheme for asymmetrically and symmetrically clipping optical (ASCOC)-OFDM for IM/DD optical systems," *EURASIP J. Adv. Sig. Proc.*, pp. 1–10, 2015.
- [68] Kuzdeba, S., Wyglinski, A.M., Hombs, B.. "Prototype Implementation of a Visual Communication System Employing Video Imagery." *IEEE Consumer Communications and Networking Conference(CCNC)*, IEEE, pp. 184-189 Las Vegas, NV, USA, ieeexplore.ieee.org/document/6488444/. Jan 2013.
- [69] Mondal, M. R. H.. "Impact of spatial sampling frequency offset and motion blur on optical wireless systems using spatial OFDM." *EURASIP Journal on Wireless Communications and Networking*, Springer, Vol 238, pp. 1-12, N/A, <https://link.springer.com/article/10.1186/s13638-016-0741-y>. (2016.).
- [70] Pei, C. C., Zhang, Z. C., Fang, W. X., and Zhang, S. J., "2D-DPSK for quasi-diffuse pixelated wireless optical," in *IEEE International Conference on Communication Technology (ICCT)*, Jinan, China, 25-28 Sep. 2011.

- [71] Dimitrov, S. and Haas, H., "Information rate of OFDM-based optical wireless communication systems with nonlinear distortion," *J. Lightw. Technol.*, vol. 31, Mar. 2013.
- [72] Taberero, A., Portilla, J., and Navarro, R., "Duality of log-polar image representations in the space and spatial-frequency domains," *IEEE Trans. Signal Process.*, vol. 47, pp. 2469-2479, Sep. 1999.
- [73] Bruce, N. D. B., Loach, D. P., and Tsotsos, J. K., "Visual correlates of fixation selection: a look at the spatial frequency domain," presented at the *Int. Conf. on Image Processing (ICIP)*, San Antonio, USA, Sep. 2007.
- [74] Kumar, B. V. K. V., Savvides, M., Venkataramani, K., and Xie, C., "Spatial frequency domain image processing for biometric recognition," presented at the *Int. Conf. on Image Processing (ICIP)*, Rochester, New York, USA, 2002.
- [75] Yu, H., Myung-Soon, K., Taehyun, J., and Sok-Kyu, L., "Equalization scheme for OFDM systems in long delay spread channels," in *15th IEEE International Symposium on Personal, Indoor and Mobile Radio Communications (PIMRC) 2004*, pp. 1297-1301 Vol.2.
- [76] Landau, O. and Weiss, A. J., "OFDM Guard Interval: Analysis and Observations," in *IEEE International Conference on Acoustics, Speech and Signal Processing (ICASSP) 2007*, pp. III-93-III-96.
- [77] Dissanayake, S. D., and Armstrong, J., "Comparison of ACO-OFDM, DCO-OFDM and ADO-OFDM in IM/DD Systems," in *Journal of Lightwave Technology*, vol. 31, no. 7, pp. 1063-1072, April, 2013.
- [78] Moghaddam, M. E., and Jamzad, M., "Motion blur identification in noisy images using fuzzy sets," *Proceedings of the Fifth IEEE International Symposium on Signal Processing and Information Technology, 2005.*, Athens, 2005, pp. 862-866.
- [79] Kurimo E., Lepistö L., Nikkanen J., Grén J., Kunttu I., Laaksonen J. (2009) The Effect of Motion Blur and Signal Noise on Image Quality in Low Light Imaging. In: Salberg AB., Hardeberg J.Y., Jenssen R. (eds) Image Analysis. SCIA 2009.
- [80] Kurimo, E.: Motion blur and signal noise in low light imaging, Master Thesis, Helsinki University of Technology, Faculty of Electronics, Communications and Automation, Department of Information and Computer Science (2008)
- [81] Nikkanen, J., Kalevo, O.: Menetelmä ja järjestelmä digitaalisessa kuvannuksessa valotuksen säätämiseksi ja vastaava laite. Patent FI 116246 B (2003)
- [82] Xiao, F., Silverstein, A., Farrell, J.: Camera-motion and effective spatial resolution. In: International Congress of Imaging Science, Rochester, NY (2006)
- [83] Wiener, N.: Extrapolation, interpolation, and smoothing of stationary time series (1992)
- [84] Yuan, W., Dana, K., Varga, M., Ashok, A., Gruteser, M., and Mandayam, N., "Computer vision methods for visual MIMO optical system," presented at the *IEEE Computer Society Conference on Computer Vision and Pattern Recognition Workshops (CVPRW)*, Colorado, USA, Jun. 2011.

- [85] Ashok, A., Gruteser, M., Mandayam, N., Taekyoung, K., Wenjia, Y., Varga, M., and Dana, K., "Rate adaptation in visual MIMO," in *8th Annual IEEE Communications Society Conference on Sensor, Mesh and Ad Hoc Communications and Networks (SECON)*, Utah, USA, Jun. 2011, pp. 583-591.
- [86] Yuan, W., Dana, K., Ashok, A., Gruteser, M., and Mandayam, N., "Dynamic and invisible messaging for visual MIMO," in *IEEE Workshop on Applications of Computer Vision (WACV)*, Colorado, USA, Jan. 2012, pp. 345-352.
- [87] Pu, Q. and Hu, W., "Smooth transmission over unsynchronized VLC links," presented at the *International Conference on Emerging Networking Experiments and Technologies (CoNEXT) Student Workshop Nice*, France, 10 Dec. 2012.
- [88] Boubezari, R., Minh, H. L., Ghassemlooy, Z., Bouridane, A., and Pham, A. T., "Data detection for Smartphone visible light communications," in *2014 9th International Symposium on Communication Systems, Networks & Digital Sign (CSNDSP)*, 2014, pp. 1034-1038.
- [89] Huiying, S. and Coughlan, J., "Reading LCD/LED Displays with a Camera Cell Phone," in *2006 Conference on Computer Vision and Pattern Recognition Workshop (CVPRW'06)*, 2006, pp. 119-119.
- [90] Kim, B. W., Kim, H. C., and Jung, S. Y., "Display Field Communication: Fundamental Design and Performance Analysis," *Journal of Lightwave Technology*, vol. 33, pp. 5269-5277, 2015.
- [91] Motahari, A. and Adjouadi, M., "Barcode Modulation Method for Data Transmission in Mobile Devices," *IEEE Transactions on Multimedia*, vol. 17, pp. 118-127, 2015.
- [92] Hartley, R., and Zisserman, A., "Multiple View Geometry in Computer Vision," Second edition, Cambridge University Press, 2003.
- [93] Kim, Y., Lee, D., and Kim, D., "Pre-Processing Images for Enhancing Reliability in Screen-to-Camera Communication," in *IEEE Wireless Communications Letters*, vol. 7, no. 6, pp. 934-937, May. 2018.
- [94] Nguyen, T., Islam, A., Yamazato, T., and Jang, Y. M., "Technical Issues on IEEE 802.15.7m Image Sensor Communication Standardization," in *IEEE Communications Magazine*, vol. 56, no. 2, pp. 213-218, Feb. 2018.
- [95] Nguyen, T., Islam, A., Hossan, T., and Jang, Y. M., "Current Status and Performance Analysis of Optical Camera Communication Technologies for 5G Networks," in *IEEE Access*, vol. 5, pp. 4574-4594, 2017.
- [96] Yamamoto, J., and Bandai, M., "A flickerless screen-camera communication using interframe difference," *2018 15th IEEE Annual Consumer Communications & Networking Conference (CCNC)*, Las Vegas, NV, 2018, pp. 1-4.
- [97] Yamsang, P., Pongyart, W., and Vanichchanunt, P., "Multilevel grey-scale visual coding for data transmission from LCD screens to Android smartphone cameras," *2017 8th International Conference of Information and Communication Technology for Embedded Systems (IC-ICTES)*, Chonburi, 2017, pp. 1-4.

- [98] Stafford, M., Rogers, A., Wu, S., Carver, C., Artan, N. S., and Dong, Z., "TETRIS: Smartphone-to-Smartphone Screen-Based Visible Light Communication," *2017 IEEE 14th International Conference on Mobile Ad Hoc and Sensor Systems (MASS)*, Orlando, FL, 2017, pp. 570-574.